UNIVERSITÀ DEGLI STUDI DI MILANO
Facoltà di Scienze Matematiche Fisiche e Naturali
Corso di Laurea Magistrale in Fisica


# Width of Long Color Flux Tubes in Yang-Mills Theory

Relatore: **Prof. Sergio Caracciolo**

Relatore Esterno: **Dott. Michele Pepe**

pacs 12.38.Gc, 11.15.Ha

Tesi di laurea magistrale

Candidato: **Alessandro Amato**
Matricola: **737441**

**Anno Accademico 2009 - 2010**

Ai miei genitori

# Contents

# Riassunto

In questa tesi abbiamo preso in considerazione la fisica di bassa energia dell'interazione forte fra due sorgenti di colore statiche.

La cromodinamica quantistica (QCD) è la teoria di campo che descrive l'interazione forte. I gradi di libertà sono rappresentati da due tipi di particelle: i quarks, fermioni elementari, e i gluoni, bosoni vettori mediatori dell'interazione.

La QCD può essere studiata in due differenti regimi. Ad alte energie, l'accoppiamento è debole e si possono utilizzare i metodi perturbativi della teoria di campo. A energie più basse, l'accoppiamento è invece forte e la dinamica è dominata da effetti non perturbativi. In quest'ultimo regime, una delle caratteristiche più rilevanti è il fenomeno del confinamento: i costituenti elementari della QCD, quarks e gluoni, non sono osservabili come stati asintoticamente liberi dello spettro.

A partire dalle evidenze sperimentali, risulta che l'energia del campo gluonico in una coppia quark–antiquark confinata aumenta linearmente con la distanza fra le due particelle. La densità di energia dell'interazione è concentrata in una regione tubolare che connette le due sorgenti e viene detta *tubo di flusso* cromoelettrico. La fisica del tubo di flusso può essere studiata in modo particolarmente efficiente nel limite in cui i quarks sono trattati come delle sorgenti statiche esterne infinitamente massive. La QCD viene allora approssimata dalla teoria di Yang-Mills, in cui i gluoni sono gli unici gradi di libertà dinamici. In questa teoria il potenziale di interazione tra una coppia statica quark–antiquark aumenta indefinitamente con andamento lineare, al crescere della distanza tra le due sorgenti.

Nel 1980 Lüscher, Symanzik e Weisz proposero una teoria di corda effettiva nel regime di basse energie, in cui il tubo di flusso è descritto come una corda vibrante. Questa corda viene considerata come un oggetto elementare, senza gradi di libertà che ne descrivono la struttura interna. È importante notare che in questo approccio viene rimossa ogni dipendenza dalla simmetria di gauge della teoria sottostante. Sebbene questa descrizione del tubo di flusso possa sembrare troppo semplificata, rappresenta invece uno strumento potente per studiarne le proprietà, portando a delle precise predizioni quantitative calcolabili analiticamente.

Una prima predizione riguarda la correzione sottodominante all'andamento

lineare del potenziale di interazione quark–antiquark. Questa correzione è della forma $-\pi(d-2)/24\,r$, dove $r$ indica la distanza tra le sorgenti di colore. Essa ha carattere universale e dipende solo dalla dimensionalità $d$ del sistema.

Una seconda predizione stabilisce che lo spessore del tubo di flusso cresce con la distanza tra le due sorgenti statiche. A temperatura zero si ottiene che tale crescita è logaritmica. Studi numerici della teoria di Yang-Mills su reticolo hanno mostrato con elevata accuratezza la validità di questa previsione.

A temperatura finita, la teoria effettiva di corda prevede invece un allargamento lineare del tubo di flusso. La descrizione effettiva di corda dipende da alcuni parametri il cui valore può essere fissato solo da un confronto con la teoria di gauge sottostante. È importante sottolineare che i dati numerici ottenuti per lo studio dell'allargamento logaritmico a temperatura zero determinano completamente la predizione della teoria effettiva a temperatura finita, senza lasciare alcun parametro libero. Dunque lo studio dell'allargamento del tubo di flusso a temperatura finita rappresenta una verifica molto stringente delle predizioni della teoria effettiva di corda.

In questa tesi sono state effettuate simulazioni Monte Carlo della teoria di Yang-Mills con gruppo di gauge $SU(2)$ in $(2+1)$ dimensioni su reticolo a temperatura finita. Abbiamo misurato con elevata accuratezza la larghezza del tubo di flusso in funzione della distanza tra la coppia di quarks statici. I risultati della simulazione numerica sono in accordo eccellente con la predizione della teoria effettiva di corda.

Lo studio numerico effettuato è molto oneroso dal punto di vista computazionale: infatti il rapporto tra segnale/rumore delle osservabili da misurare decresce esponenzialmente con la distanza tra le sorgenti. Sfruttando un algoritmo proposto recentemente da Lüscher e Weisz, è stato possibile effettuare questo studio per la prima volta, fornendo dati sulla larghezza del tubo di flusso in una teoria di gauge non–Abeliana.

# Introduction

During the 50s there was a significant development in particle physics, with the improvement of scattering experiments exploiting a continuous increase of energy. These experiments detected a large number of new strongly interacting particles that were called hadrons. The study of the properties of the hadrons led to group them into multiplets with similar physical behavior.

In 1963 Gell-Mann and Zweig proposed a model that could explain the multiplets by introducing new elementary particles called quarks. However at that time, the quark model was simply a useful scheme for classifying hadrons.

According to this hypothesis quarks are elementary fermions of spin 1/2, with fractional electric charge. Each hadron is the bound state of a quark and an antiquark. In particular, two main hadrons families appear: mesons, consisting in a bound state of a quark–antiquark pair, and baryons, made of three quarks or three antiquarks.

There exist 6 different kinds of quarks, called flavors: *up*, *charm* and *top*, with positive electric charge, $q = +2/3$; *down*, *strange* and *bottom*, with negative charge $q = -1/3$.

Despite these successes, the original model was not able to account for some phenomenological aspects. First, no isolated quark was ever observed. Second, a particular excited state of the baryonic spectrum, $\triangle^{++}$, with spin 3/2 e and charge +2 was detected. This particle could only be interpreted as the completely symmetric bound state of three quarks with parallel spin,

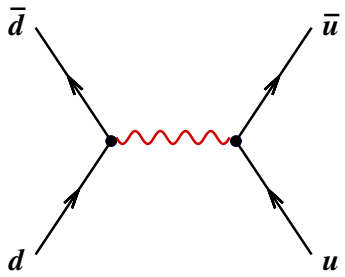


Figure 1: *In QCD the quarks interact by exchanging vector bosons (wiggly line) that are referred to as gluons. They carry $SU(3)$ quantum numbers and couple to all flavors of quarks with equal strength proportional to the gauge coupling $g$.*

but this was in contradiction with the fermionic nature of quarks.

The solution of the second puzzle was proposed in 1965 by Han, Nambu and, independently, by Greenberg. They proposed to assign a new quantum number to quarks: the *color*. With this new internal degree of freedom, the wave function of $\triangle^{++}$, symmetric with respect to quantum observed numbers, could be made antisymmetric in agreement with the Fermi-Dirac statistics.

This proposal, called "color hypothesis", assumes that quarks transform under the fundamental representation of a global $SU(3)$ symmetry. As this new quantum number was not observed in experiments, it was postulated that hadrons are singlet states with respect to $SU(3)$ transformations. Hence the action that describes strong interactions must be invariant under that symmetry. Later the $SU(3)$ group was promoted to be a local symmetry group for strong interaction, leading to the formulation of QCD as a non-Abelian gauge theory [1, 2].

An important feature of this theory is the property of asymptotic freedom. At the end of the '60s, at SLAC accelerator in Stanford, scattering experiments were performed at high energies where electrons were made to collide over hadrons. The results of these experiments showed that the cross sections of such processes were dominated by electromagnetic interactions.

Later, in 1973 Gross,Wilczek e Politzer found that such behavior was indeed a feature of quantum chromodynamics. In fact they realized that the coupling constant of the strong interaction depends on the energy scale at which the theory is considered. For high energy processes, the coupling is small and the theory is weakly interacting; instead, at low energy scales it becomes strong [1, 2].

This behavior suggests that QCD has two different regimes: at short distances, the coupling is small and it is the natural parameter for a perturbative expansion. At large distances, the coupling becomes strong and non-perturbative effects are dominant.

However as far as Gell-Mann and Zweig proposed this theory, one of the most striking feature is the conjecture that the physically observed states are singlets states of the color symmetry. This is what we refer to *quark confinement*. If it has to be a fundamental theory, QCD must include this feature as well.

Let us consider an hadron consisting of a quark-antiquark pair, and let $V(R)$ be the energy of that state. If $V$ increases with the interquark distance, we have a confining theory. In fact, attempts to separate such state would result in an infinite energy cost. Moreover there exists a distance at which the energy is enough to create a new quark-antiquark pair from the vacuum. When that happens, the phenomenon of "hadronization" [1, 3] takes place and the original system separates into two parts. This could explain why there are no isolated quarks in Nature.

In this context it was proposed the flux tube picture of confinement.

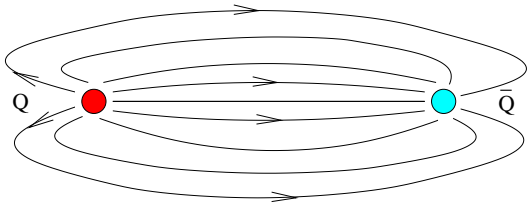


Figure 2: A tube of gluonic flux connects quarks and antiquarks. The strength of this string is 14 tons.

The field lines from a quark cannot end, instead, as in Fig. 2, they cluster together, forming a tube of flux connecting the quark and the antiquark. This tube is a real physical object, and becomes larger as the quark and antiquark are pulled apart. The resulting force is constant at long distances, and it can be determined from the slope of the famous Regge trajectories [3]. In physical units, it has a strength of about 14 tons.

In this work we study the low energy aspects of the strong interactions. A useful simplification consists in giving the quarks an infinite mass and decoupling them from the gluon dynamics. In this approximation, quarks do not contribute to any virtual process, including string-breaking processes. This enables us to focus on the dynamics of the gluon field described by the Yang-Mills theory.

In 1980 Luscher, Symanzic and Weisz proposed an effective string theory of the flux tube. Physics is described through the oscillations of a string connecting the quark to the anti-quark. In this picture the color flux tube is described as a vibrating string. It is important to note that the string has no internal degrees of freedom and any dependence of the gauge symmetry group has been removed. Although, at first sight, this seems to be a very poor description of the confining string, it is a very powerful tool to investigate the properties of the color flux tube. In fact it provides a systematic low-energy description of the quark–antiquark interactions and it leads to precise quantitative predictions.

One of the predictions of the effective string theory is the Lüscher term: a correction to the linear behavior of the interaction potential between the two sources, that turns out to be universal.

In this work we focus on the predictions of the effective string theory to the broadening of the color flux tube. At zero temperature we expect a logarithmic behavior. Numerical simulations of $(2+1)-d$ Yang-Mills $SU(2)$ theory confirmed this prediction with high accuracy.

At finite temperature the broadening of the flux tube should be linear instead.

It is important to remark that the effective string theory depends on two low energy parameters, that can be only fixed by comparison with numerical simulations of the underlying Yang-mills gauge theory. Data obtained at

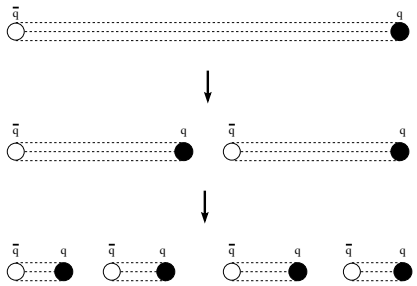

Figure 3: *String breaking by quark-antiquark pair production.*

zero temperature, completely fix these parameters and at finite temperature the theory has no free parameters left. Hence, studying the broadening of the flux tube at finite temperature will result in a stringent check of the effective string theory.

In this thesis, simulations have been performed on $(2+1)-d$ Yang-Mills theory with $SU(2)$ gauge group on a lattice at finite temperature. The broadening of the flux tube has been measured with great accuracy and the data perfectly agree with the effective string theory predictions.

This dissertation will procede as follow. In Chapter 1 we briefly review some basic facts about non–Abelian gauge theory on the lattice: the path integral formulation of quantum field theory, Yang-Mills theory in the continuum and then its regularization on the lattice. In Chapter 2 the effective string theory is introduced. We calculate analytically the corrections to the static quark potential and the predictions on the broadening of the flux tube at zero and finite temperature. The necessary statistical tools used to implement numerical simulations are discussed in Chapter 3. The Monte Carlo method is reviewed, together with the main update algorithms we used in our simulations. Finally, in Chapter 4, we show and discuss the results of the numerical study we performed on $(2+1)-d$ Yang-Mills $SU(2)$ theory.

# Chapter 1

# Lattice Gauge Theory

In this Chapter we describe the Lattice Gauge Theory (LGT) formalism as a non–perturbative regularization of field theory. In the first Section we will review the Feynman path integral, or functional integral formulation of quantum field theory. Then we will focus on Yang-Mills and its regularization on a lattice.

## 1.1 Path Integral Formalism

In this Section we introduce some fundamental tools of lattice gauge theories: quantum field theory in its path integral formulation, Wick rotation to imaginary time coordinates leading to Euclidean field theory, and the discretization of space-time in form of a lattice. These concepts are being illustrated using a scalar field theory.

### 1.1.1 Path Integral for QFT

Let us start considering the quantum mechanics of a particle in one space dimension. The Hamiltonian appears to be

$$H = \frac{p^2}{2m} + V(x) \equiv H_0 + V. \tag{1.1}$$

The quantum mechanical transition amplitude is

$$\langle x', t'|x, t\rangle = \langle x'|e^{-iH(t'-t)}|x\rangle. \tag{1.2}$$

Inserting a complete set of coordinate eigenstates,

$$1 = \int dx_1 \, |x_1\rangle\langle x_1| \ , \tag{1.3}$$

into the matrix element, taking $T = (t' - t)$ and $\Delta t = (t_1 - t)$, we obtain

$$\langle x', t'|x, t\rangle = \int dx_1 \, \langle x'|e^{-iH(T-\Delta t)}|x_1\rangle\langle x_1|e^{-iH\Delta t}|x\rangle. \tag{1.4}$$

Now we divide $T$ into $n$ equal parts, $T = n\Delta t$. We then insert a $(n-1)$ complete sets obtaining:

$$\langle x', t'|x, t\rangle = \int dx_1 \dots dx_{n-1} \ \langle x'|e^{-iH\Delta t}|x_{n-1}\rangle \times \\ \times \langle x_{n-1}|e^{-iH\Delta t}|x_{n-2}\rangle \dots \langle x_1|e^{-iH\Delta t}|x\rangle \ . \quad (1.5)$$

In the following we set $x \equiv x_0$ and $x' \equiv x_n$.

When $n$ becomes larger then $\Delta t$ is smaller and smaller and the matrix elements can be rewritten using only the first term of the Baker-Campbell-Hausdorff-formula, performing a good approximation to the exponential:

$$\langle x_{k+1}|e^{-iH\Delta t}|x_k\rangle \approx \\ \langle x_{k+1}|e^{-iH_0\Delta t}e^{-iV\Delta t}|x_k\rangle \ = \langle x_{k+1}|e^{-iH_0\Delta t}|x_k\rangle \, e^{-iV(x_k)\Delta t} \ . \quad (1.6)$$

If we consider the fact that the potential $V$ is a function of the space only coordinates, the remaining matrix element can be calculated by means of Fourier transform with the following result:

$$\langle x_{k+1}|e^{-iH\Delta t}|x_k\rangle \approx \sqrt{\frac{m}{2\pi i\Delta t}} \ \exp i\Delta t \left[\frac{m}{2}\left(\frac{x_{k+1}-x_k}{\Delta t}\right)^2 - V(x_k)\right]. \quad (1.7)$$

Reiterating this operation for every matrix element, we obtain for the amplitude (1.2) the final form:

$$\langle x'|e^{-iHT}|x\rangle = \left(\frac{2\pi i\Delta t}{m}\right)^{-n/2} \int dx_1 \dots dx_{n-1} \prod_{k=0}^{n-1} e^{i\Delta t\left[\frac{m}{2}\left(\frac{x_{k+1}-x_k}{\Delta t}\right)^2 - V(x_k)\right]}. \quad (1.8)$$

Let us explore now the limit $n \to \infty$: the exponent becomes the classical action

$$\sum_{k=0}^{n-1} \Delta t \left[\frac{m}{2}\left(\frac{x_{k+1}-x_k}{\Delta t}\right)^2 - V(x_k)\right] \\ \longrightarrow \int_0^T dt \left[\frac{m}{2}\left(\frac{dx}{dt}\right)^2 - V(x)\right] = \int_0^T dt \, L(x, \dot{x}) \equiv S \quad (1.9)$$

for a path $x(t)$ from $x$ to $x'$ with $x_k = x(k\Delta t)$.

We can interpret $x_k$ integrations as an exploration of all possible paths $x(t)$ of the system. It is useful to introduce then the notation

$$\left(\frac{m}{2\pi i\Delta t}\right)^{n/2} \ dx_1 \dots dx_{n-1} \longrightarrow \text{const.} \prod_t dx(t) \equiv \mathcal{D}x \quad (1.10)$$

we then obtain the path integral representation of the quantum mechanical amplitude:

$$\langle x'|e^{-iHT}|x\rangle = \int \mathcal{D}x \ e^{iS}. \quad (1.11)$$

It is possible to generalize the paths $x_i(t)$ with $i = 1, 2, 3$ for a particle in 3 dimensions as:

$$\mathcal{D}x = \prod_t \prod_i dx_i(t). \tag{1.12}$$

In this way the quantum mechanical transition amplitude is written as an integral over contributions from all possible paths weighted by the classical action from the starting point to the final point.

It is possible to translate the procedure outlined here to a field theory context. Let us consider a scalar field $\phi(x)$, where $x = (\vec{x}, t)$ labels space-time coordinates. $\phi(\vec{x}, t)$ evolves in time through:

$$\phi(\vec{x}, t) = e^{iHt}\, \phi(\vec{x}, t = 0)\, e^{-iHt}. \tag{1.13}$$

Vacuum expectation values are the main object we consider in field theory. These are made up by (time ordered) products of field operators. So we are interested in the Green's functions:

$$\langle 0|\phi(x_1)\phi(x_2)\dots\phi(x_n)|0\rangle, \qquad t_1 > t_2 > \dots > t_n. \tag{1.14}$$

These essentially contain all physical informations of the system.

Deriving the functional integral representation for quantum field theory from the beginning, would be rather complicate. We shall restrict ourselves to translating the quantum mechanical concepts to field theory by means of analogy. This consists in translating the variables $x_i(t)$ into fields $\phi(\vec{x}, t)$. The rules for the translation are then

$$\begin{aligned} x_i(t) &\longleftrightarrow \phi(\vec{x}, t) \\ i &\longleftrightarrow \vec{x} \\ \prod_{t,i} dx_i(t) &\longleftrightarrow \prod_{t,\vec{x}} d\phi(\vec{x}, t) \equiv \mathcal{D}\phi \\ S = \int dt\ L &\longleftrightarrow S = \int dt\, d^3x\ \mathcal{L}, \end{aligned}$$

where $S$ is the classical action.

For scalar field theory we might consider the following Lagrangian density:

$$\begin{aligned} \mathcal{L} &= \frac{1}{2}\left((\dot{\phi}(x))^2 - (\nabla\phi(x))^2\right) - \frac{m_0^2}{2}\phi(x)^2 - \frac{g_0}{4!}\phi(x)^4 \\ &= \frac{1}{2}(\partial_\mu\phi)(\partial^\mu\phi) - \frac{m_0^2}{2}\phi(x)^2 - \frac{g_0}{4!}\phi(x)^4. \end{aligned} \tag{1.15}$$

The mass $m_0$ and coupling constant $g_0$ bear a subscript 0, since they are bare, unrenormalized parameters.

The analogy to quantum mechanical path integral case drives us to represent the Greens functions in terms of *functional integrals*:

$$\langle 0|\phi(x_1)\phi(x_2)\dots\phi(x_n)|0\rangle = \frac{1}{Z}\int \mathcal{D}\phi\ \phi(x_1)\phi(x_2)\dots\phi(x_n)\, e^{iS} \tag{1.16}$$

with

$$Z = \int \mathcal{D}\phi\ e^{iS}. \tag{1.17}$$

These integrals are meant over all classical field configurations.

There are some issues that must be clarified. It is important to understand how could be performed the projection onto the ground state $|0\rangle$ and if these integrals, that contain oscillating integrands due to the imaginary exponents are convergent. In the following we shall discuss, how the introduction of imaginary times helps in answering these questions.

### 1.1.2 Euclidean Functional Integral

Green's functions can be introduced also in the quantum mechanical case, e.g.

$$G(t_1, t_2) = \langle 0|X(t_1)X(t_2)|0\rangle, \qquad t_1 > t_2. \tag{1.18}$$

It is possible to relate these Green's functions to quantum mechanical amplitudes at imaginary times by analytic continuation. Let us consider the matrix element

$$\langle x', t'|X(t_1)X(t_2)|x, t\rangle = \langle x'|e^{-iH(t'-t_1)}Xe^{-iH(t_1-t_2)}Xe^{-iH(t_2-t)}|x\rangle \tag{1.19}$$

for $t' > t_1 > t_2 > t$. Let all times to be purely imaginary as $t = -i\tau$. Thus we obtain:

$$\langle x'|e^{-H(\tau'-\tau_1)}Xe^{-H(\tau_1-\tau_2)}Xe^{-H(\tau_2-\tau)}|x\rangle. \tag{1.20}$$

We can expand the time evolution operator in imaginary times after inserting a complete set of energy eigenstates as[1]:

$$e^{-H\tau} = \sum_{n=0}^{\infty} e^{-E_n\tau}|n\rangle\langle n| = |0\rangle\langle 0| + e^{-E_1\tau}|1\rangle\langle 1| + \dots, \tag{1.21}$$

Then a ground state projector is obtained if we look at the previous equation for large $\tau$. If we perform the limit $\tau' \to \infty$ and $\tau \to -\infty$ the matrix element becomes:

$$\langle x'|0\rangle\langle 0|Xe^{-H(\tau_1-\tau_2)}X|0\rangle\langle 0|x\rangle \tag{1.22}$$

and similarly

$$\langle x'|e^{-H(\tau'-\tau)}|x\rangle \longrightarrow \langle x'|0\rangle\langle 0|x\rangle. \tag{1.23}$$

[1] Ground state energy has been normalized to $E_0 = 0$.

We can then express the Green's function at imaginary times $G_E(\tau_1, \tau_2) = \langle 0|Xe^{-H(\tau_1-\tau_2)}X|0\rangle$ as

$$G_E(\tau_1, \tau_2) = \lim_{\substack{\tau'\to\infty \\ \tau\to-\infty}} \frac{\langle x'|e^{-H(\tau'-\tau_1)}Xe^{-H(\tau_1-\tau_2)}Xe^{-H(\tau_2-\tau)}|x\rangle}{\langle x'|e^{-H(\tau'-\tau)}|x\rangle} \,. \tag{1.24}$$

As we have seen before, path integral can be used to represent both denominator and numerator. However we now have to use for imaginary times:

$$\langle x|e^{-H\Delta\tau}|y\rangle \approx \sqrt{\frac{m}{2\pi\Delta\tau}}\ \exp -\Delta\tau \left[\frac{m}{2}\left(\frac{x-y}{\Delta\tau}\right)^2 + V(x)\right]. \tag{1.25}$$

This leads to the path integral representation

$$G_E(\tau_1, \tau_2) = Z^{-1}\int \mathcal{D}x\ x(\tau_1)x(\tau_2)\, e^{-S_E} \tag{1.26}$$

$$S_E = \int d\tau \left[\frac{m}{2}\left(\frac{dx}{d\tau}\right)^2 + V(x(\tau)\right]. \tag{1.27}$$

The Green's functions at real times (1.18) can be obtained from $G_E$ by means of analytical continuation, $G(t_1, t_2) = G_E(it_1, it_2)$. The analytical continuation has to be done in such a way that all time arguments are rotated simultaneously counter-clockwise in the complex $t$-plane. This is the so-called *Wick rotation*.

Now we turn to field theory again. Let us consider the Green's functions continued to imaginary times $t = -i\tau$:

$$G_E((\vec{x}_1, \tau_1), \ldots, (\vec{x}_n, \tau_n)) = G((\vec{x}_1, -i\tau_1), \ldots, (\vec{x}_n, -i\tau_n)). \tag{1.28}$$

In analogy to the quantum mechanical case their functional integral representation can be written as:

$$G_E(x_1, \ldots, x_n) = \frac{1}{Z}\int \mathcal{D}\phi\ \phi(x_1)\ldots\phi(x_n)\, e^{-S_E} \tag{1.29}$$

with

$$Z = \int \mathcal{D}\phi\ e^{-S_E} \tag{1.30}$$

and

$$\begin{aligned} S_E &= \int d^3x d\tau \left[\frac{1}{2}\left(\frac{d\phi}{d\tau}\right)^2 + \frac{1}{2}(\nabla\phi)^2 + \frac{m_0^2}{2}\phi^2 + \frac{g_0}{4!}\phi^4\right] \\ &= \int d^4x \left[\frac{1}{2}(\partial_\mu\phi)^2 + \frac{m_0^2}{2}\phi^2 + \frac{g_0}{4!}\phi^4\right]. \end{aligned} \tag{1.31}$$

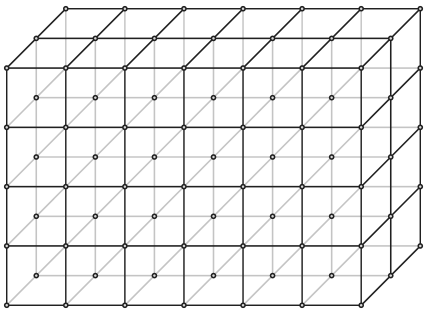

Figure 1.1: *A representation of a* 3*–dimensional lattice.*

As we performed a Wick rotation the metric of Minkowski space changed according to

$$-ds^2 = -dt^2 + dx_1^2 + dx_2^2 + dx_3^2 \;\rightarrow\; d\tau^2 = dx_1^2 + dx_2^2 + dx_3^2 \tag{1.32}$$

that is the metric of a Euclidean space. Therefore in that context we will refer to *Euclidean Greens functions* $G_E$ and of *Euclidean functional integrals*. Remarkably, as $S_E$ is real, the integrals of interest are now real and no undesired oscillations occur.

From now on we shall remain in Euclidean space and suppress the subscript $E$, so that $S \equiv S_E$ means the Euclidean action.

### 1.1.3 Field Theories on a Lattice

We derived the path integral representation of quantum mechanics as a limit of a discretization in time $\tau$. After performing a Wick rotation, fields depend on the four Euclidean coordinates. It is then possible to introduce a discretized space-time in form of a lattice, for example a hypercubic lattice as in Fig. 1.1, specified by

$$x_\mu = a n_\mu, \qquad n_\mu \in \mathbf{Z}. \tag{1.33}$$

The quantity $a$ is called the lattice spacing and the scalar field $\phi(x)$ is now defined on the lattice points $x$ only. The derivative is replaced by finite differences:

$$\partial_\mu \phi \longrightarrow \Delta_\mu \phi(x) \equiv \frac{1}{a}(\phi(x + a\hat{\mu}) - \phi(x)), \tag{1.34}$$

and space-time integrals are replaced by sums:

$$\int d^4x \quad \longrightarrow \sum_x a^4 \; . \tag{1.35}$$

We can now rewrite the action Eq. (1.31) for a discretized $\phi^4$-theory as:

$$S = \sum_x a^4 \left[ \frac{1}{2} \sum_{\mu=1}^{4} (\Delta_\mu \phi(x))^2 + \frac{m_0^2}{2} \phi(x)^2 + \frac{g_0}{4!} \phi(x)^4 \right]. \tag{1.36}$$

In the functional integrals the measure

$$\mathcal{D}\phi = \prod_x d\phi(x) \tag{1.37}$$

involves the lattice points $x$ only. So we have a discrete set of variables to integrate. If the lattice is taken to be finite, we just have finite dimensional integrals.

Discretization of space-time on the lattice has one very important consequence. Due to a non-zero lattice spacing a cutoff in momentum space arises. The cutoff can be observed by having a look at the Fourier transformed field

$$\tilde{\phi}(p) = \sum_x a^4 \; e^{-ipx} \; \phi(x). \tag{1.38}$$

The Fourier transformed functions are periodic in momentum-space, so that we can identify $p_\mu \cong p_\mu + 2\pi/a$ and restrict the momenta to the so-called Brillouin zone $-\pi/a < p_\mu \leq \pi/a$.

The inverse Fourier transformation is now equipped with an ultraviolet cutoff $|p_\mu| \leq \pi/a$ :

$$\phi(x) = \int_{-\pi/a}^{\pi/a} \frac{d^4p}{(2\pi)^4} \; e^{ipx} \; \tilde{\phi}(p). \tag{1.39}$$

Therefore field theories on a lattice are regularized in a natural way.

Aiming to perform numerical simulations of field theories one has to deal with finite lattices. Let us assume a hypercubic lattice with length $L_1 = L_2 = L_3 = L$ in every spatial direction and length $L_4 = T$ in Euclidean time,

$$x_\mu = a n_\mu, \qquad n_\mu = 0, 1, 2, \ldots, L_\mu - 1, \tag{1.40}$$

with finite volume $V = L^3 T$.

In a finite volume one has to specify boundary conditions. One can impose periodic b.c. $\phi(x) = \phi(x + aL_\mu \hat{\mu})$, where $\hat{\mu}$ is the unit vector in the $\mu$-direction, as well a Dirichlet b.c. $\phi(0) = \phi(aL_\mu \hat{\mu}) = 0$ . They imply that the momenta are also discretized,

$$p_\mu = \frac{2\pi}{a} \frac{l_\mu}{L_\mu} \qquad \text{with } l_\mu = 0, 1, 2, \ldots, L_\mu - 1, \tag{1.41}$$

and therefore momentum-space integration is replaced by finite sums

$$\int \frac{d^4p}{(2\pi)^4} \; \longrightarrow \; \frac{1}{a^4 L^3 T} \sum_{l_\mu}. \tag{1.42}$$

Now, all functional integrals have turned into regularized and finite expressions.

If we want to recover the physics in the continuum in an infinite space-time, we have to take the infinite volume limit and the continuum limit $a \longrightarrow$

0. Constructing the continuum limit of a lattice field theory is nontrivial as we will see.

The formulation of Euclidean quantum field theory on a lattice bears a useful analogy to statistical mechanics. Functional integrals have the form of partition functions and we can set up the following correspondence:

| Euclidean field theory | Statistical Mechanics |
|---|---|
| generating functional $\int \mathcal{D}\phi \; e^{-S}$ | partition function $\sum e^{-\beta \mathcal{H}}$ |
| action $S$ | Hamilton function $\beta \mathcal{H}$ |
| mass $m$ $G \sim e^{-mt}$ | inverse correlation length $1/\xi$ $G \sim e^{-\frac{x}{\xi}}$ |

This formal analogy allows to use well established methods of statistical mechanics in field theory and vice versa.

## 1.2 Non Abelian Gauge Theory

In this Section we will review some basic aspects of non abelian gauge theories. We will start from the continuum formulation and then move to the lattice one. As we are dealing with the pure gauge theory for the rest of our work, we will focus on that. However we will use fermion matter fields, and their transformation laws under the gauge group to explain concepts such as parallel transport and covariant derivative.

### 1.2.1 Continuum formulation

QCD describes the relativistic dynamics of quarks, that are massive fermions described by Dirac 4-spinors $\overline{\psi}_\alpha(x)^c$ and $\psi_\alpha(x)^c$. The spacetime position is denoted by $x$, the Dirac index by $\alpha = 1, 2, 3, 4$ and the color index is labeled by $c = 1, 2, 3$. The fermionic part of the QCD action is a bilinear function in the fields $\overline{\psi}$ and $\psi$ [1, 2]:

$$S = \int \mathrm{d}^4 x \left[\overline{\psi}(x) \cdot \left(i\partial\!\!\!/ - m\right) \psi(x)\right] \tag{1.43}$$

where $\gamma^\mu$ are the Dirac matrices, $\overline{\psi} = \gamma_0 \psi^\dagger$ and $\partial\!\!\!/ = \partial_\mu \gamma^\mu$. The internal product "$\cdot$" represents the contraction of the color index $c$:

$$\overline{\psi} \cdot \psi = \sum_{c=1}^{3} \overline{\psi}^{\,c} \, \psi^c. \tag{1.44}$$

It is possible to generalize the theory and implement a global symmetry $SU(N)$. At that purpose we let the color index runs from 1 to $N$. This means that $\psi(x)$ belongs to a vectorial space $V_x$ isomorph to $\mathbb{C}^N$.

The action is then invariant under a global transformation of the from:

$$\psi(x) \to \psi'(x) = \Lambda^{-1}\psi(x), \qquad \Lambda \in SU(N)\ . \tag{1.45}$$

A gauge theory needs the implementation of a local symmetry, requiring that the action fulfills a larger class of transformations:

$$\begin{aligned} \psi'(x) &= \Lambda^{-1}(x)\,\psi(x), \\ \overline{\psi}\,'(x) &= \psi(x)\,\Lambda(x), \end{aligned} \qquad \Lambda \in SU(N) \tag{1.46}$$

where $\Lambda(x)$ depends on $x$. In order to promote the global symmetry to a local one, the ordinary derivative must be substituted with a covariant one:

$$\partial_\mu \longrightarrow D_\mu = \partial_\mu + A_\mu(x) \tag{1.47}$$

where $A_\mu$ is the gauge field. It belongs to the algebra $su(N)$ of the gauge group, hence it is an hermitian traceless matrix. $A_\mu$ transforms according to:

$$A'_\mu(x) = \Lambda^{-1}(x)(\partial_\mu + A_\mu(x))\Lambda(x) \tag{1.48}$$

and from (1.48) we obtain the transformation of the covariant derivative:

$$D'_\mu\psi'(x) = \Lambda^{-1}(x)D_\mu\psi(x). \tag{1.49}$$

When we replace $\partial_\mu \to D_\mu$ in (1.43), the action becomes invariant under local gauge transformations:

$$S = \int \mathrm{d}^4x \left[\overline{\psi}(x) \cdot \left(i\not{D} - m\right) \cdot \psi(x)\right] \tag{1.50}$$

Another reason to require this substitution can be found when we evaluate $\psi(x + \mathrm{d}x) - \psi(x)$. The gauge transformation matrix depends on $x$ and the difference between $\Lambda(x + \mathrm{d}x)$ and $\Lambda(x)$ must be taken into account. This is obtained by the introduction of a parallel transporter that maps the vectorial space $V_x$, related to the vector $\psi(x)$ into $V_{x+\mathrm{d}x}$.

Each curve $\mathscr{C}_{yx}$ from $x$ to $y$ can be associated to a $SU(N)$ matrix, that defines a mapping from $V_x$ to $V_y$. This matrix fulfills the following transformation law:

$$U\left(\mathscr{C}_{y,x}\right) \to U'\left(\mathscr{C}_{y,x}\right) = \Lambda^{-1}(y)U\left(\mathscr{C}_{y,x}\right)\Lambda(x) \tag{1.51}$$

under a local gauge transformation given by:

$$\psi(x) \to \psi'(x) = \Lambda^{-1}(x)\psi(x) \tag{1.52}$$

$$\psi(y) \to \psi'(y) = \Lambda^{-1}(y)\psi(y). \tag{1.53}$$

Using the parallel transporter operator $U(\mathscr{C}_{x+\mathrm{d}x,x})$ on a straight path from $x$ to $x + \mathrm{d}x$, covariant differential can be written as:

$$D\psi(x) = \psi(x + \mathrm{d}x) - U\left(\mathscr{C}_{x+\mathrm{d}x,x}\right)\psi(x) \tag{1.54}$$

from which we obtain (1.47). As the path $\mathscr{C}_{x+\mathrm{d}x,x}$ is infinitesimal the operator $U(\mathscr{C}_{x+\mathrm{d}x,x})$ is a matrix close infinitely to the identity:

$$U\left(\mathscr{C}_{x+\mathrm{d}x,x}\right) = \mathbb{1} - A_\mu(x)\mathrm{d}x^\mu. \tag{1.55}$$

From the action (1.50) we observe that the field $A_\mu$ mediates the interactions between the fermionic fields:

$$i\overline{\psi}(x) \cdot A_\mu(x) \cdot \psi(x) \tag{1.56}$$

This field belongs to the $su(N)$ algebra, and can be rewritten as a combination of $N^2 - 1$ generators $T^a$ of the group:

$$\left(A_\mu(x)\right)_{ij} = -ig_s \sum_{a=1}^{N^2-1} A_{\mu,a}(x) T^a_{ij} \tag{1.57}$$

$T^a$ satisfies commutation relations proper to the group:

$$[T^a, T_b] = if_{abc}T_c, \qquad \mathrm{Tr}\left(T^a T_b\right) = \frac{1}{2}\delta_{ab} \tag{1.58}$$

where $f_{abc}$ are the structure constants of the group itself.

The gluon field is identified with the $N^2 - 1$ components of $A_{\mu,a}$. Let us write explicitly the color index in the interaction terms between fermions and the field $A_\mu$ (1.56):

$$g_s \sum_{i,j,a} \overline{\psi}_i(x) A_{\mu,a}(x) T^a_{ij} \psi_j(x) \tag{1.59}$$

where $g_s$ is the coupling constant of the theory.

### 1.2.2 Yang-Mills Action

Let us now discuss the action for the gluon field $A_\mu$. This is a functional of only the gauge fields and is required to be invariant under the transformation (1.48) $S_{\mathrm{YM}}[A] = S_{\mathrm{YM}}[A']$. To construct an action with this property we define the field strength $F_{\mu\nu}$ as the commutator of two covariant derivative:

$$F_{\mu\nu}(x) = [D_\mu, D_\nu] = \partial_\mu A_\nu(x) - \partial_\nu A_\mu(x) + [A_\mu(x), A_\nu(x)] \tag{1.60}$$

From a geometrical point of view this tensor is related to the parallel transport of a vector around and infinitesimal parallelogram $\mathscr{C}_{xx}$ [4]:

$$U\left(\mathscr{C}_{xx}\right) = \mathbb{1} - F_{\mu\nu}(x)\mathrm{d}x^\mu \mathrm{d}y^\nu \tag{1.61}$$

Let us write down the transformation law of $F$:

$$F'_{\mu\nu} = \Lambda^{-1}(x) F_{\mu\nu}(x) \Lambda(x). \tag{1.62}$$

If we explicit the generators $T^a$ of $SU(N)$ we can factorize the strength tensor as:

$$F_{\mu\nu}(x)_{ij} = -ig_s \sum_{a=1}^{N^2-1} F_{\mu\nu,a}(x) T^a_{ij} \tag{1.63}$$

where each component $F_{\mu\nu,a}$ is:

$$F_{\mu\nu,a} = \partial_\mu A_{\nu,a} - \partial_\nu A_{\mu,a} + g_s f_{abc} A^b_\mu A^c_\nu. \tag{1.64}$$

$F_{\mu\nu}$ is used to build up gauge invariant terms in the gluonic part of the Lagrangian. These are quadratic in $A_\mu$ and its derivatives and we consider the Yang-Mills choice:

$$S_{\mathrm{YM}} = -\frac{1}{2g_s^2} \int \mathrm{d}^4x \mathrm{Tr}\left[(F_{\mu\nu})^2\right] = -\frac{1}{4} \int \mathrm{d}^4x (F^a_{\mu\nu})^2. \tag{1.65}$$

If we use the explicit form (1.60) of $F_{\mu\nu}$, it is apparent that $S_{\mathrm{YM}}$ contains a kinetic term quadratic in the derivatives $(\partial A)$ plus a quartic and cubic terms that account for the autointeraction of $A_\mu$.

We already stated that a non abelian gauge theory could be considered without any matter field being described only by the action (1.65). In that case it is called *pure*. In this work we focus on Yang-Mills theory, when quarks are threated as external static sources.

Once the action (1.65) has been introduced it is possible to define the quantum expectation value for physical observables using the functional integral. As we stated in the previous Chapter, these live in an Euclidean spacetime.

The observables must be a function of the gauge potential $O(A_\mu(x))$ and must be invariant under $SU(N)$ transformation. The expectation value is:

$$\langle O \rangle = \frac{1}{Z} \int D\left[A_\mu\right] O\left(A_\mu\right) \exp\left(-S\left[A_\mu\right]\right) \tag{1.66}$$

where $Z$ is the partition function of the theory

$$Z = \int D\left[A_\mu\right] \exp\left(-S\left[A_\mu\right]\right) \ . \tag{1.67}$$

Eq.(1.66) represents a mean over field configurations with a measure proportional to $\exp\left(-S\left[A_\mu\right]\right)$.

### 1.2.3 Lattice Formulation

We want to define the gauge theory, outlined in the previous Section, on a lattice. As we already discussed in Section 1.1, this implies a discretization of spacetime, that now consists of lattice points, called *sites*, connected by

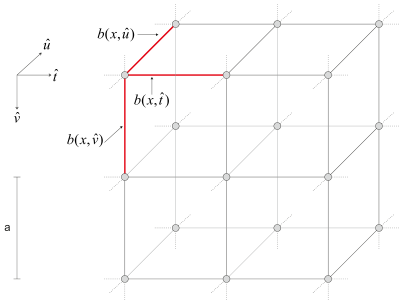


Figure 1.2: *Notation for links in a* 3*–dimensional cubic lattice.*

*links*, as it is shown in Fig.1.2. In fact, local gauge transformation are now defined on the site $x$ of the lattice:

$$\psi(x) \to \psi'(x) = \Lambda^{-1}(x)\psi(x) \ . \tag{1.68}$$

In order to make gauge invariant the product of nearest-neighbors matter fields, we need the smallest parallel transporters, that exist on a lattice. The corresponding paths are called links.

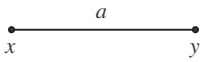


Figure 1.3: *Link b between lattice points x and y*

The gauge field $A_\mu$ introduced in the previous Section, is obtained from the infinitesimal parallel transporter (1.55). Then when we are on the lattice it replaces the gauge field $A^a_\mu(x)$.

$$A_\mu \longrightarrow U(b) \in G \tag{1.69}$$

with each link $b = \langle x + a\hat{\mu}, x\rangle$ and $G$ representing the gauge group of the theory. The link variables transform as

$$U(x,y) \longrightarrow \Lambda(x)U(x,y)\Lambda^{-1}(y) \tag{1.70}$$

In order to describe the dynamics of the link variables, we need a discretized version of the Yang-Mills action (1.65). Therefore we need to find a candidate for the tensor $F_{\mu\nu}$ on the lattice, where the smallest closed path $\square$ is represented by a square of side $a$ delimited by 4 links. The parallel transporter around such elementary loop is the plaquette variable, namely the product of link variable around it:

$$\begin{aligned} P_x = U(b(x+\hat{\mu}a, x))U(b(x+\hat{\mu}a+\hat{\nu}a, x+\hat{\mu}a))\cdot \\ \cdot U(b(x+\hat{\nu}a, x+\hat{\mu}a+\hat{\nu}a))U(b(x, x+\hat{\nu}a)). \end{aligned} \tag{1.71}$$

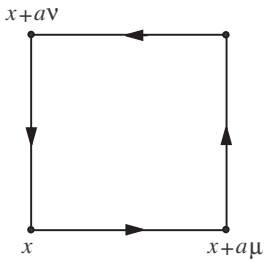


Figure 1.4: *A plaquette p lying on the plane* $\mu - \nu$

In Fig. 1.4 it is displayed a plaquette located at the four vertices $x, x + \hat{\mu}a, x + \hat{\mu}a + \hat{\nu}a$ e $x + \hat{\nu}a$.

Plaquette is the main component of the action proposed by Wilson [5] for lattice gauge theory. It is defined as:

$$S[U] = \beta \sum_{\square} \left[1 - \frac{1}{N} \mathrm{Re}\,\mathrm{Tr}\, P_x\right] \tag{1.72}$$

for $SU(N)$ as the gauge group. Sum is meant over all lattice plaquette with just one orientation. Action (1.72) is gauge invariant, as it depends only on $\mathrm{Tr}\, P_x$. Under a gauge transformation (1.70), the cyclic property of trace ensures that:

$$\mathrm{Tr}\, P'_x = \mathrm{Tr}\, P_x \tag{1.73}$$

that finally makes $S$ gauge-invariant.

If we write down the dependence of the link variable from $A_\mu(x)$ we obtain:

$$U(b(x + \hat{\mu}a, x)) \equiv e^{-aA_\mu(x)} \ . \tag{1.74}$$

When we substitute this expression in the action (1.72) the result is [4]:

$$S = -\frac{\beta}{4N} \sum_x a^4 \mathrm{Tr}\, F_{\mu\nu}(x) F^{\mu\nu}(x) + \mathscr{O}\left(a^5\right) \tag{1.75}$$

This ensures that $S$ coincides with the Yang-Mills action when $a \to 0$ by identifying

$$\beta = \frac{2N}{g_s^2}. \tag{1.76}$$

Hence we found that Wilson action is a discretized version of (1.65).

For the quantum theory we have to specify how to do functional integrals. The integral over all gauge field configurations on the lattice amounts to an integral over all link variables $U(b)$. So, for the expectation value of any

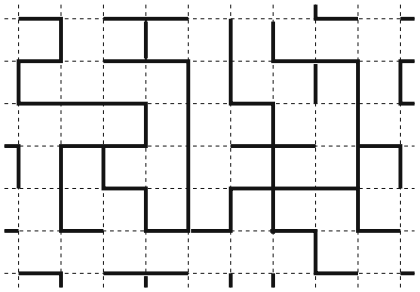

Figure 1.5: *Representation of a maximal tree on a $2D$ sub-lattice. The fat lines represent link variables that are set to $\mathbb{1}$ and omitted in the integration.*

observable $A$ we write

$$\langle A \rangle = \frac{1}{Z} \int \prod_b dU(b)\ A\ e^{-S_W}, \tag{1.77}$$

where the Haar measure $dU(b)$ for a given link $b$ is the invariant integration over the group manifold (e.g. a 3-sphere for $SU(2)$), normalized to

$$\int dU = 1. \tag{1.78}$$

As a shorthand, we shall write

$$\mathcal{D}U \equiv \prod_b dU(b). \tag{1.79}$$

It is worth noticing here that no gauge fixing appears to be necessary. The total "volume of the gauge group" is unity.

### 1.2.4 Gauge Invariance and Gauge Fixing

In this Section we discuss in more detail the freedom of choosing a gauge and address the different roles of gauge fixing in the continuum and on the lattice. We argue that physical observables have to be gauge-invariant. We stress that all the gauge properties discussed here for pure gauge theory can be taken over to the full theory with fermions.

Let us begin our discussion of gauge fixing with a kind of gauge that is particular for the lattice. We show that in a certain set of link variables, a so-called maximal tree, the link variables can be set to the identity element $\mathbb{1}$ and left out in the integration of the gauge field. We start with an arbitrary configuration of link variables $U_\mu(x)$. In the beginning of our construction all gauge transformation matrices $\Lambda(x)$ are set to the identity $\mathbb{1}$. We pick a single-link variable $U_{\mu_0}(x_0)$ and set the transformation matrix $\Lambda(x_0 + \hat{\mu_0})$

at the endpoint of the link to the value $U_{\mu_0}(x_0)$, keeping all other $\Lambda(x)$ at $\mathbb{1}$. The link $U_{\mu_0}(x_0)$ thus is transformed to

$$U_{\mu_0}(x_0)' = \Lambda(x_0)\, U_{\mu_0}(x_0)\, \Lambda(x_0+\hat{\mu}_0)^\dagger = \mathbb{1}\, U_{\mu_0}(x_0)\, U_{\mu_0}(x_0)^\dagger = \mathbb{1} \quad (1.80)$$

The transformation with the nontrivial $\Lambda(x_0+\hat{\mu_0})$ will also affect all link variables starting at the site $x_0+\hat{\mu_0}$, in particular

$$U_{\mu_1}(x_0+\hat{\mu}_0)' = \Lambda(x_0+\hat{\mu}_0)\, U_{\mu_1}(x_0+\hat{\mu}_0) \quad (1.81)$$

For these transformed links we can repeat the step of (1.80) and choose the matrices $\Lambda$ at their endpoints such that also these links are transformed to the identity $\mathbb{1}$. The whole procedure can be repeated until we hit a link $U_{\mu^*}(x^*)$ which connects to another link that already has been transformed to $\mathbb{1}$ before. If we wanted to transform also this particular link, according to (1.81) we would transform the other link, which is already at $\mathbb{1}$, away from the identity. This restricts the set of links that can be transformed to $\mathbb{1}$ to a cluster of links which does not contain closed loops. Let us now discuss the consequences of the freedom to fix the gauge on a maximal tree (or a subset of it). We consider the vacuum expectation value of some gauge-invariant observable $O$. Gauge invariance of $O$ implies

$$O[U'] = O[U]\ . \quad (1.82)$$

Also the action and the measure are gauge-invariant, i.e.,

$$S_{\mathrm{YM}}[U'] = S_{\mathrm{YM}}[U] \quad (1.83)$$

$$\int \mathcal{D}[U'] = \int \mathcal{D}[U] \quad (1.84)$$

These equations imply that the whole integrand and measure are unchanged when setting the links in a maximal tree to $\mathbb{1}$. Since the construction of a maximal tree works for any particular choice of link variables, we can keep the links in the maximal tree at $\mathbb{1}$ throughout the whole integration $\int \mathcal{D}[U]$. Since the Haar measure is normalized to 1 the links in the maximal tree can be omitted in the integration altogether.

Thus, we can summarize the procedure of fixing the gauge to a maximal tree as follows. Select a maximal tree, or a smaller set of links without closed loops, and set the links in this set to $\mathbb{1}$. Subsequently, integrate over all link variables that are not contained in the chosen set. The expectation value of a gauge-invariant observable is unaffected, whether we fix the gauge or not.

The role of gauge fixing on the lattice is very different from the role it plays in the continuum. Fixing the gauge on the lattice is a step which we can implement to simplify some calculations or to make the interpretation of observables more transparent (see the discussion of the Wilson loop below). However, fixing the gauge is not a necessary step to make vacuum expectation values of operators well defined and computable.

There is a certain gauge, the so-called *temporal gauge*, which has a corresponding counterpart in the continuum. On a lattice with infinite temporal extent we can set all time-like links to $\mathbb{1}$, i.e., we can set

$$U_4(x) = \mathbb{1} \quad \forall x \ . \tag{1.85}$$

We remark that this is not a maximal tree but a smaller set. In the (Euclidean) continuum theory the temporal gauge is defined by $A_4(x) = 0$, which matches the lattice definition due to the relation $U_4 = \exp(iaA_4)$. We will make use of the temporal gauge when we introduce and discuss the Wilson loop.

## 1.3 Quarks in Yang-Mills Theory

In this Section we present the observables that allow one to determine the potential between two static color sources. These observables are the so-called Wilson and Polyakov loops which we first introduce and only later give their interpretation.

### 1.3.1 The Wilson Loop

We already stated that that physical observables have to be gauge-invariant. A prototype of a gauge-invariant object, made from only the gauge fields, is the trace of a product of link variables along a closed loop :

$$L[U] = \ \mathrm{tr} \left[ \prod_{(x,\mu)\in\mathfrak{L}} U_\mu(x) \right] \tag{1.86}$$

Here $\mathfrak{L}$ is a closed loop of links on the lattice and the product in (1.86) runs over all these links. The Wilson loop which we introduce now is of that type. A Wilson loop $W_\mathfrak{L}$ is made from four pieces, two so-called *Wilson lines* $S(\mathbf{m},\mathbf{n},n_t)$, $S(\mathbf{m},\mathbf{n},0)$ and two temporal transporters $T(\mathbf{n},n_t)$, $T(\mathbf{m},n_t)$. The Wilson line $S(\mathbf{m},\mathbf{n},n_t)$ connects the two spatial points $\mathbf{m}$ and $\mathbf{n}$ along some path $\mathcal{C}_{\mathbf{m},\mathbf{n}}$ with all link variables restricted to time argument $n_t$ :

$$S(\mathbf{m},\mathbf{n},n_t) = \prod_{(\mathbf{k},j)\in\mathcal{C}_{\mathbf{m},\mathbf{n}}} U_j(\mathbf{k},n_t) \tag{1.87}$$

The temporal transporter $T(\mathbf{n},n_t)$ is a straight line of $n_t$ link variables in time direction, all situated at spatial position $\mathbf{n}$ :

$$T(\mathbf{n},n_t) = \prod_{j=0}^{n_t-1} U_4(\mathbf{n},j) \tag{1.88}$$

Attaching the four pieces to each other gives a closed loop $\mathfrak{L}$:

$$\mathfrak{L}: \quad (\mathbf{m}, n_t) \xrightarrow{S} (\mathbf{n}, n_t) \xrightarrow{T^\dagger} (\mathbf{n}, 0) \xrightarrow{S^\dagger} (\mathbf{m}, 0) \xrightarrow{T} (\mathbf{m}, n_t) \tag{1.89}$$

The Wilson loop $W_\mathfrak{L}$ is obtained by taking the trace,

$$W_\mathfrak{L}[U] = \text{tr}\left[S(\mathbf{m}, \mathbf{n}, n_t) T(\mathbf{n}, n_t)^\dagger S(\mathbf{m}, \mathbf{n}, 0)^\dagger T(\mathbf{m}, n_t)\right] \tag{1.90}$$

If the piece of loop $\mathcal{C}_{\mathbf{m},\mathbf{n}}$ used in $S(\mathbf{m}, \mathbf{n}, n_t)$ is a straight line we speak of a planar Wilson loop. Note that this can be the case only if $\mathbf{m}$ and $\mathbf{n}$ fall on a common coordinate axis. Otherwise the Wilson loop is called nonplanar.

### 1.3.2 Physical Interpretation of the Wilson Loop

In the temporal gauge (1.85), discussed in Section 1.2.4, the temporal transporters become trivial,

$$T(\mathbf{n}, n_t) = \prod_{j=0}^{n_t - 1} U_4(\mathbf{n}, j) = \mathbb{1} \tag{1.91}$$

and we obtain the following chain of identities

$$\langle W_\mathfrak{L} \rangle = \langle W_\mathfrak{L} \rangle_{\text{temp}} = \left\langle \text{tr}\left[S(\mathbf{m}, \mathbf{n}, n_t) S(\mathbf{m}, \mathbf{n}, 0)^\dagger\right] \right\rangle_{\text{temp}} \tag{1.92}$$

where in the first step we have used the fact that the expectation value of a gauge-invariant observable remains unchanged when fixing the gauge. The temporal gauge used in (1.92) makes explicit that the Wilson loop is the correlator of two Wilson lines $S(\mathbf{m}, \mathbf{n}, n_t)$ and $S(\mathbf{m}, \mathbf{n}, 0)$ situated at time slices $n_t$ and 0. The correlator behaves for large total temporal extent $T$ of the Euclidean lattice as (a, b are summed);

$$\left\langle \text{tr}\left[S(\mathbf{m}, \mathbf{n}, n_t) S(\mathbf{m}, \mathbf{n}, 0)^\dagger\right] \right\rangle_{\text{temp}} = \sum_k \langle 0 | \widehat{S}(\mathbf{m}, \mathbf{n})_{ab} | k \rangle \langle k | \widehat{S}(\mathbf{m}, \mathbf{n})^\dagger_{ba} | 0 \rangle e^{-tE_k} \tag{1.93}$$

where the Euclidean time argument $t$ is related to $n_t$ via $t = a n_t$ with $a$ being the lattice spacing. The sum in (1.93) runs over all states $|k\rangle$ that have a nonvanishing overlap with $S(\mathbf{m}, \mathbf{n})^\dagger |0\rangle$. In the next paragraph we will argue that the states $|k\rangle$ with nonvanishing overlap are states describing a static quark–antiquark pair located at spatial positions $\mathbf{m}$ and $\mathbf{n}$. Thus in (1.93) the term with the lowest energy $E_1$ is expected to be the state describing our static quark–antiquark pair. Higher states could be, e.g., this pair plus additional particle–antiparticle combinations with the quantum numbers of the vacuum. The energy $E_1$ is thus identified with the energy of

the quark–antiquark pair, that is the static potential $V(r)$ at spatial quark separation $r$,

$$E_1 = V(r) \quad \text{with} \quad r = a|\mathbf{m} - \mathbf{n}| \ . \tag{1.94}$$

Combining (1.91), (1.93) and (1.94) we obtain

$$\langle W_{\mathfrak{L}} \rangle \propto e^{-tV(r)}(1 + \mathcal{O}(e^{-t\Delta E})) = e^{-an_t V(r)}(1 + \mathcal{O}(e^{-an_t \Delta E})) \ . \tag{1.95}$$

Thus we find that we can calculate the static quark–antiquark potential from the large $n_t$ behavior of the Wilson loop. The corrections in (1.95) are exponentially suppressed, where $\Delta E$ is the difference between $V(r)$ and the first excited energy level of the quark–antiquark pair.

### 1.3.3 Wilson Line and the Quark–Antiquark Pair

To complete our physical interpretation of the Wilson loop we still need to show that the states $S(\mathbf{m}, \mathbf{n})^\dagger |0\rangle$ do indeed have overlap with a quark–antiquark pair. However we will just show that $S(\mathbf{m}, \mathbf{n})$ has the same transformation properties as a quark–antiquark pair under a gauge transformation. According to our discussion in Section 1.2, a quark–antiquark pair at spatial positions $a\mathbf{m}$, $a\mathbf{n}$ is described by a product of fields

$$Q(\mathbf{m}, \mathbf{n}) \equiv \psi(\mathbf{m})^a_\alpha \, \overline{\psi}(\mathbf{n})^b_\beta \tag{1.96}$$

The quark fields carry spinor $(\alpha, \beta)$ and color $(a, b)$ indices. However, here we are not interested in the dependence of the potential on the spinor indices, and we ignore them in the definition of $Q(\mathbf{m}, \mathbf{n})_{ab}$. $Q(\mathbf{m}, \mathbf{n})_{ab}$ is not gauge-invariant. According to (1.46), it transforms under gauge transformations as

$$Q(\mathbf{m}, \mathbf{n})_{ab} \to \Lambda(\mathbf{m}) Q(\mathbf{m}, \mathbf{n})_{a'b'} \Lambda^\dagger(\mathbf{n}) \tag{1.97}$$

From the discussion following the gauge transformation properties of link variables (1.51), we know that the products of link variables, transform exactly as required:

$$S(\mathbf{m}, \mathbf{n})_{ab} \to \Lambda(\mathbf{m}) S(\mathbf{m}, \mathbf{n})_{a'b'} \Lambda^\dagger(\mathbf{n}) \tag{1.98}$$

Thus we have at least verified that the Wilson line has the same transformation properties as the quark–antiquark pair.

### 1.3.4 Polyakov Loop

Let us conclude this Section with discussing a modification of the Wilson loop, the so-called Polyakov loop [6] (also called thermal Wilson line). Here we work with boundary conditions for the gauge fields that are periodic in the time direction. We make the temporal extent $n_t$ of the Wilson loop as large as possible on our lattice, i.e., we set $n_t = N_T$ , where $N_T$ is the total

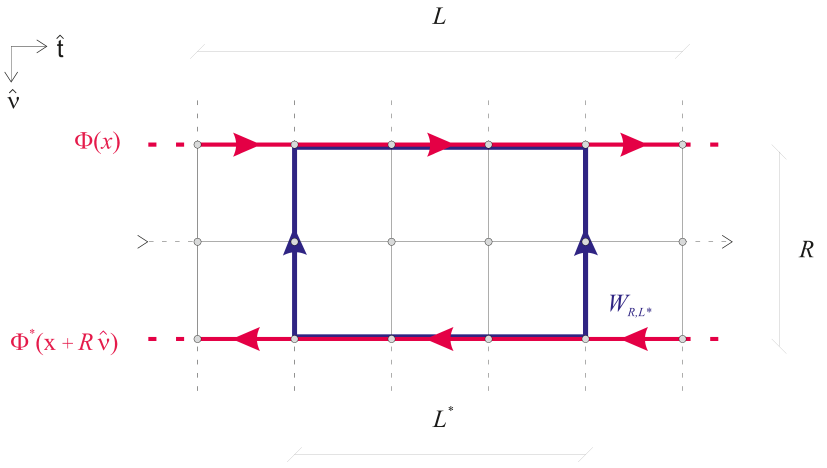


Figure 1.6: *A representation in a bi–dimensional lattice of a Wilson loop* $W_{R,L^*}$ *(blue) and a pair of Polyakov loops* $\Phi(x)$ *and* $\Phi^*(x + R\hat{\nu})$ *(red).*

number of lattice points in time direction. Then the spatial pieces of the Wilson loop sit on top of each other but are oriented in opposite direction. Due to the periodic boundary conditions we cannot gauge-transform all temporal links to $\mathbb{1}$. We can, however, gauge the spatial pieces of our loop to $\mathbb{1}$. Then the Wilson loop reduces to the two disconnected paths (compare (1.88)) $T(\mathbf{m}, N_T)$, $T(\mathbf{n}, N_T)^\dagger$ of temporal link variables, located in space at the two positions $\mathbf{m}$ and $\mathbf{n}$. Both these paths wind around the temporal direction of the lattice but have opposite orientations. We can make this new observable gauge-invariant by taking the trace for each of the two loops individually. This is simply a rearrangement of the color indexes and leaves the interpretation of the observable the same. In this way we introduce the so-called Polyakov loop

$$\Phi(\mathbf{m}) = \mathrm{tr}\left[\prod_{j=0}^{N_t-1} U_4(\mathbf{m}, j)\right] . \tag{1.99}$$

Being a trace over a closed loop, this quantity appears to be gauge-invariant. We now can abandon our special gauge and obtain ($r = a|\mathbf{m} - \mathbf{n}|$):

$$\langle \Phi(\mathbf{m})\, \Phi(\mathbf{n})^\dagger \rangle \propto e^{-aN_T V(r)}(1 + \mathcal{O}(e^{-aN_T \Delta E})) \tag{1.100}$$

In Chapter 4 we will present a numerical evaluation of the static potential that is based on the correlator of two Polyakov loops.

## 1.4 The Static Quark Potential

Having introduced the Wilson loop as an observable for the static quark potential $V(r)$, we now discuss the general form of $V(r)$. The observables

of the theory, when considering the limit $\beta \to 0$, can be written as power series in $\beta$ [4, 7], with a finite convergence radius. This procedure is the analogous of the high temperature expansion of statistical mechanics and it takes the name of *strong coupling expansion*. It is of relevant interest the result obtained with this tool for the static quark potential. Two sources at distance $R$ are confined if the interact through a potential that is rising with $R$. Within the context of pure gauge theory we can characterize this potential if we consider a rectangular Wilson loop $W_{\mathscr{C}_{R,L}}$. For large $L$ it behaves like:

$$W_{\mathscr{C}_{R,L}} \sim C\mathrm{e}^{-LV(R)}, \qquad L \to \infty \tag{1.101}$$

Using the strong coupling expansion, it is possible to derive the behavior of large Wilson loop [5, 4, 8]. As an example, if we consider the gauge group $SU(2)$:

$$W_{\mathscr{C}_{R,L}} \simeq 2\exp(-\ln(u)RL)\left[1 + 4u^4 RL\right] \tag{1.102}$$

using the expansion parameter $u = \beta/4 + \beta^3/96 + \mathcal{O}(\beta^5)$. From (1.102) on can see the so called *area law*:

$$W_{\mathscr{C}_{R,L}} \sim C\mathrm{e}^{-\sigma RL}, \qquad R, L \to \infty \tag{1.103}$$

The static quark potential can then be extracted using (1.95):

$$V(R) \sim \sigma R, \qquad R \to \infty \tag{1.104}$$

where the linear rising behavior of $V(R)$ is manifest. The theory is then confining within the limit $\beta \to 0$. An important parameter is the *string tension*:

$$\sigma \equiv \lim_{R\to\infty} \frac{1}{R} V(R) = -\lim_{R,L\to\infty} \frac{1}{RL} \ln W(\mathscr{C}_{R,L}) \tag{1.105}$$

that represent the limiting attractive force between the two sources. Numerical results [9] have proven that the area law (1.103) is the dominant part of a Wilson loop even outside the strong coupling regime.

Let us briefly sketch the physical implications of the static QCD potential, in particular the role of the linear term. The linearly rising term in the potential between a static quark–antiquark pair implies that the energy keeps rising linearly as one tries to pull the two constituents apart. Thus the quark and the antiquark are confined in a strongly bound meson state. The physical mechanism that leads to the linearly rising term is the formation of a flux tube between the two sources.

Direct experimental evidence for the linearly rising potential is seen when the mass of hadrons is plotted as a function of their total spin and a linear behavior is found. Since for a linearly rising potential the energy rises linearly with the angular momentum, this experimental finding confirms the linear term. In the next Chapter we will present an effective string model for describing the infrared feature of the flux tube generated by the quark–antiquark pair.

## 1.5 The Continuum Limit

Lattice actions may differ in various aspects. They may use different discretization of derivatives or the lattice grid, which is usually taken to be hypercubic, may vary in its structure. However, when removing the lattice cutoff, i.e., in the limit $a \to 0$, physical observables should agree with the experimental value and become independent of $a$. In general this will imply that the bare parameters have a nontrivial dependence on the cutoff a, meaning that they are functions $g(a)$, $m(a)$, etc. As we send $a \to 0$ the values of the bare parameters will have to be changed in order to keep physics constant.

If we consider a mass $m$ as a physical observable, this should be of the form:

$$m = \hat{m}(g_s)/a \tag{1.106}$$

where $\hat{m}(g_s)$ is a dimensionless function of $g_s$. In order to approach the continuum limit, we have to vary $g_0$ such that when $a \to 0$ the observable $m$ remains fixed. That is to say, it is necessary to found a critical value $g_s^*$ such that:

$$\lim_{g_s \to g_s^*} \hat{m}(g_s) = 0 \tag{1.107}$$

The mass $\hat{m}$ can be also seen as the inverse of a correlation length $\hat{\xi} = 1/\hat{m}$ that in contrast diverges in the continuum limit. This is a sign of a phase transition, a critical point of the statistical system. This can be interpreted in a meaningful physical way: if we want the lattice results to be valid in the continuum physics, we have to require that the system looses memory of the underlining lattice structure: indeed this happens when the correlation length of the system diverges.

This running of the bare parameters is addressed by the so-called renormalization group. Considering the lattice spacing a as the inverse of our energy scale, we write

$$-\frac{\mathrm{d}g}{\mathrm{d}a} = \beta(g) \ . \tag{1.108}$$

The $\beta$–function may be expanded in a power series around $g = 0$, with coefficients determined by perturbation theory. For $SU(N)$ pure gauge theory the result reads

$$\begin{aligned} \beta(g) &= -\beta_0 g^3 - \beta_1 g^5 + \mathcal{O}(g^7) \\ \beta_0 &= \frac{1}{(4\pi)^2}\frac{11}{3}N \\ \beta_1 &= \frac{1}{(4\pi)^4}\frac{34}{3}N^2 \end{aligned} \tag{1.109}$$

These first two coefficients of the expansion are universal, independent of the regularization scheme. The differential equation (1.108) with (1.109)

can be solved, using separation of variables, and one obtains

$$a(g) = \frac{1}{\Lambda_L} \left(\beta_0 g^2\right)^{-\frac{\beta_1}{2\beta_0^2}} \exp\left(-\frac{1}{2\beta_0 g^2}\right) \left(1 + \mathscr{O}\left(g^2\right)\right) \tag{1.110}$$

The integration constant $\Lambda_L$ is used to set the scale by fixing the value of $g$ at some $a$. This is peculiar because the pure gauge theory in $d = 4$ has no dimensional parameters. This phenomenon is associated with dimensional transmutation and it is a pure quantum effect.

Inverting the relation (1.110) one obtains the coupling $g$ as a function of the scale $a$, the so-called running coupling,

$$g(a)^{-2} = \beta_0 \ln(a^{-2}\Lambda_L^{-2}) + \frac{\beta_1}{\beta_0} \ln(\ln\left(a^{-2}\Lambda_L^{-2}\right)) + \mathcal{O}(1/\ln\left(a^{-2}\Lambda_L^{-2}\right)) \tag{1.111}$$

Vanishing lattice spacing corresponds to vanishing coupling $g$. This behavior is called *asymptotic freedom*.

However in our study we consider $d = 3$ Yang-Mills theory, where the gauge coupling $g^2$ has dimension of $[M]$. A mass scale is then already present in the classical theory. This means that the dimensionless parameter $\beta$ in the Wilson action has the form:

$$\beta \equiv \frac{2N}{g_{s,3}^2 a} \tag{1.112}$$

This feature determines a behavior similar to the asymptotic freedom of the theory in $d = 4$. In fact from (1.112), we obtain that in order to approach the continuum limit $a \to 0$ we have to send $\beta \to \infty$.

We have shown in (1.110) and (1.112) that the lattice spacing $a$ decreases with decreasing $g$. Hence we conclude that we have to study the limit where the parameter $\beta$ of the Wilson action:

$$\beta \to \infty \tag{1.113}$$

If one performs such a limit, then the physical volume of the box is proportional to $a^4$ and thus shrinks to zero, unless we also increase the numbers of lattice points in the spatial ($N$ points) and temporal ($N_T$ points) directions of our lattice. One would first perform the so-called thermodynamic limit

$$N \to \infty\,, \quad N_T \to \infty\,, \tag{1.114}$$

and only after that step the continuum limit (1.113) would be taken. However, since in a numerical calculation this is not possible, one is reduced to calculate the physical observables for a few values of $\beta$, giving rise to different values of $a$. The numbers of lattice points $N$, $N_T$ are always chosen such that the physical extension

$$L = a\,N\,, \quad T = a\,N_T \tag{1.115}$$

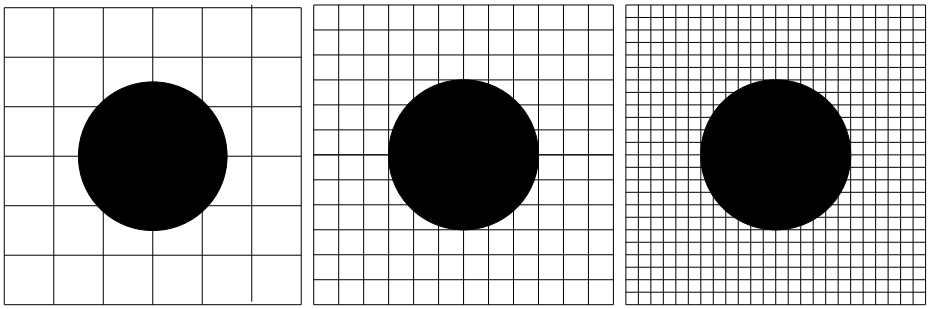

Figure 1.7: *2-dimensional lattices with finer lattice spacing a*

of the box remains fixed for the different values of $a$. Studying the a–dependence of the results at fixed physical volume allows one to analyze the dependence on the scale $a$ and to extrapolate the results to $a \to 0$. The extrapolation to $a = 0$ can then be repeated for different physical sizes $L$, $T$ which in the end allows one to extrapolate the data to infinite physical volume.

# Chapter 2

# Effective String Theory

Lattice gauge theory is a powerful tool that enables us to study the confinement phenomenon which arises between two static color charges. One interesting problem in that context is the construction of an effective string theory that describes the infrared behavior of that system. In fact, starting from the studies on confinement dynamics in Yang-Mills theory, it has been argued that the interaction between two static color charges can be described with a theoretical string model.

In the following we outline the main features of this effective theory, starting from the chromo-electric flux tube. Then we describe the quantitative predictions that follows from this description.

## 2.1 Chromo-electric flux tubes

In the Yang-Mills Theory the gluons are the only dynamical degrees of freedom. The quarks are infinitely massive and they enter the theory as external color sources. Interaction between two static charges in Yang-Mills theory is established by the exchange of gluons, described by the dynamics of the field $A_\mu$, introduced in Section 1.2.1. Similarly to what happens in electrodynamics, we can associate chromo-electric and chromo-magnetic vector fields to the derivatives of the gluonic potential $A_\mu$. How this field is distributed is a peculiar feature of confinement.

Energy density of chromo-electric field is very different from the one that arises between two electric charges. The linear shape of the static quark potential (1.104) suggests that the gluonic field is mainly concentrated in a tubular region called *flux tube* which links the two sources.

Outside this region the energy density of chromo-electric field is highly suppressed, unlike the dipole generated field in electrodynamics.

### 2.1.1 Flux Tube's Width

Now we would like to focus on the structure of the flux tube. The energy density of the chromo-electric field can be expressed by the connected correlation function [10]:

$$\rho(x) \propto \langle q\bar{q}| \operatorname{Tr} E^2(x) |q\bar{q}\rangle - \langle q\bar{q}|q\bar{q}\rangle \langle \operatorname{Tr} E^2(x)\rangle \tag{2.1}$$

where $|q\bar{q}\rangle$ is the ground state of a quark-antiquark pair. When we regularize the theory on a lattice this equation becomes:

$$\rho(x) \propto \frac{\langle W_{\mathscr{C}}\, P_x\rangle - \langle W_{\mathscr{C}}\rangle \langle P_x\rangle}{\langle W_{\mathscr{C}}\rangle} \tag{2.2}$$

where $W_{\mathscr{C}}$ is the Wilson of Eq. (1.90) on a rectangular path and $P_x$ is the plaquette defined in (1.71) localized in $x$ coplanar to $\mathscr{C}$. At finite temperature, we can consider a pair of Polyakov loops, defined in Eq. (1.99). The lattice operator then becomes:

$$\rho(x) \propto \frac{\langle \Phi_0^*\, \Phi_R\, P_x\rangle - \langle \Phi_0^*\, \Phi_R\rangle \langle P_x\rangle}{\langle \Phi_0^*\, \Phi_R\rangle} \tag{2.3}$$

where $\Phi_0$ and $\Phi_R$ are two Polyakov loops separated by $R$ lattice spacing and again $P_x$ is a plaquette localized in $x$. Within this setting the flux depends on the spatial coordinates of the plaquette, on its orientation, on the separation $R$ between the Polyakov loops and on the length $L$ of the lattice in the temporal direction. It does not depend on the temporal coordinate of the plaquette. Different possible orientations of the plaquette measure different components of the flux.

The width of the flux tube is defined as the second moment of the probability distribution $\rho(x)$ [10]:

$$w^2 = w^2(R/2) = \frac{\int \mathrm{d}^2 x_\perp x_\perp^2 \rho(x)}{\int \mathrm{d}^2 x_\perp \rho(x)} \tag{2.4}$$

where $x_\perp$ parametrizes the transverse displacement with respect to the line connecting the two quarks and the flux tube width is evaluated in the symmetry point $R/2$ of the domain. This gives us with a reasonable estimate of the width of the distribution $\rho$.

In general, the width $w^2$ can be a function of the interquark distance $R$. From the flux tube picture we expect $w^2$ to grow much slower than $R^2$ as $R \to \infty$ [10]. Within the framework of Yang-Mills $SU(2)$ gauge theory described by the Wilson action (1.72) in $d = 4$, we can verify this assumption using the strong coupling expansion of $w^2$ in the limit $R \to \infty$ [10]:

$$w_\infty^2 = 4\left\{u^4 + 2u^6 + \frac{92}{3}u^8 + \dots\right\} \tag{2.5}$$

where $u = \frac{\beta}{4} + \mathcal{O}(\beta^3)$ and $\beta$ is the coupling constant appearing in Wilson action. At small $\beta$, the strong coupling expansion is convergent and the width of flux tube is not only growing slower than $R^2$, but approaches a constant.

### 2.1.2 "Roughening" Transition

In the strong coupling regime, the width of the flux tube tends to a constant value when the distance between the two sources becomes large. Now we want to know if this behavior still holds at weak coupling.

If $w_\infty^2$ is finite in this regime, we expect that $(\sigma\, w_\infty^2)$, extrapolates smoothly with $\beta$, where $\sigma$ is the string tension defined in (1.105). Using the strong coupling series for $\sigma$ obtained in [11] we get [10]:

$$\left(\sigma\, w_\infty^2\right)^{-1} = \frac{-1}{4u^4 \ln u}\left\{1 - 2u^2 - 4u^4\left(\frac{20}{3} + \frac{1}{\ln u}\right) + 4u^6\left(\frac{2179}{475} + \frac{2}{\ln u}\right) - u^8\left(\frac{244903}{1215} - \frac{48}{\ln u} - \frac{16}{(\ln u)^2}\right) + \ldots\right\} \quad (2.6)$$

So rather than approaching a constant $\left(\sigma\, w_\infty^2\right)^{-1}$ seems to vanish at about

$$\beta_r \simeq 1.9 \quad (2.7)$$

If we found that $\beta_r$ still resides in the region where strong coupling expansion makes sense, (2.7) gives us a hint that the limiting width $w_\infty^2$ diverges for values of $\beta$ greater than $\beta_r$.

Numerical simulation [12] for $SU(2)$ in $d = 4$ showed that the changeover from the strong-coupling behavior to the weak-coupling occurs rather sharply over a range of about 10% in $\beta \gtrsim 2$. This transition is quite fast: analytic results in strong coupling regime are in good agreement with numerical estimates also for $\beta$ near to 2. We could argue that strong coupling expansion is reasonable for $\beta \lesssim \beta_r$.

These arguments enable us to interpret (2.7) as a key point in asserting that for $\beta > \beta_r$ the width of the flux tube grows indefinitely with the distance $R$ between quarks. This behavior has been named "flux tube delocalization". Then $\beta_r$ reveals a discontinuity in the physics of the system that is called *roughening transition*.

In conclusion, the confining regime of a gauge theory consists in two regions separated by the value $g_r = \sqrt{2N/\beta_r}$ of the coupling constant, where the strong coupling expansion ceases to converge[10, 13].

## 2.2 Effective Theory

An effective theory describing the infrared behavior of the confining dynamics of two static quarks was proposed by Luscher, Symanzik and Weisz

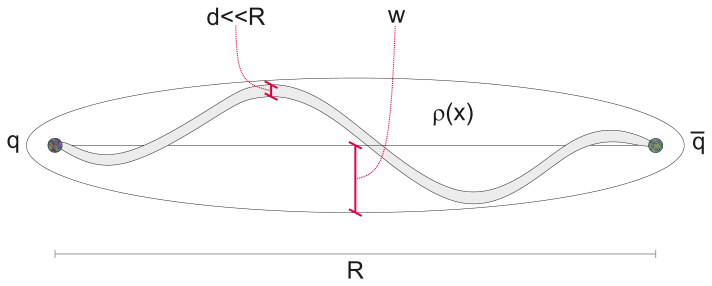


Figure 2.1: *Fluctuating string between two sources at a distance R. Oscillations' amplitudes determine the width w of the distribution ρ(x) of the chromo-electric field. In order for this description to hold the width d of the string has to be negligible compared to the length R.*

in 1980 [14, 15]. This proposal emerged from both analytical results obtained in Yang-Mills theory and experimental evidence of Regge trajectories in mesonic spectroscopy [16, 3].

The idea consists in the effective description of the flux tube as a vibrating string that connects the two sources. This string is assumed to be thin (Figure 2.1), that is to say that we get rid of any internal structure of the flux tube and any dependence on the gauge symmetry group is gone.

In that picture the potential is generated by the dynamics of such string and its quantum fluctuation are responsible for the density distribution of the chromo-electric field $\rho(x)$. However it is important to stress that this description is expected to hold only in the infrared regime of the theory, where the distance $R$ between quarks is sufficiently large that the string can be considered thin. So we are dealing with low energy aspects of strong interactions.

As we already showed in Section 1.3 in a finite temperature setting the interquark potential can be extracted by looking at the correlator of two Polyakov loops in the confined phase. The correlation function of two loops $\Phi_x$ at a distance $R$ and at a temperature $T = 1/L = 1/aN_t$, being $L$ the extension of the lattice in the temporal direction, is given by

$$\langle \Phi_0 \, \Phi_R^* \rangle \equiv e^{-F(R,L)}$$

where the free energy $e^{-F(R,L)}$ is expected to be described, as a first approximation, by the so called "area law":

$$F(R, L) \sim \sigma L R + k(L).$$

This however correctly describes the Polyakov loops correlator only in the strong coupling phase. As we discussed, the confining regime consists in two phases: the strong coupling and the rough phase. These two phases are related to two different behaviors of the quantum fluctuation of the flux tube around its equilibrium position [15]. In the strong coupling phase these

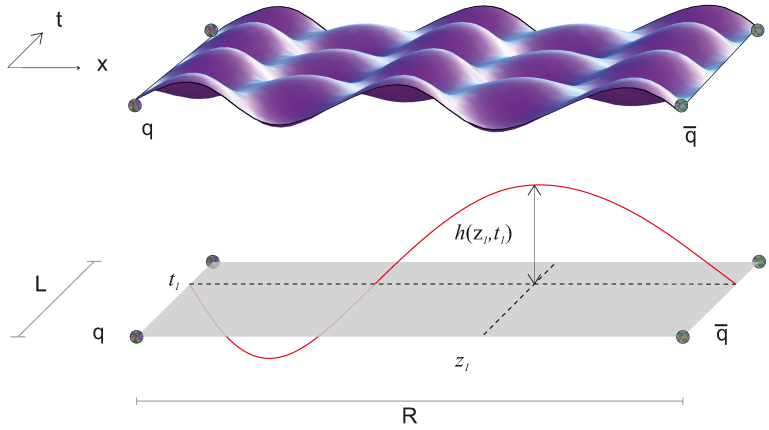


Figure 2.2: *The time evolution of the string produces a two dimensional surface. A real scalar field $h(z,t)$ describes the displacements from the rest position (grey rectangle $R \times L$) of the thin string that connects the two quarks at distance $R$.*

fluctuations are massive, while in the rough phase they become massless. In the rough phase the flux-tube fluctuations can be described by a suitable two dimensional massless quantum field theory, where the fields describe the transverse displacements of the flux tube. We expect this QFT to be the effective low energy description of some fundamental string theory. This observation enables us to decouple the degrees of freedom of the glue field into two groups: those that describe the state inside the thin flux tube and those describing its position in space.

Let us consider two static sources in a $d$ dimensional spacetime where $x_0$ represents the time coordinate. If the quarks are located at $x = (0, 0, \ldots)$ and $x = (0, R, \ldots)$ the time evolution of the string forms a two dimensional surface of parameters $x_0$ and $x_1$ which is called worldsheet. If the evolution extends for a period $L$, the worldsheet of the equilibrium configuration is a rectangle $\mathscr{R}_{R,L}$. The displacements of the string from its rest position can be specified by a $d-2$ component vector field

$$\vec{h}(z,t)\,, \quad 0 \le z \le R\,, \quad \vec{h}(0,t) = \vec{h}(R,t) = 0\ .$$

The effective action should fulfill some general requirements [15]: it should be local, the lagrangian must be invariant under Poincaré transformation in the $(z,t)$ plane and $O(2)$ rotation and translation of the field vector $\vec{h}$. We might expect the action to be a non-renormalizable one. This is not a problem however because the high frequency fluctuations of the field $\vec{h}$ have to be cut off anyway: if $\vec{h}$ wiggles with a wavelength which is not much larger than the diameter of the thin flux tube, the internal degrees of freedom of the tube are excited and the description of the state in terms of $\vec{h}$ breaks down.

At a more formal level, it has been proposed to write the expectation value of two Polyakov loops as a string functional integral.

$$\langle P(x)^* P(x+R)\rangle \equiv Z\left[-S_{\text{eff}}(R,L)\right] = e^{-\sigma RL+k} Z_\Gamma(R,L) \tag{2.8}$$

At that purpose we are going to investigate functional integrals such as:

$$Z_\Gamma = \int_\Gamma \mathcal{D}\vec{h}(z,t) e^{-\frac{\sigma}{2}\int_0^L dt \int_0^R dz \left[\left(\partial_t \vec{h}\right)^2 + \left(\partial_z \vec{h}\right)^2 + V\left(\partial_t \vec{h}, \partial_z \vec{h}\right)\right]} \tag{2.9}$$

where $z$ and $t$ are the parameters of a two dimensional rectangle with sides $R$ and $L$, $h_i(z,t)$ $(i = 1,\ldots,d-2)$ are fields, defined over that rectangle, which are subject to certain boundary condition (symbolized by $\Gamma$) and $V$ is a polynomial which depends only on derivatives of $\vec{h}$.

In the following Sections we will derive the corrections for the interquark potential coming from the effective string model and its predictions for the broadening $w^2$ of the color flux tube.

## 2.3 Free Bosonic String

A description of the string dynamics is then achieved by a bosonic QFT. We do not know however the true form of the potential $V$ in (2.9). In a first approximation we can neglect it and deal with a theory with $d-2$ free bosons. The action becomes:

$$\begin{aligned} S_h^1 &= \int_0^L \int_0^R \mathrm{d}^2 z \left\{\frac{1}{2}\partial_a h \partial_a h\right\} \\ &= \int_0^L \int_0^R \mathrm{d}^2 z \left\{\frac{1}{2} h(-\partial_a^2) h\right\} \end{aligned} \tag{2.10}$$

where $(\partial_a^2)$ is the laplacian acting on functions defined over the rectangle. The partition function (2.9) becomes a Gaussian functional integral, which we can solve:

$$Z_h(R,L) \propto \left[\det(-\partial_a^2)\right]^{-\frac{d-2}{2}}. \tag{2.11}$$

The form of the laplacian $\partial_a^2$ depends directly on the domain of the fluctuating string. Hence (2.11) depends strictly on the boundary conditions imposed on the rectangle $\mathscr{R}_{R,L}$, that are different depending on which observable we are considering. Wilson loop has Dirichlet boundary conditions over the whole perimeter of the rectangle. On the other hand, for the correlator of two Polyakov loops, we have Dirichlet boundary conditions in the spatial direction and periodic boundary condition in temporal direction. The determinant of the laplacian is given by the product of the eigenvalues $\lambda_{mn}$:

$$\det(-\partial_a^2) = \prod_{mn} \lambda_{mn} \tag{2.12}$$

We will now address the calculation of the determinant as in [17]. In this step we will make use of $\zeta$ function regularization. Let us introduce the function:

$$\zeta\left(s,-\Delta_\Gamma\right) := \sum_{n,m}{}' \frac{1}{(\lambda_{mn})^s} \tag{2.13}$$

where the $'$ means that the sum extends over all non zero eigenvalues. The determinant of $-\Delta_\Gamma$ is now defined as:

$$\ln\det\left(-\Delta_\Gamma\right) := -\frac{d}{ds}\zeta\left(s,-\Delta_\Gamma\right)\big|_{s=0} \tag{2.14}$$

We shall verify that $\zeta\left(s,-\Delta_\Gamma\right)$ has an analytic continuation, which is regular at $s=0$, so that the r.h.s. of (2.14) is well defined. Using the integral representation of the $\Gamma$ function we get:

$$\begin{aligned}\zeta\left(s,-\Delta_\Gamma\right) &= \sum_{n,m}{}' \frac{1}{\Gamma(s)}\int_0^\infty e^{-\lambda_{nm}t}t^{s-1}dt \\ &= \frac{1}{\Gamma(s)}\int_0^\infty \left(\sum_{n,m}{}' e^{-\lambda_{nm}t}\right)t^{s-1}dt\end{aligned} \tag{2.15}$$

For an elliptic operator of order 2 in two dimensions there exists an asymptotic expansion

$$\sum_{n,m}{}' e^{-\lambda_{nm}t} \xrightarrow[t\to 0^+]{} \sum_{k=0}^{\infty} c_k^{'} t^{\frac{k-2}{2}} \tag{2.16}$$

the coefficients $c_k^{'}$ are called Seeley coefficients. It is possible to show [17] that $\zeta\left(s,-\Delta_\Gamma\right)$ is regular around $s=0$ and we obtain:

$$\zeta\left(s,-\Delta_\Gamma\right) = c_2^{'} \tag{2.17}$$

As $\zeta\left(s,-\Delta_\Gamma\right)$ is analytic we expand around $s=0$ and obtain the determinant as the coefficient of the linear term. We consider cylindrical boundary conditions for the laplacian so that:

$$\lambda_{mn} = -\pi^2\left(\frac{m^2}{L^2}+\frac{n^2}{R^2}\right) \quad \text{with} \quad \begin{array}{l} n=1,2,3,\ldots \\ m=0,\pm 2,\pm 4,\ldots \end{array} \tag{2.18}$$

The last equation can be rewritten as:

$$\lambda_{mn} = -\pi^2\left(\frac{m^2}{(L/2)^2}+\frac{n^2}{R^2}\right) \quad n\in\mathbb{N}_0, m\in\mathbb{Z} \tag{2.19}$$

Now let us put (2.19) into (2.15). We obtain:

$$\zeta\left(s,-\Delta_\Gamma\right) = \frac{1}{\Gamma(s)}\int_0^\infty dt\left(\sum_{m=-\infty}^{\infty}\sum_{n=1}^{\infty} e^{-\pi^2\left(\frac{m^2}{(L/2)^2}+\frac{n^2}{R^2}\right)t}\right)t^{s-1}\ . \tag{2.20}$$

From the inversion formula of the $\Theta$ series one gets:

$$\sum_{m=-\infty}^{\infty} e^{-\pi^2 \frac{m^2}{(L/2)^2} t} = \frac{L}{\sqrt{\pi \mathrm{t}}} \sum_{m=1}^{\infty} e^{-m^2 \frac{(L/2)^2}{t}} + \frac{L}{2\sqrt{\pi \mathrm{t}}} \ . \tag{2.21}$$

Inserting the last relation into (2.20) gives:

$$\begin{aligned} \zeta\left(s, -\Delta_\Gamma\right) = \frac{1}{\Gamma(s)} \int_0^\infty t^{s-1} \frac{L}{\sqrt{\pi t}} \sum_{m,n=1}^{\infty} e^{-\left[\frac{\pi^2 n^2 t}{R^2} + \frac{m^2 (L/2)^2}{t}\right]} dt \\ + \frac{1}{\Gamma(s)} \int_0^\infty t^{s-1} \frac{L}{2\sqrt{\pi \mathrm{t}}} \sum_{n=1}^{\infty} e^{-\frac{\pi^2 n^2 t}{R^2}} dt \ . \end{aligned} \tag{2.22}$$

The $t$ integration can now be done and we get in the limit $s \to 0$:

$$\zeta\left(s, -\Delta_\Gamma\right) = \left[ 2 \sum_{m,n=1}^{\infty} \frac{e^{-mn\pi \frac{L}{R}}}{m} - \pi \frac{L}{R} \sum_{n=1}^{\infty} n \right] s + \mathcal{O}\left(s^2\right) \tag{2.23}$$

We now need the value $\zeta(-1)$ of the zeta Riemann function. The regularization is straightly forward if we take the $t$-independent part of

$$\zeta(-1) = \sum_{n=1}^{\infty} n := t - \text{independent part of } \sum_{n=1}^{\infty} n\, e^{-nt} \ . \tag{2.24}$$

So we get:

$$\begin{aligned} \sum_{n=1}^{\infty} n e^{-nt} &= -\frac{d}{dt} \sum_{n=1}^{\infty} e^{-nt} = -\frac{d}{dt} \left( \frac{1}{e^t - 1} \right) \\ &= \frac{e^t}{\left(1 - e^t\right)^2} \sim \frac{1}{t^2} - \frac{1}{12} + \frac{t^2}{240} + \mathcal{O}\left(t^3\right) \ . \end{aligned} \tag{2.25}$$

From the above equation we obtain that $\zeta(-1) = -1/12$. We now insert these results into equation (2.14):

$$\begin{aligned} -\frac{d}{ds} \zeta\left(s, -\Delta_\Gamma\right) \big|_{s=0} &= -2 \sum_{n=1}^{\infty} \sum_{m=1}^{\infty} \frac{e^{-mn\pi \frac{L}{R}}}{m} + \sum_{n=1}^{\infty} \pi n \frac{L}{R} \\ &= 2 \log \prod_{n=1}^{\infty} \left( 1 - e^{-\pi \frac{L}{R} n} \right) - \frac{\pi}{12} \frac{L}{R} \\ &= 2 \log \left[ e^{-\frac{\pi}{24} \frac{L}{R}} \prod_{n=1}^{\infty} \left( 1 - e^{-\pi \frac{L}{R} n} \right) \right] \end{aligned} \tag{2.26}$$

Introducing the Dedekind $\eta$-function

$$\eta(q) = q^{\frac{1}{24}} \prod_{n=1}^{\infty} \left(1 - q^n\right), \qquad q = \mathrm{e}^{-\pi L/R} \tag{2.27}$$

we can rewrite (2.26) in a more compact form:

$$\det(-\partial_a^2) = \eta(q)^2 \ . \tag{2.28}$$

To leading order, the exact expression for the partition function is:

$$Z_0 = e^{-\sigma RT}\eta(q)^{2-d} \tag{2.29}$$

When expanded in powers of $q$, this formula leads to the representation [18]:

$$Z_0 = \sum_{n=0}^{\infty} w_n e^{-E_n^0 L} \tag{2.30}$$

with some positive integral weights $w_n$ and energies $E_n^0$ given by:

$$E_n^0 = \sigma r + \frac{\pi}{r}\left\{-\frac{1}{24}(d-2) + n\right\} \tag{2.31}$$

In particular the splitting between successive energy levels is equal to $\pi/r$ to this order in perturbation theory.

Now we are able to derive the correction for the free energy due to the fluctuations of the flux tube in the context of free string approximation:

$$\triangle_0 F(R,L) = -\ln Z_0(R,L) = (d-2)\ln\eta(q) \ . \tag{2.32}$$

Under modular transformations the Dedekind $\eta$ function fulfills the following relation:

$$\eta(\tau) = \frac{1}{\sqrt{-i\tau}}\eta(-\tau^{-1}) \tag{2.33}$$

Using this property we can obtain the correction $\triangle F$ within the two different region separated by $R = L/2$.
For $2R < L$ we have:

$$\triangle_0 F(R,L) = (d-2)\left[-\frac{\pi L}{24R} + \sum_{n=1}^{\infty}\ln(1-\mathrm{e}^{-\pi n L/R})\right] \tag{2.34}$$

instead for $2R > L$:

$$\triangle_0 F(R,L) = (d-2)\ \left[-\frac{\pi R}{6L} + \frac{1}{2}\ln\frac{2R}{L} + \sum_{n=1}^{\infty}\ln(1-\mathrm{e}^{-4\pi n R/L})\right] \tag{2.35}$$

The exponentially small corrections coming from the subleading terms in (2.34) are negligible unless we are in the intermediate region $R \sim L/2$. In fact, neglecting the summation in (2.34) we can extract the potential:

$$V(R) \simeq \sigma R + \mu + \frac{\gamma}{R}, \qquad \gamma = -\frac{\pi(d-2)}{24}. \tag{2.36}$$

It has been pointed out [14, 15] that the coefficient $\gamma$ is universal, that is to say, it does not depend on the underling gauge theory, but just on the transverse degrees of freedom of the oscillating string.

On the other hand in (2.35) the first two term are proportional respectively to $R$ and to $T = 1/L$. The latter can be interpreted as a finite temperature correction that lowers the string tension as the temperature increases. Extracting the dominant part of (2.35), the static potential takes the form:

$$V(R) \equiv \frac{1}{L}F(R,L) = \sigma R - \frac{\pi T^2 (d-2)}{6} R + \mu \tag{2.37}$$

where $\mu = \frac{k(L)}{L}$. From Eq. (2.37) we see that there exists a temperature $T_c$ where the string tension vanish and eventually leads to a deconfinement transition. This temperature appears to be:

$$T_c = \sqrt{\frac{6\sigma}{\pi(d-2)}}. \tag{2.38}$$

The existence of the deconfinement transition has been verified throughout many numerical simulations within the context of Yang-Mills theory [19]. However the value $T_c$ in (2.38) turns out to be rather far from the value obtained in Montecarlo simulations. This might support the existence of higher order terms in the effective string action.

The expression obtained for $2R > L$, can also be reinterpreted as a low temperature result [20]. If we look at the temporal direction as a spatial direction and vice-versa, the correlator between the two Polyakov loops becomes the temporal evolution for a time $R$ of a torelon of length $L$. The difference now is that the spatial boundary conditions of the fluctuating string are periodic and no longer fixed. With these different spatial boundary conditions the coefficient of the Lüscher term turns out to be 4 times larger [17] as one can read out from the expansion (2.35).

In conclusion we can recognize two regions in the effective string theory:

- $2R \ll L$, extremely low temperature regime [1]
- $2R \gg L$ finite temperature regime.

In what follows we will add a self-interaction part in the action and derive the consequences it brings.

## 2.4 Corrections to the Free String

In the last Section we calculated the first leading correction term that came from the effective string model. Now we want to turn on the autointeraction

[1] We note that the string representation is an effective description holding only for large $R$. So the requirement $2R \ll L$ means that $L$ is very large.

of the string, inserting a potential in the effective action. This will bring us subleading correction to the Lücher term. When one considers field theories on manifolds with boundaries [18], the possible interaction terms are localized either on the world-sheet or at its boundaries. Moreover, any terms that are formally removable by a field transformation can be dropped, since their effects on the energy spectrum amount to a renormalization of the coupling constants multiplying the interactions of lower dimensions. It turns out that in $d$ spacetime dimensions the only interaction term with coupling $b$ of dimension [length] is

$$S_1 = \frac{b}{4}\int_0^L \left\{ \left(\partial_z \vec{h}\cdot\partial_z\vec{h}\right)_{z=0} + \left(\partial_z \vec{h}\cdot\partial_z\vec{h}\right)_{z=R} \right\} dt \tag{2.39}$$

At second order the couplings have dimension [length]$^2$ and the complete list of terms is

$$\begin{aligned} S_2 &= \frac{1}{4}c_2\int_0^R dz\int_0^T dt \left(\partial_a\vec{h}\partial_a\vec{h}\right)\left(\partial_b\vec{h}\partial_b\vec{h}\right) \\ S_3 &= \frac{1}{4}c_3\int_0^R dz\int_0^T dt \left(\partial_a\vec{h}\partial_b\vec{h}\right)\left(\partial_a\vec{h}\partial_b\vec{h}\right) \end{aligned} \tag{2.40}$$

In the following paragraphs we will demonstrate that, using the so-called open-closed string symmetry, the coefficients of the interaction terms have to fulfill several constraints. In particular it will turn out that $b = 0$, that means that no boundary term is needed. It will be also important to review some existent string models, in order to gain some further understanding in deriving an interacting effective string theory.

### 2.4.1 Boundary Term

In this Section we would like to calculate the corrections to the free energy when we insert a boundary term in the action [21]. Let's consider the $d = 3$ case. We have:

$$S_1 = \frac{b}{4}\int_0^L \left\{ \left(\partial_z h\partial_z h\right)_{z=0} + \left(\partial_z h\partial_z h\right)_{z=R} \right\} dt \tag{2.41}$$

We are mainly interested in a finite temperature confining gauge theory, so the $z$-dependence of the eigenfunctions can be factored out as:

$$\sin\left(\frac{n\pi z}{R}\right) \quad n\in\mathbb{N}_0 \tag{2.42}$$

so that in (2.41):

$$\frac{\partial h}{\partial z} = \frac{n\pi}{R}\cos\left(\frac{n\pi z}{R}\right)[\ldots] \tag{2.43}$$

where the dots represent the $t$-dependence of the eigenfunction. We thus have:

$$\left(\frac{\partial h}{\partial z}\right)^2_{z=0,R} = \frac{n^2\pi^2}{R^2}\cos^2\left(\frac{n\pi z}{R}\right)\Big|_{z=0,R}[\ldots] = \frac{n^2\pi^2}{R^2}[\ldots]\ . \tag{2.44}$$

As it is concerned with the momentum in the compactified direction, the eigenvalues are:

$$\frac{4\pi^2 m^2}{L^2} \quad m \in \mathbb{Z} \tag{2.45}$$

The eigenvalues of the $(-\Delta)$ operator can be rewritten as

$$\pi^2\left(\frac{n^2}{\rho^2} + \frac{m^2}{\tau^2}\right) \quad \text{with} \quad \rho = R,\, \tau = L/2 \tag{2.46}$$

If we consider the boundary term as a perturbation of the pure free string action, then we can derive the corrections to the potential to first order in $b$ as a perturbation expansion. We then have:

$$\begin{aligned} S = \sigma RL + \frac{\sigma}{2}\int_0^L dt \int_0^R dz \left[(\partial_t h)^2 + (\partial_z h)^2\right] \\ + \frac{\sigma b}{4}\int_0^L dt \left[(\partial_z h)^2_{z=0} + (\partial_z h)^2_{z=R}\right] \end{aligned} \tag{2.47}$$

Let us notice that the eigenvalues of the unperturbed problem are known, so the double integral in (2.47) can be written in a simpler way:

$$\int_0^L dt \int_0^R dz \left[(\partial_t h)^2 + (\partial_z h)^2\right] = \pi^2\left(\frac{n^2}{\rho^2} + \frac{m^2}{\tau^2}\right)\int_0^L dt \int_0^R dz (\ldots)_{[z,t]^2} \tag{2.48}$$

where the notation $(\ldots)_{[z,t]^2}$ represents the squared modulus of the complete, unperturbed eigenfunction. We understand from (2.44) that the two addends in the integral in (2.47) are equal and their contribution can be written as:

$$\int_0^L dt \left[(\partial_z h)^2_{z=0} + (\partial_z h)^2_{z=R}\right] = 2\frac{n^2\pi^2}{R^2}\int_0^L dt (\ldots)_{[t]^2} \tag{2.49}$$

where $(\ldots)_{[t]^2}$ is the squared modulus of the $t$-dependent part of the eigenfunction. So when we consider the free string action, it involves terms like:

$$\frac{\sigma}{2}\pi^2\left(\frac{n^2}{\rho^2} + \frac{m^2}{\tau^2}\right)\int_0^L dt \int_0^R dz (\ldots)_{[z,t]^2} \tag{2.50}$$

but when we turn on the boundary terms it modifies according to:

$$\frac{\sigma}{2}\pi^2\left(\frac{n^2}{\rho^2} + \frac{m^2}{\tau^2}\right)\int_0^L dt \int_0^R dz (\ldots)_{[z,t]^2} + \frac{\sigma b}{2}\frac{n^2\pi^2}{R^2}\int_0^L dt (\ldots)_{[t]^2} \tag{2.51}$$

We can solve these integrals to obtain the following shorter expressions:

$$\begin{aligned}\int_0^L dt \int_0^R dz(\ldots)_{[z,t]^2} &= C_2 RL \\ \int_0^L dt(\ldots)_{(t)^2} &= C_1 L\end{aligned} \tag{2.52}$$

where $C_{1,2}$ are pure numbers. We can now rewrite (2.51) as:

$$\begin{aligned}&\sigma\frac{\pi^2}{2}\left(\frac{n^2}{\rho^2}+\frac{m^2}{\tau^2}\right)C_2 RL + \frac{\sigma b}{2}\frac{n^2\pi^2}{R^2}C_1 L \\ &= \sigma RL\frac{\pi^2}{2}C_2\left[\left(\frac{n^2}{\rho^2}+\frac{m^2}{\tau^2}\right)+k\frac{bn^2}{\rho^2 R}\right] \\ &= \sigma\frac{\pi^2}{2}C_2 RL\left\{\frac{m^2}{\tau^2}+\frac{n^2}{\tilde{R}^2}\right\}\end{aligned} \tag{2.53}$$

where $k = C_1/C_2$ and $\tilde{R} = R\left(1+k\frac{b}{R}\right)^{-1/2}$. So when we add the boundary term we get similar results as in the free case provided that we replace:

$$R \longrightarrow \tilde{R} = R\left(1+k\frac{b}{R}\right)^{-1/2} \tag{2.54}$$

### 2.4.2 Nambu-Goto action and NLO corrections

In this paragraph we will point out the connection of (2.9) with fundamental string theories. As an example we mention Nambu's model [22]:

$$Z_N[\mathcal{C}] = \int\limits_{\phi|_{\partial B=\mathcal{C}}} \mathcal{D}\phi\,(\xi_1,\xi_2)\, e^{-\sigma\int_B d^2\xi\sqrt{g}} \tag{2.55}$$

where

$$g = \det \partial_a\phi^\mu\partial_b\phi_\mu \quad \text{with} \quad a,b=1,2;\mu=1,\ldots,d. \tag{2.56}$$

The fields $\phi_\mu$ are mapping from a compact two-dimensional parameter space $B \subset \mathbb{R}^2$ into a $d$-dimensional euclidean spacetime, thus defining a surface in $d$ dimensions. This surface is bounded by a closed loop $\mathcal{C}$, which in the following we take to be a rectangle of sides $R \times L$. The functional integral (2.55) represents a summation over all surfaces which are bounded by that rectangle, each weighted by an action corresponding to its area. Finally, $\sigma$ is the string tension defined in (1.105).

Reparametrizations of $B$ form an invariance group of (2.55) and one may

choose a special gauge:

$$\begin{aligned}\phi_1 &= z \\ \phi_2 &= t \\ \phi_3 &= h_1(z,t) \\ &\vdots \\ \phi_d &= h_{d-2}(z,t)\end{aligned} \tag{2.57}$$

where now $z$ and $t$ parametrize the rectangle, which corresponds to the minimal surface with boundary $\mathcal{C}$. With this choice we do not allow for overlapping configurations as the functions $h_i(z,t)$ are single-valued. From (2.55) and (2.57) we obtain:

$$\begin{aligned}\sqrt{g} &= \left[1 + \left(\partial_t \vec{h}\right)^2 + \left(\partial_z \vec{h}\right)^2 + \left(\partial_t \vec{h} \times \partial_z \vec{h}\right)^2\right]^{1/2} \\ &\xrightarrow{d=3} \left[1 + (\partial_t h)^2 + (\partial_z h)^2\right]^{1/2}\end{aligned} \tag{2.58}$$

We are interested in the case $d = 3$ where the axial component vanishes and we are left with only one transverse degree of freedom. We proceed expanding the square root, but before doing that let us rewrite the action in terms of dimensionless variables:

$$\begin{aligned}\phi &= \sqrt{\sigma} h, \\ \xi_0 &= \frac{t}{L} \\ \xi_1 &= \frac{z}{R}\end{aligned} \tag{2.59}$$

so we are left with:

$$S[\phi] = \sigma RL \int_0^1 \mathrm{d}\xi_0 \int_0^1 \mathrm{d}\xi_1 \sqrt{1 + \frac{1}{\sigma L^2}(\partial_0\phi)^2 + \frac{1}{\sigma R^2}(\partial_1\phi)^2}. \tag{2.60}$$

We recognize in (2.60) that the expansion parameter is $(\sigma RL)^{-1}$ and the second order expansion of the square root gives for the partition function:

$$Z_N = \int_\Gamma \mathcal{D}[\phi] e^{-\sigma RL - S'[\phi]} \tag{2.61}$$

where

$$S'(\phi) = S_{bs}(\phi) - \frac{1}{8\sigma LR} S_I(\phi) + \mathcal{O}\left(\frac{1}{(\sigma LR)^2}\right) \tag{2.62a}$$

$$S_{bs}(\phi) = \frac{1}{2} \int_0^1 \mathrm{d}\xi_0 \int_0^1 \mathrm{d}\xi_1 \left[\frac{R}{L}(\partial_0\phi)^2 + \frac{L}{R}(\partial_1\phi)^2\right] \tag{2.62b}$$

$$S_I(\phi) = \int_0^1 \mathrm{d}\xi_0 \int_0^1 \mathrm{d}\xi_1 \left[\frac{R}{L}(\partial_0\phi)^2 + \frac{L}{R}(\partial_1\phi)^2\right]^2. \tag{2.62c}$$

We note that the first term in (2.61) is proportional to the area of the surface, while the corrections comes from the dynamics of the field $\phi$ that we could now identify with the fluctuating string describing the flux tube. The term $S_{bs}$ is exactly the free string contribution to the action which we already worked out in Section (2.3). The interacting term $S_I$ gives rise to subleading correction to the free energy which one can calculate [17]:

$$\triangle_I F(R,L) = -\frac{\pi^2 L}{1152\sigma R^3}\left[2E_4(q) - E_2^2(q)\right] \tag{2.63}$$

$E_2$ and $E_4$ are the first and second Eisenstein series:

$$E_2(q) = 1 - 24\sum_{n=1}^{\infty}\sigma(n)q^n \tag{2.64}$$

$$E_4(q) = 1 + 240\sum_{n=1}^{\infty}\sigma_3(n)q^n \tag{2.65}$$

where $q = \exp(-\pi L/R)$, $\sigma_1(n)$ and $\sigma_3(n)$ are, respectively, the sum of all divisors of $n$ and of their cubes (1 and $n$ are included in the sum). We note that these corrections are proportional to $R^{-3}$. We can now easily extend Eq. (2.38) so as to keep into account the next-to-leading order in the Nambu-Goto action expansion. To this end, the modular transformation properties of the Eisenstein series are [23]:

$$E_2(\tau) = -\left(\frac{i}{\tau}\right)^2 E_2\left(-\frac{1}{\tau}\right) + \frac{6i}{\pi\tau} \tag{2.66}$$

$$E_4(\tau) = \left(\frac{i}{\tau}\right)^4 E_4\left(-\frac{1}{\tau}\right) \tag{2.67}$$

Performing a modular transformation so as to reach the large $R$ limit we find:

$$E_2\left(i\frac{L}{2R}\right) = -\frac{4R^2}{L^2}E_2\left(i\frac{2R}{L}\right) + \frac{12R}{\pi L} \sim -\frac{4R^2}{L^2} \tag{2.68}$$

$$E_4\left(i\frac{L}{2R}\right) = \frac{16R^4}{L^4}E_4\left(i\frac{2R}{L}\right) \sim \frac{16R^4}{L^4} \tag{2.69}$$

so that:

$$-\frac{1}{8\sigma \mathrm{LR}}\langle S_I\rangle \sim -\frac{\pi^2 R}{72\sigma \mathrm{L}^3}. \tag{2.70}$$

We finally have:

$$F(L,R) \sim \sigma \mathrm{LR}\left(1 - \frac{\pi}{6L^2\sigma} - \frac{\pi^2}{72\sigma^2 L^4}\right) \tag{2.71}$$

This result agrees with the conjecture reported in [19] which states that if the world sheet bordered by the two Polyakov loops is described by a Nambu-Goto type action then the string tension should vanish at the critical point with a square root singularity: $\sigma(T) \sim (T_c - T)^2$. This behavior is compatible with (2.71) only if we assume:

$$\sigma(T) = \sigma(0)\sqrt{1 - \frac{T^2}{T_c^2}} \quad \text{with} \quad T_c^2 = \frac{3\sigma(0)}{\pi} \tag{2.72}$$

which turns out to be in much better agreement with the results of MC simulations. Inserting this value into (2.71) we find:

$$F(L,R) \sim \sigma \frac{R}{T}\left(1 - \frac{1}{2}\left(\frac{T}{T_c}\right)^2 - \frac{1}{8}\left(\frac{T}{T_c}\right)^4\right) \tag{2.73}$$

which is exactly the expansion to the next-to-leading order of (2.72). Many numerical investigations have confirmed with high accuracy the validity of this expectation. However this result should be considered with great caution, since it predicts a critical index 1/2 for the deconfinement transition, that disagrees with Monte Carlo simulations.

In what follows we will mainly use the zero temperature value of the string tension referring to it as $\sigma$.

### 2.4.3 Open-Closed String Duality

We will now address the question whether the constants $b, c_2, c_3$ shall satisfy some relation in order to meet the underlying quantum field physics. The string partition function is required to match the Polyakov loop correlation function at large $L$ and $R$. We usually consider the Polyakov loop to run along the time axis, forming topologically closed loops around the periodic boundary conditions in this direction. This let us interpret the Polyakov loop correlation function as the partition function of the gauge theory in presence of a static quark-antiquark pair.

We could however take the compactified dimension to be a spatial direction. In that case the field theoretical interpretation of such loop would be an operator that creates (or annihilates) a closed flux tube wrapping around the world at time $t_1$ and transverse spatial position $\vec{z}_\perp = (z_1, \ldots, z_{d-2})$. In this setting it is therefore expected [24] that the loop correlation function at zero transverse momentum has a spectral representation of the form:

$$\int d\vec{z}_\perp \left\langle P\left(t_1, \vec{z}_\perp\right)^* P\left(t_2, \vec{z}_\perp + R\hat{e}\right)\right\rangle = \sum_{n=0}^{\infty} |v_n|^2 \, e^{-\tilde{E}_n |t_1 - t_2|} \tag{2.74}$$

where the exponent $\tilde{E}_n$ and the coefficients $v_n$ are the energies and the transition matrix elements of the possible intermediate states. Through the

properties [24] of the Radon transform, (2.74) implies that the correlation function itself can be expanded in a series of Bessel functions according to:

$$\left\langle P\left(t_1,\vec{z}_\perp\right)^* P\left(t_2,\vec{z}_\perp+R\hat{e}\right)\right\rangle = \sum_{n=0}^{\infty}\left|v_n\right|^2 2R\left(\frac{\tilde{E}_n}{2\pi R}\right)^{\frac{1}{2}(d-1)} K_{\frac{1}{2}(d-3)}\left(\tilde{E}_n R\right) \quad (2.75)$$

Even if the energy values and the transition matrix are not known, this equation severely constrains the possible analytic form of the Polyakov loop correlation function. So the question is whether the partition function in the effective string theory can be expanded, at large $L$ and $R$, in a series of Bessel functions of the form (2.75). Failing in this would imply that the effective theory cannot provide an asymptotically exact description of the Polyakov loop.

Using the modular transformation property of the $\eta$-function:

$$\eta(q)=\left(\frac{2R}{T}\right)^{1/2}\eta\left(\tilde{q}\right), \quad \tilde{q}=e^{-4\pi R/T} \quad (2.76)$$

the leading-order expansion (2.29) can be rewritten as a series of exponentials

$$Z_0=\left(\frac{T}{2R}\right)^{\frac{d-2}{2}}\sum_{n=0}^{\infty} w_n e^{-\tilde{E}_n^0 R} \quad (2.77)$$

where the weights $w_n$ are the same as in expansion (2.30) but the closed string energies are:

$$\tilde{E}_n^0=\sigma T+\frac{4\pi}{T}\left[-\frac{1}{24}(d-2)+n\right]. \quad (2.78)$$

Since their arguments grow proportionally to $\sigma TR$ in this limit, the Bessel functions in (2.75) could be expanded as:

$$\begin{aligned}\left\langle P\left(t_1,\vec{z}_\perp\right)^* P\left(t_2,\vec{z}_\perp+R\hat{e}\right)\right\rangle = \sum_{n=0}^{\infty}\left|v_n\right|^2\left(\frac{\tilde{E}_n}{2\pi R}\right)^{\frac{d-2}{2}} e^{-\tilde{E}_n R}\times \\ \times\left[1+\frac{(d-2)(d-4)}{8\tilde{E}_n R}+\ldots\right]\end{aligned} \quad (2.79)$$

where to leading order we may replace $\tilde{E}_n$ with $\tilde{E}_n^0$ and drop all subleading terms in the squared bracket. Hence the free string partition function (2.77) has in any dimension $d$ the required form, and open-closed string duality thus holds to this order of the perturbation expansion.

At next-to-leading order we find the boundary term $S_1$. The partition function is obtained by replacing in $Z_0$ the variable $\tilde{R} = R\left(1 + k\frac{b}{R}\right)^{-1/2}$. We obtain:

$$\begin{aligned} Z_b = Z_0\big|_{R=\tilde{R}} = \left(\frac{T}{2R}\right)^{\frac{d-2}{2}} \sum_{n=0}^{\infty} w_n e^{-\tilde{E}_n^0 R} \\ \times \left[1 + \frac{kb}{2}\left(\tilde{E}_n^0 - \sigma L\right) + \frac{bk}{4R}(d-2)\right] \end{aligned} \tag{2.80}$$

From the previous discussion we know that $\tilde{E}_n = \tilde{E}_n^0 + O(b)$ and when this relation is inserted in (2.79) one understands that the $b/R$ term inside the square bracket in (2.80) cannot be matched. Thus we conclude that $b = 0$ is the only possible coupling which is consistent with the requirement of open-closed string duality.

A similar argument can also be applied to examine the next order terms $S_2$ and $S_3$ in perturbation theory, which have couplings $c_2$ and $c_3$. The computation is rather involved but it can be showed [18] that open-closed string duality holds if:

$$(d-2)c_2 + c_3 = \frac{d-4}{2\sigma} \, . \tag{2.81}$$

For general $d$ a generalization of the Lüscher and Weisz' argument provides a further constraint on the next-to-leading order coefficients [25]:

$$c_2 + c_3 = -\frac{1}{8} \, . \tag{2.82}$$

Thus for any value of $d$, the two constraints (2.81) and (2.82) completely fix the effective action at this perturbative order. The two terms $S_2$ and $S_3$ are actually equals in $d = 3$ and we find that the next-to-leading order term is given by:

$$S_{nlo} = -\frac{\sigma}{8}\int_0^R dz \int_0^L dt \, (\partial_a h \partial_a h)^2 \tag{2.83}$$

We shall remark that the expansion (2.60) of the Nambu-Goto action satisfies these two constraints.

## 2.5 Broadening of the Color Flux Tube

We are now going to describe in detail the predictions to the broadening of the flux tube, resulting from the leading and next-to-leading order terms in the effective string theory. In the following we consider the theory in $d = 3$

dimensions. The action at next-to-leading order is given by:

$$S[h] = S_0[h] + S_{nlo}[h] \tag{2.84}$$

$$S_0[h] = \frac{\sigma}{2}\int_0^L dt \int_0^R dz \left[(\partial_t h)^2 + (\partial_z h)^2\right] \tag{2.85}$$

$$S_{nlo}[h] = -\frac{\sigma}{8}\int_0^L dt \int_0^R dz \left[(\partial_t h)^2 + (\partial_z h)^2\right]^2 \tag{2.86}$$

The squared width of the string is defined as:

$$w^2(z) = \langle h(z,t)^2\rangle = \frac{\int \mathcal{D}[h]\,(h(z,t)-h_0)^2 \exp(-S[h])}{\int \mathcal{D}[h]\exp(-S[h])} \tag{2.87}$$

At next-to-leading order we have to replace the field with $h(z,t) \to h(z,t) + \alpha\partial_\mu\partial_\mu h(z,t)$, where $\alpha$ is a low energy parameter. As we did for the calculation of the boundary term, we consider the term $S_{nlo}$ as subleading and perform a perturbative expansion around the free action $S_0$. Following [26] we get:

$$\begin{aligned} w^2(z) = w^2_{lo}(z) &- \left\langle h(z,t)^2 S_2\right\rangle_0 + 2\alpha\left\langle (\partial_\mu h(z,t))^2\right\rangle_0 \\ &+ \alpha^2\left\langle (\partial_\mu\partial_\mu h(z,t))^2\right\rangle_0 \\ &- \frac{\alpha^2}{(LR)^2}\int dt\,dt'dz\,dz'\left\langle \partial_\mu\partial_\mu h(z,t)\cdot\partial_\mu\partial_\mu h\left(z',t'\right)\right\rangle_0 \end{aligned} \tag{2.88}$$

Where $\langle\ldots\rangle_0$ represents the vacuum expectation value with respect to the free-string action and $w^2_{lo}(x) = \left\langle h(z,t)^2\right\rangle_0$ is the result of the squared width at leading order. If we define $G\left(z,t;z',t'\right) = \langle h(z,t)h\left(z',t'\right)\rangle_0$ as the free field propagator, then:

$$\left\langle h(z,t)^2 S_2\right\rangle_0 = \frac{1}{2}\left(T_1 - 2T_2\right) - T_1 \tag{2.89}$$

where $T_1$ and $T_2$ are given by:

$$T_1 = \lim_{\epsilon,\epsilon'\to 0}\int_0^L dt' \int_0^R dz'\,\partial_{\mu'}G(z,t;z',t')\,\partial_{\mu''}G(z'',t'';z,t)\,\partial_{\nu'}\partial_{\nu''}G(z',t';z'',t'') \tag{2.90}$$

$$T_2 = \lim_{\epsilon,\epsilon'\to 0}\int_0^L dt' \int_0^R dz'\,\partial_{\mu'}G(z,t;z',t')\,\partial_{\nu''}G(z'',t'';z,t)\,\partial_{\mu'}\partial_{\nu''}G(z',t';z'',t'') \tag{2.91}$$

where $z'' = z' + \epsilon$ and $t'' = t' + \epsilon$. These quantities are divergent for $(z,t) = (z',t')$, and the above integrals have been regularized by the point-splitting method. We finally have:

$$\begin{aligned} \left\langle h(z,t)\cdot\partial_{\mu'}\partial_{\mu'}h\left(z',t'\right)\right\rangle_0 &= \partial_{\mu'}\partial_{\mu'}G(z,t;z',t') \\ \left\langle \partial_\mu\partial_\mu h(z,t)\cdot\partial_{\nu'}\partial_{\nu'}h\left(z',t'\right)\right\rangle_0 &= \partial_\mu\partial_{\mu'}\partial_{\nu'}\partial_{\nu'}G(z,t;z',t') \end{aligned} \tag{2.92}$$

In Appendix A we will show that the free field propagator can be written as:

$$G(z,t;z',t') = \frac{1}{\pi\sigma}\sum_{n=1}^{\infty}\sin\left(\frac{n\pi z}{R}\right)\sin\left(\frac{n\pi z}{R}\right)\frac{e^{-n\pi(t-t')/R}+q^n e^{n\pi(t-t')/R}}{n\,(1-q^n)} \tag{2.93}$$

with

$$u = \frac{L}{2R}, \quad q = e^{-2\pi u} \tag{2.94}$$

As we already discussed in Section 2.1.1, we are interested in the string width at the midpoint $R/2$. In (2.93) the $t$-dependence has been dismissed due to translational invariance in the temporal direction. At leading order the squared width $w_{lo}^2(z)$ is ultraviolet divergent again and has been regularized with point splitting method:

$$w_{lo}^2(R/2) = \frac{1}{2\pi\sigma}\log\frac{R}{R_0} + \frac{1}{\pi\sigma}\log\frac{\eta(2iu)}{\eta^2(iu)} \tag{2.95}$$

where the low energy parameter is given by

$$R_0 = \frac{\pi}{2}\sqrt{\epsilon^2+\epsilon'^2}. \tag{2.96}$$

Now we have to evaluate (2.89). Since (2.93) is valid only for $(t-t') \in [0,L]$, it is useful to split the integral over $t$, such as $\int_0^L dt = \int_0^{\epsilon'} dt + \int_{\epsilon'}^L dt$. We get:

$$\begin{aligned}
T_1 = {} & \frac{\pi}{\sigma^2 R^4}\sum_{n=1}^{\infty}\sum_{m=1}^{\infty}(-1)^{m+n}\sum_{k=1}^{\infty}\frac{k}{1-q^k}\left(e^{-k\pi\epsilon'/r}+q^k e^{n\pi(t-t')/r}\right) \\
& \times\int_0^R dz\cos\frac{\pi(2kz+k\epsilon)}{R}\Big[\cos\frac{\pi(2(m-n)z+(2m-1)\epsilon)}{R} \\
& \times\frac{1}{(1-q^{2n-1})\,(1-q^{2m-1})}\int_0^{\epsilon'}dt\left(e^{-2\pi(n+m-1)t/R}+e^{-2\pi(n+m-1)(L-t)/R}\right) \\
& +\cos\frac{\pi(2(m+n-1)z+(2m+1)\epsilon)}{R} \\
& \times\frac{1}{(1-q^{2n-1})\,(1-q^{2m-1})}\int_{\epsilon'}^{L}dt\left(e^{-2\pi(n+m)t/R}q^{2m-1}+e^{-2\pi(m-n)t/R}q^{2n-1}\right)\Big]
\end{aligned} \tag{2.97}$$

while the $T_2$ term appears to be:

$$\begin{aligned}
T_2 = {} & \frac{T_1}{2} - \sum_{n=1}^{\infty}\sum_{m=1}^{\infty}(-1)^{m+n}\frac{E_2(iu)}{24R^4\sigma^2}\int_0^R dz\cos\frac{2\pi(m-n)z}{R} \\
& \times\frac{1}{(1-q^{2n-1})\,(1-q^{2m-1})}\int_{\epsilon'}^{L}dt\left(e^{-2\pi(n-m)t/R}q^{2m-1}+e^{-2\pi(m-n)t/R}q^{2n-1}\right) \\
& -\frac{E_2(iu)}{96\sigma^2R^2}
\end{aligned} \tag{2.98}$$

where $E_2$ is the second Eisenstein series and the last term comes from the contribution of the integration $\int_0^{\epsilon'} dt$ after the limit $\epsilon' \to 0$ has been taken. Note that two identities hold:

$$\begin{aligned}\partial_x\partial_x G(x,t;x',t') &= -\partial_t\partial_t G(x,t;x',t'),\\ \partial_{x'}\partial_{x'}\partial_x\partial_x G(x,t;x',t') &= \partial_{y'}\partial_{y'}\partial_y\partial_y G(x,t;x',t'),\end{aligned} \tag{2.99}$$

thus we get that both $\langle(\partial_\mu h(x,t))^2\rangle_0$ and $\langle(\partial_\mu\partial_\mu h(x,t))^2\rangle_0$ vanish. Remarkably, the two terms in (2.88) proportional to $\alpha$ and $\alpha^2$ are zero at the next-to-leading order, simplifying the form of the squared width. The calculation of $T_1$ and $T_2$ is quite complicated, however we shall note that the next-to-leading contribution to $w^2$ does not introduce any new low-energy parameters. The final expression is:

$$w^2(R/2) = \left(1 + \frac{4\pi f(\tau)}{\sigma R^2}\right) w_{lo}^2(R/2) - \frac{f(\tau)+g(\tau)}{\sigma^2 R^2}, \tag{2.100}$$

where $\tau = iu$ and

$$f(\tau) = \frac{E_2(\tau) - 4E_2(2\tau)}{48} \tag{2.101}$$

$$g(\tau) = i\pi\tau\left(\frac{E_2(\tau)}{12} - q\frac{d}{dq}\right)\left(f(\tau) + \frac{E_2(\tau)}{16}\right) + \frac{E_2(\tau)}{96}. \tag{2.102}$$

As we already pointed out, the Dedekind $\eta$-function and the Eisenstein series, obey the following transformation properties under the transformation $\tau \to -\tau^{-1}$:

$$\eta(\tau) = \frac{1}{\sqrt{-i\tau}}\eta(-\tau^{-1}) \tag{2.103}$$

$$E_2(\tau) = \frac{1}{\tau^2}\,E_2(-\tau^{-1}) - \frac{6}{i\pi\tau}\ . \tag{2.104}$$

Using these relations, we can convert the expression (2.100) in a form useful in the limit $R \gg L$. The temperature is still small, so to be in the confined phase and the string length $R$ is much larger than the inverse temperature $L$. The derivative of the second Eisenstein series is:

$$q\,\frac{\mathrm{d}}{\mathrm{d}q}\,E_2(\tau) = \frac{1}{12}\left[E_2(\tau)^2 - E_4(\tau)\right] \tag{2.105}$$

with $E_4(t)$ given by (2.65) and its inversion property by (2.69). A bit of algebra then shows that in the limit $R \gg L$ the broadening of the tube

width is:

$$w_{lo}^2(R/2)\frac{3L\Big[-1+LR\sigma\Big]+\pi R\Big[E_2\Big(\frac{iR}{L}\Big)-E_2\Big(\frac{2iR}{L}\Big)\Big]}{3L^2R\sigma}$$
$$+\frac{1}{144\pi L^3R\sigma^2}\Big[18L^2-18\pi RL\,E_2\Big(\frac{iR}{L}\Big)+\pi^2R^2\,E_2\Big(\frac{iR}{L}\Big)^2+30\pi RL\,E_2\Big(\frac{2iR}{L}\Big)$$
$$-2\pi^2R^2\,E_2\Big(\frac{iR}{L}\Big)\,E_2\Big(\frac{2iR}{L}\Big)-\pi^2R^2\Big[E_4\Big(\frac{iR}{L}\Big)-8E_4\Big(\frac{2iR}{L}\Big)\Big]\Big] \quad (2.106)$$

where $w_{lo}^2(R/2)$ is the expansion of (2.95) for high temperatures and takes the form:

$$w_{lo}^2(R/2)=\frac{\log\Big[\frac{R}{4R_0}\Big]}{2\pi\sigma}+\frac{\log\Big[\sqrt{\frac{L}{R}}\eta\left(\frac{iR}{L}\right)\eta\left(\frac{2iR}{L}\right)^{-2}\Big]}{\pi\sigma} \quad (2.107)$$

In the Chapter 4 we will check the results of the effective string theory with the numerical study in the $(2+1)-d$ Yang-Mills $SU(2)$ gauge theory. We will find a perfect agreement between the analytic predictions and data of Monte Carlo simulations.

# Chapter 3

# Numerical Simulations

In the context of quantum field theory, analytical results are mostly restricted to very simple systems, perhaps with substantial approximations. This is the reason why numerical simulations became a very important tool, to support and orient theoretical investigations.

The formulation of lattice gauge theory provides a natural way to implement numerical simulations. The vacuum expectation value of an observable in the quantized euclidean gauge field theory on a lattice is formally given by the functional integral:

$$\langle O \rangle = \frac{1}{Z} \int \prod_b dU(b) O\left(\{U(b)\}\right) \exp\left(-S\left[U\right]\right) \tag{3.1}$$

$$Z = \int \prod_b dU(b) \exp\left(-S\left[U\right]\right) \tag{3.2}$$

where in our case $S$ is the Wilson action (1.72). The integration must be performed over all configurations of the link variables $U(b)$ of the lattice. If we want to evaluate the integral by numerical methods, the lattice must be finite, so (3.1) and (3.2) are multidimensional definite integrals.

Even if the integration variables are finite, the configuration space is still too large to be directly evaluated. In fact a $32 \times 32$ bi-dimensional lattice has 1024 sites and if we want to compute the expectation value of any observable, we have to sum over all possible configurations of the 2048 link variables. Considering $Z_2$ variables, the number of operations amounts to $2^{2048} \sim 3 \times 10^{600}$, that is fair beyond the actual computational resources.

This is the reason why these integrations are carried out by means of statistical tools. In this Chapter we discuss the *Monte Carlo* method and how this is achieved, by constructing a so-called Markov chain. We then present an algorithm called *Multi-level* [27] proposed by Lüscher and Weisz, that will enhance the efficiency in measuring the observables.

## 3.1 The Monte Carlo Method

The Monte Carlo method consists in sampling the space $U$ of possible configuration by generating an ensemble $\{U_i\}_{i=1}^{N}$. The result of the integration is estimate by an arithmetic mean of the integrand, evaluated on each configuration $U_i$.

For example if one has to calculate the multidimensional integral

$$I = \int_D \mathrm{d}^d x \, f(\vec{x}) \tag{3.3}$$

we sample the domain $D$ by choosing $N$ independent values of the vector $\vec{x}$. These values are used perform an estimate $I_{MC}$ of $I$:

$$I_{MC} = \frac{1}{N} \sum_{n=1}^{N} f(\vec{x}_n), \qquad \lim_{N\to\infty} I_{MC} = I \tag{3.4}$$

The variance of the function $f$ allows for an estimate of the error in $I_{MC}$:

$$\sigma^2(f) = \int_D \mathrm{d}^d x \, (f(\vec{x}) - I)^2 \tag{3.5}$$

So that the standard deviation of $I_{MC}$ over all possible samples $\{\vec{x}\}_{i=1}^{N}$ is obtained from:

$$\sigma^2 \left(I_{MC}\right) = \int_D \mathrm{d}^d x_1 \cdots \int_D \mathrm{d}^d x_N \; (I_{MC} - I) = \frac{\sigma^2(f)}{N} \tag{3.6}$$

The central limit theorem ensures that if $N$ is large enough then $I_{MC}$ is distributed normally around the expected value $I$ with standard deviation $\sigma(f)/\sqrt{N}$. Hence the accuracy of the result depends on the number $N$ of total configurations as $N^{-1/2}$.

### 3.1.1 Importance Sampling

The Boltzmann factor $\exp(-S)$ has to be taken into account in the path integral of Eq.(3.1). Depending on the action $S$ it will give different importance to different field configurations. When summing over the configurations it is therefore more important to consider the configurations with larger weight than those with smaller weight. The central idea of the importance sampling Monte Carlo method is to approximate the huge sum by a comparatively small subset of configurations, which are sampled according to the weight factor. The expectation value of some function $f(x)$ with regard to a probability distribution with density $\rho(x)$ is given by

$$\langle f \rangle_\rho = \frac{\int \mathrm{d}x \, \rho(x) f(x)}{\int \mathrm{d}x \, \rho(x)} \tag{3.7}$$

In the importance sampling Monte Carlo integration this expectation value is approximated by an average over $N$ values,

$$\langle f \rangle_\rho = \lim_{N\to\infty} \frac{1}{N} \sum_{n=1}^{N} f(x_n) \tag{3.8}$$

where $x_n$ are randomly sampled with the normalized probability density

$$\mathrm{d}P(x) = \frac{\rho(x)\,\mathrm{d}x}{\int \mathrm{d}x\,\rho(x)} \tag{3.9}$$

Path integral in (3.1) is of the form (3.7) and thus suitable for importance sampling. We may therefore write the expectation of an operator $O$ as

$$\langle O \rangle = \lim_{N\to\infty} \frac{1}{N} \sum_{n=1}^{N} O[U_n] \tag{3.10}$$

with each of the $U_i$ sampled according to the probability distribution density

$$\mathrm{d}P(U) = \frac{e^{-S[U]} \prod_b dU(b)}{\int e^{-S[U]} \prod_b dU(b)} \tag{3.11}$$

the so-called Gibbs measure. The gauge field configurations $U_i$ are the random variables. We approximate the integral using a sample of $N$ such configurations.

### 3.1.2 Markov Chains

When one performs a numerical simulation is not able to sample the whole set $\{U_i\}_{i=1}^N$. One instead starts from some arbitrary configuration and then constructs a stochastic sequence of configurations that relax to equilibrium distribution $P(U)$. This is done with a so-called homogeneous Markov chain or Markov process

$$U_0 \to U_1 \to U_2 \to \ldots \tag{3.12}$$

In this Markov chain, configurations $U_i$ are generated subsequently. The index $i$ labels the configurations in the order they appear in the chain; it is often referred to as computer time, not to be mistaken with the Euclidean time. The change of a field configuration to a new one is called an "update" or a Monte Carlo step.

A Markov process is characterized by a conditional transition probability, i.e. the probability to get $U'$ when starting from $U$:

$$P(U_i = U' | U_{i-1} = U) = T(U'|U) \tag{3.13}$$

This probability depends only on the configurations $U'$ and $U$ but not on the index $i$. The transition probabilities $T(U'|U)$ obey

$$0 \leq T(U'|U) \leq 1 \tag{3.14}$$

$$\sum_{U'} T(U'|U) = 1 \tag{3.15}$$

The inequality simply delimits the range of a probability. The sum states that the total probability to jump from some configuration $U$ to any target configuration $U'$ is equal to 1. Let us now discuss an important restriction for $T(U'|U)$. Once it is in equilibrium, the Markov process cannot have sinks or sources of probability. Thus the probability to hop into a configuration $U'$ at the step $U_{i-1} \to U_i$ has to be equal to the probability for hopping out of $U'$ at this step. The corresponding balance equation reads as

$$\sum_{U} T(U'|U)P(U) = \sum_{U} T(U|U')P(U') \tag{3.16}$$

On the left-hand side we sum the transition probability $T(U'|U)$ leading into the final configuration $U'$ over all starting configurations $U$, weighted by the probability $P(U)$ that the system actually is in the configuration $U$. This expression gives the total probability to end up in $U'$ and has to equal the probability to hop out of $U'$, which we compute on the right-hand side. It is given by the probability $P(U')$ of finding the system in the configuration $U'$ times the sum of the transition probability $T(U|U')$ over all final configurations $U$ the system could jump into.

Before we discuss a solution of the balance equation (3.16), let us note an important property. The sum on the right-hand side can be calculated explicitly by using the normalization property. We find

$$\sum_{U} T(U'|U)P(U) = P(U') \tag{3.17}$$

showing that the equilibrium distribution $P(U)$ is a fixed point of the Markov process. Once the equilibrium distribution is obtained, the system stays there upon applying $T$. Starting the process from an arbitrary start configuration $U_0$ with initial distribution $P^{(0)}(U) = \delta(U - U_0)$, one eventually obtains the equilibrium distribution $P(U)$ by applying the transition matrix iteratively:

$$P^{(0)} \xrightarrow{T} P^{(1)} \xrightarrow{T} P^{(2)} \xrightarrow{T} \ldots \xrightarrow{T} P \quad (= \text{equilibrium distribution}) \tag{3.18}$$

For an elementary proof of this property see, e.g., [28].

Let us address an important point. In order to obtain correct results, the Markov chain must be able to access all configurations. If the transition matrix $T(U|U')$ is strictly positive for all pairs $U$, $U'$ then the process is

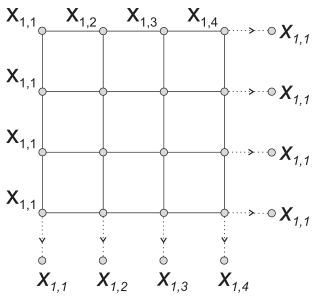


Figure 3.1: *Periodic boundary conditions over the lattice.*

aperiodic and every configuration can be eventually reached. This property is called strong ergodicity. In an actual calculation one starts to measure observables only after a sufficient number of equilibrating Monte Carlo steps. The subtle question is when one can assume that the distribution of the considered configurations is already close enough to the equilibrium distribution. This decision is usually based on the measurement of certain observables and correlations. A sufficient condition for a solution of the balance equation (3.16) can be obtained, by requiring that the equality holds term-wise,

$$T(U'|U)P(U) = T(U|U')P(U') \tag{3.19}$$

This sufficient condition is known as the *detailed balance* condition. Although other solutions are known, most algorithms use the detailed balance condition.

### 3.1.3 Lattice and Boundary Conditions

In our simulations we applied Monte Carlo method to the pure gauge theory on a 3–dimensional lattice.

We chose a cubic lattice with lattice spacing $a$. The number of lattice point in the temporal direction are $N_T$, so that the extension of the system is $L = a\,N_T$. The two spatial direction consist of $N$ sites, and the spatial extension amounts to $R = a\,N$. These two numbers $N_T$ and $N$ must be large to avoid finite size effects.

As we are dealing with a finite lattice, boundary conditions have to be implemented. For gauge fields, one uses periodic boundary conditions. This changes the topology of the underlying manifold as that of a torus in three dimensions.

## 3.2 Update Algorithms

In this Section we will describe some update algorithms. We will start with the famous Metropolis algorithm proposed in 1953 by Metropolis, Rosen-

bluth and Teller. Then will describe the Heat Bath and Overrelaxation methods, that we used in our simulations.

### 3.2.1 Metropolis

The Metropolis algorithm [29], which advances the Markov chain from a configuration $U_{i-1}$ to some new configuration $U_i$, consists of the following steps (we use $P(U) \propto \exp(-S[U])$:

**Step 1:** Choose some candidate configuration $U$ according to some a priori selection probability $T_0(U'|U)$, where $U = U_{i-1}$ and $U' = U_i$.

**Step 2:** Accept the candidate configuration $U'$ as the new configuration $U_i$ with the acceptance probability

$$T_A(U'|U) = \min\left(1, \frac{T_0(U|U')\exp(-S[U'])}{T_0(U'|U)\exp(-S[U])}\right) . \tag{3.20}$$

If a suggested change is not accepted, the unchanged configuration is considered again in the Markov chain and included in the measurements.

**Step 3:** Repeat these steps from the beginning.

The total transition probability $T = T_0 T_A$ fulfills the detailed balance condition:

$$\begin{aligned} T(U'|U)\exp(-S[U]) &= \\ &= T_0(U'|U)\min\left(1, \frac{T_0(U|U')\exp(-S[U'])}{T_0(U'|U)\exp(-S[U])}\right)\exp(-S[U]) \\ &= \min(T_0(U'|U)\exp(-S[U]), T_0(U|U')\exp(-S[U'])) \\ &= T(U|U')\exp(-S[U'])) \end{aligned} \tag{3.21}$$

due to the positivity of all factors and the symmetry of the min operation. In many cases one uses a symmetric selection probability which obeys

$$T_0(U'|U) = T_0(U|U') . \tag{3.22}$$

In this case (3.20) simplifies to

$$T_A(U'|U) = \min(1, \exp(-\Delta S)) \quad \text{with} \quad \Delta S = S[U'] - S[U] . \tag{3.23}$$

In particular for symmetric $T_0$, the information necessary to decide on acceptance or rejection comes only from the change of the action $\Delta S$ with regard to the change of the configuration. If this change is local, e.g., just involves a single link variable $U_\mu(n)$, then $\Delta S$ may be determined from the field values in the local neighborhood. The application to $SU(N)$ Wilson

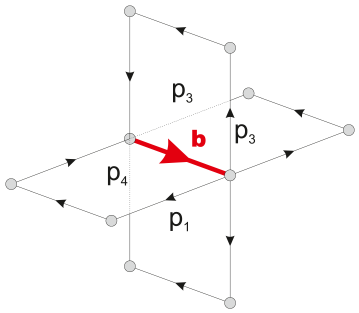


Figure 3.2: *In 3 dimensions a link b is shared by 4 plaquettes.*

gauge action (1.72) is now straightforward. Starting from some configuration $U$, the candidate configuration $U'$ for the Metropolis update differs from the configuration $U$ by the value of only a single link variable $U_\mu(n)$. In 3 dimensions this link is shared by four plaquettes (see Fig.3.2), and only these four plaquettes are affected when changing $U_\mu(n) \to U_\mu(n)'$. Their local contribution to the action is

$$\begin{aligned} S[U_\mu(n)']_{\text{loc}} &= \frac{\beta}{N} \sum_{i=1}^{4} \text{Re tr } \left[\mathbb{1} - U_\mu(n)' P_i\right] = \frac{\beta}{N} \text{Re tr} \left[4\,\mathbf{1} - U_\mu(n)' A\right] \\ A &= \sum_{i=1}^{4} P_i = \sum_{\nu \neq \mu} \big( U_\nu\,(n+\hat{\mu})\, U_{-\mu}\,(n+\hat{\mu}+\hat{\nu})\, U_{-\nu}\,(n+\hat{\nu}) \\ &\quad + U_{-\nu}\,(n+\hat{\mu})\, U_{-\mu}\,(n+\hat{\mu}-\hat{\nu})\, U_\nu\,(n-\hat{\nu}) \big) \end{aligned} \tag{3.24}$$

Here the $P_i$ are products of the other three gauge link variables that build up the plaquettes together with $U_\mu(n)'$. These products are called *staples* and we have written explicitly the sum A over all staples. For the change of the action we obtain

$$\Delta S = S[U_\mu(n)']_{\text{loc}} - S[U_\mu(n)]_{\text{loc}} = -\frac{\beta}{N} \text{Re tr} \left[(U_\mu(n)' - U_\mu(n))A\right] \tag{3.25}$$

where $A$ is not affected by the change of $U_\mu(n)$. An important part of the algorithm is the choice of the candidate link $U_\mu(n)'$. It should be an element of $SU(N)$ not too far away from the old link $U_\mu(n)$, such that the average acceptance probability (3.20) for the candidate does not become too small. A standard technique is to use

$$U_\mu(n)' = X U_\mu(n) \tag{3.26}$$

where $X$ is a random element of the gauge group $SU(N)$ in the vicinity of $\mathbb{1}$. To achieve a symmetric selection probability $T_0$, $X$ and $X^{-1}$ have to be chosen with equal probability. Based on equations (3.24), (3.25), and (3.26),

a realization of the Metropolis algorithm with single link variable updates and symmetric selection probability $T_0$ may be briefly summarized:

**Step 1** : Given some gauge field configuration, choose a site $n$, a direction $\mu$ and a candidate value $U_\mu(n)'$ according to some symmetric selection probability $T_0$, using, e.g., (3.26).

**Step 2** : Compute the sum over the staples and from this the change of the action $\Delta S$ according to (3.25). Compute a random number $r$ uniformly distributed in the interval $[0, 1)$. Accept the new variable $U_\mu(n)'$ if $r \leq \exp(-\Delta S)$ and reject it otherwise.

**Step 3:** Repeat these steps from the beginning.

We point out that the change in Step 2 is always accepted if the action decreases or remains invariant, i.e., $\exp(-\Delta S) \geq 1$.

In the next Section we will describe another Monte Carlo algorithm, called *Heatbath*, the one that used in our simulation. It successfully optimizes the local acceptance rate.

### 3.2.2 Heat Bath

The Heat Bath method combines steps 1 and 2 of the single link Metropolis update into a single step. In this algorithm, one chooses the new value $U_\mu(n)'$ according to the local probability distribution defined by the surrounding staples

$$\mathrm{d}P(U) = \mathrm{d}U \exp\left(\frac{\beta}{N} \mathrm{Re\ tr}\,[U\ A]\right) \tag{3.27}$$

The sum of staples $A$ is calculated according to (3.24) and all links, except for $U = U_\mu(n)'$, are held fixed and therefore $A$ is constant. Note that $\mathrm{d}U$ denotes the Haar integration measure of the gauge group. This may be computationally quite demanding. It has the advantage, however, that the link variable always changes. The implementation depends on the details of the gauge group and of the action. We present in detail the Heat Bath method for the gauge group $SU(2)$ with Wilson action. For this case there exists an efficient method to find a new link element. This group has the peculiar feature that a sum of two $SU(2)$ elements is proportional to another $SU(2)$ matrix. We use this property and write the sum of staples $A$ from (3.25) in the form

$$A = aV \quad \text{with} \quad a = \sqrt{\det[A]} \tag{3.28}$$

where it can be shown that $\det[A] \geq 0$. If $\det[A]$ vanishes one chooses a random $SU(2)$ matrix for $U$. Otherwise we find that $V = A/a$ is a properly normalized $SU(2)$ matrix. Inserting (3.28) in the probability distribution (3.28), we obtain (for $SU(2)$ we have set $N = 2$ in this equation)

$$\mathrm{d}P(U) = \mathrm{d}U \exp\left(\frac{1}{2} a\,\beta\ \mathrm{Re\ tr}\,[U\ V]\right) \tag{3.29}$$

The Haar measure $\mathrm{d}U$ is invariant under group multiplication and we may also write it as $\mathrm{d}(UV)$. If we define a matrix $X$ by the product $X = UV$, the local probability distribution for $X$ is

$$\mathrm{d}P(X) = \mathrm{d}X \exp\left(\frac{1}{2} a\,\beta\ \mathrm{Re\ tr}\,[X]\right) \tag{3.30}$$

If we generate a matrix $X$ distributed accordingly, the candidate link is obtained by

$$U_\mu(n)' = U = XV^\dagger = XA^\dagger \frac{1}{a} \tag{3.31}$$

We therefore have reduced the problem to generating matrices $X$ distributed according to (3.30). If we represent an $SU(2)$ matrix as a vector $x = (x_0, \mathbf{x})$ of four real component

$$U = x_0 \mathbb{1} + i\,\mathbf{x}\cdot\boldsymbol{\sigma} \tag{3.32}$$

$$\text{with} \quad \det[U] = |\mathbf{x}|^2 = x_0^2 + |\mathbf{x}|^2 = \sum_{i=0}^{3} x_i^2 = 1 \tag{3.33}$$

where $\boldsymbol{\sigma}$ denotes the three Pauli matrices, then the Haar measure in equation (3.30) may be written in terms of these real parameters. For $X$ in representation (3.32) with $x \in \mathbb{R}^4$, the Haar measure reads

$$\mathrm{d}X = \frac{1}{\pi^2}\ \mathrm{d}^4x\ \delta\left(x_0^2 + |\mathbf{x}|^2 - 1\right) \tag{3.34}$$

$$= \frac{1}{\pi^2}\ \mathrm{d}^4x\ \frac{\theta(1-x_0^2)}{2\sqrt{1-x_0^2}}\left[\delta\left(|\mathbf{x}| - \sqrt{1-x_0^2}\right) + \delta\left(|\mathbf{x}| + \sqrt{1-x_0^2}\right)\right] \tag{3.35}$$

where in the second line we have used the formula for the Dirac delta of functions. We rewrite the volume element as

$$\mathrm{d}^4x = \mathrm{d}|\mathbf{x}||\mathbf{x}|^2\mathrm{d}^2\Omega\,\mathrm{d}x_0 \tag{3.36}$$

where $\mathrm{d}^2\Omega$ denotes the spherical angle element in the integration over the 3–vector $\mathbf{x}$. We can use the Dirac deltas to remove the $|\mathbf{x}|$ integration. Only the first Dirac delta in (3.34) contributes and from now on $|\mathbf{x}|$ is frozen to $\sqrt{1-x_0^2}$. The Haar measure assumes the form

$$\begin{aligned}\mathrm{d}X &= \frac{1}{\pi^2}\,\mathrm{d}^2\Omega\,\mathrm{d}x_0\,\frac{(1-x_0^2)\theta(1-x_0^2)}{2\sqrt{1-x_0^2}} \\ &= \frac{1}{2\pi^2}\,\mathrm{d}^2\Omega\,\mathrm{d}x_0\,\sqrt{1-x_0^2}\,\theta(1-x_0^2)\end{aligned} \tag{3.37}$$

Note that in the matrix representation chosen for $X$ we have $|x_0| \leq 1$ and therefore we could have omitted the step function $\theta$. Due to $\mathrm{tr}\,[X] = 2x_0$, we end up with the distribution for $X$ in the form (using $\mathrm{d}^2\Omega = \mathrm{d}\cos\vartheta\mathrm{d}\varphi$):

$$\mathrm{d}P(X) = \frac{1}{2\pi^2}\,\mathrm{d}\cos\vartheta\mathrm{d}\varphi\,\mathrm{d}x_0\,\sqrt{1-x_0^2}\,e^{a\beta x_0} \tag{3.38}$$

with $x_0 \in [-1,1]$, $\cos\vartheta \in [-1,1]$, and $\varphi \in [0,2\pi)$. In order to find a random matrix $X$ we have to determine random variables $x_0$, $\vartheta$, and $\varphi$ according to this distribution. Since the distribution for the three variables factorizes, we can generate them independently:

**Random variable $x_0$:** The task is to find values $x_0$ distributed according to $\sqrt{1-x_0^2}\,e^{a\beta x_0}$. Following [30] we introduce a variable $\lambda \to x_0 = 1-2\lambda^2$, so that

$$\mathrm{d}x_0\sqrt{1-x_0^2}\,e^{a\beta x_0} \propto \mathrm{d}\lambda\ \lambda^2\sqrt{\lambda^2}e^{-2a\beta\lambda^2} \tag{3.39}$$

After this transformation we need to generate $\lambda$ with the polynomially modified Gaussian distribution density

$$p_1(\lambda) = \lambda^2 e^{-2a\beta\lambda^2} \tag{3.40}$$

and accept it with an accept/reject step using the square root function

$$p_2(\lambda) = \sqrt{1-\lambda^2} \tag{3.41}$$

Algorithms to compute random numbers with Gaussian distributions are described in, e.g., [31, 32]. We proceed as follows [30]:
*Step 1:* One starts with a triplet of random numbers $r_i$ with $i = 1,2,3$ uniformly distributed in $(0,1]$. Then

$$\lambda^2 = -\frac{1}{2a\beta}\left(\ln(r_1) + \cos^2(2\pi r_2)\ln(r_3)\right) \tag{3.42}$$

follows the required distribution.
*Step 2:* We correct for the factor $p_2(\lambda)$ and thus accept only those values of $\lambda$ which obey

$$r \le \sqrt{1-\lambda^2} \Rightarrow r^2 \le 1-\lambda^2 \tag{3.43}$$

where $r$ is a random variable uniformly distributed in $[0,1)$. The accepted values give $x_0 = 1-2\lambda^2$ following the requested distribution.

**Random variable $|\mathbf{x}|$:** Actually this random variable was removed when we integrated it out using the Dirac delta of (3.34). However, in this step the length was frozen to $|\mathbf{x}| = \sqrt{1-x_0^2}$ and we now can compute it from the $x_0$ determined in the last step.

**Random variables $\cos\vartheta$ and $\varphi$:** The angular variables correspond to the direction of $\mathbf{x}$ and are uniformly distributed. A possible method is to choose three random numbers $r_1$, $r_2$ and $r_3$ uniformly distributed in $[-1,1)$ and to accept them when $r_1^2 + r_2^2 + r_3^2 \le 1$. This 3-vector is then normalized to length $|\mathbf{x}| = \sqrt{1-x_0^2}$.

After these steps we end up with a vector $(x_0, \mathbf{x})$ and from that we can compute the matrix $X$ using representation (3.32).

### 3.2.3 Overrelaxation

This method tries to change the variables as much as possible in order to speed up the decorrelation of the configurations. One utilizes the property that in the Metropolis algorithm new configurations are always accepted if they do not change the action. Like for the Heat Bath algorithm the starting point is the probability distribution (3.27) of a single link variable $U_\mu$ in the background of its neighbors which we hold fixed with the sum of staples $A$ calculated according to (3.24). The idea of the overrelaxation method is to find a new value $U'$ which has the same probability weight as $U$ and thus is automatically accepted. Let us first illustrate the idea for the gauge group $U(1)$. In that case we can write $U = \exp(i\varphi)$ and for the sum of staples obtain $A = a\exp(i\alpha)$. The exponent for the local probability (3.27), the local action, can be written as

$$\beta\,\mathrm{Re}\,(U\,A) = \beta a\,\mathrm{Re}\,(e^{i\varphi}e^{i\alpha}) = \beta a\cos(\varphi+\alpha) \tag{3.44}$$

Obviously the reflection of $(\varphi+\alpha) \to -(\varphi+\alpha)$ or, equivalently, the change $\varphi \to (2\pi - 2\alpha - \varphi)$ leaves the local action invariant and thus is always accepted.

For the non-abelian groups one suggests a change according to the ansatz

$$U \to U' = V^\dagger\, U^\dagger\, V^\dagger \tag{3.45}$$

with a gauge group element $V$ chosen such that the action is invariant. For the gauge group $SU(2)$ the sum of staples $A$ is proportional to a group matrix and one constructs $V = A/a$ with the real number $a = \det[A]$. The matrix $V$ is now unitary. We find

$$\mathrm{tr}\,[U'\,A] = \mathrm{tr}\,[V^\dagger\, U^\dagger\, V^\dagger] = a\,\mathrm{tr}\,[V^\dagger\, U^\dagger] = \mathrm{tr}\,[A^\dagger\, U^\dagger] = \mathrm{tr}\,[U\,A] \tag{3.46}$$

In the last step we have used the reality of the trace for $SU(2)$ matrices. This choice for $U'$ indeed leaves the action invariant. Also the selection probability $T_0$ is symmetric, since $U' = V^\dagger\, U^\dagger\, V^\dagger$ implies $U = V^\dagger\, U'^\dagger\, V^\dagger$. In the rare case that $\det[A]$ vanishes, any random link variable is accepted.

The overrelaxation algorithm alone is not ergodic. It samples the configuration space on the subspace of constant action. This is called the microcanonical ensemble. Since one wants to determine configurations according to the canonical ensemble, i.e., distributed according to the Boltzmann weight, one has to combine the overrelaxation steps with other updating algorithms, such as Metropolis or Heat Bath steps.

### 3.2.4 Random Numbers

We end this Section spending a few words on the generation of random numbers. The central step of the Monte Carlo procedure needs random

numbers. In the computer programs these are the so-called *pseudo* random numbers, generated reproducibly by algorithms. Typical Monte Carlo runs may need $\mathcal{O}(10^{12})$ random numbers. Therefore, utmost care has to be taken in selecting a proper generator.

High-quality generators with extremely long guaranteed periods $\mathcal{O}(10^{171})$ are available and use the so-called lagged Fibonacci method. In our simulation we used the *ranlux* [31, 33] generator, that is an improvement of the known Marsaglia-Zaman [34] algorithm.

## 3.3 Multilevel Algorithm

Once we have implemented the update step of our simulation, we are able to create the configurations $\{U_i\}_{i=1}^{N}$ of link variables. Through these configurations we want to compute expectation value of the correlator of two Polyakov loops

$$G(r) \equiv \langle \Phi(x)^* \, \Phi(x + r\hat{v}) \rangle \tag{3.47}$$

where the Polyakov loop is defined in (1.99). The expectation value $G(r)$ is then evaluated by a statistical mean over $N$ such configurations.

We need to evaluate this observable over a wide range of distances $r$ between the two sources. In the previous Chapters we pointed out that the signal we are going to measure is exponentially decreasing:

$$G(r) \sim \mathrm{e}^{-\sigma A} \tag{3.48}$$

where $\sigma$ is the string tension and $A$ is the area of the minimal surface bounded by the two Polyakov loops. For a lattice with temporal extension $L$ we have $A = r \times L$. The error in measuring this observable depends on the standard deviation $s$ and on the number $N$ of measurements:

$$\delta G \simeq \frac{s}{\sqrt{N}}. \tag{3.49}$$

The relative error can be estimated by

$$\frac{\delta G(r)}{G(r)} \sim \frac{s}{\sqrt{N}} \, \mathrm{e}^{\sigma r L} \tag{3.50}$$

where $s$ can be considered independent of the separation between the two sources. This means that if $r$ is doubled, the same relative error is obtained by an exponentially increasing number $N$ of configurations. In fact the relative error on $G(2r)$ is:

$$\frac{\delta G(2r)}{G(2r)} \sim \frac{s}{\sqrt{N_{2r}}} \, \mathrm{e}^{\sigma 2 r L} \tag{3.51}$$

and in order to achieve the same accuracy (3.50) the total number $N_{2r}$ of configuration must increase as

$$N_{2r} \sim N\, \mathrm{e}^{2\sigma(A_f - A_i)} = N\, \mathrm{e}^{2\sigma r L}. \tag{3.52}$$

An accurate measurement of the static quark potential could require a total amount of computational time that is too large.

### 3.3.1 Exponential Error Reduction

The idea of the algorithm is to reduce the short wavelength fluctuations. By freezing the Monte Carlo dynamics of a suitably chosen set of lattice links, one splits the lattice into different sub-lattices non communicating among themselves. Then the observables are built up combining independent measurements performed within every sub-lattice.

Suppose we can decouple the measured signal (3.48) within $k$ factors and that each of them is evaluated independently:

$$G(r) \sim \mathrm{e}^{-\sigma A} = \left(\mathrm{e}^{-\frac{\sigma A}{k}}\right)^k = (F)^k \tag{3.53}$$

Performing the expectation value of each factor over $N$ configuration, the relative error is given by:

$$\frac{\delta F}{F} \sim \frac{s'}{\sqrt{N}}\, \mathrm{e}^{\frac{\sigma A}{k}} \tag{3.54}$$

the standard deviation $s'$ is considered of the same order of $s$. Using error propagation, the relative error on $G$ is:

$$\frac{\delta G(r)}{G(r)} \simeq \sqrt{\left(\frac{\delta F_1}{F_1}\right)^2 + \ldots + \left(\frac{\delta F_k}{F_k}\right)^2} \sim \frac{s'}{\sqrt{N}}\, \mathrm{e}^{\frac{\sigma A}{k}} \sqrt{k} \tag{3.55}$$

The ratio $\mathcal{R}$ between the error obtained with this prescription and the one achieved through a direct measurement is then:

$$\mathcal{R} = \frac{s'}{s} \sqrt{k} \mathrm{e}^{-k}\ . \tag{3.56}$$

We then obtained an exponential reduction of the relative error. This happens because when we perform $k$ expectation values over $N$ measurements, the final result on $G$ could be regarded as obtained from $N^k$ distinct configurations.

However this procedure can be applied only if we show that the expectation value of $G(r)$ can be decoupled into $k$–independent factors, that are evaluated individually.

In 2002 Lüscher and Weisz [27] showed that exponential error reduction can be applied when measuring the correlation function of two Polyakov

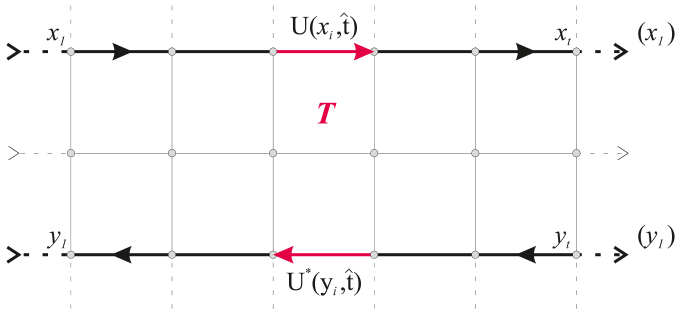


Figure 3.3: *Two Polyakov loops. The red marked links represent a* 2*–link operator.*

loops. We decompose the product of two Polyakov loop $\Phi(x)^*\,\Phi(x+r\hat{v})$ in more elementary pieces, called 2–link operators.

In Fig.3.3 these operators are identified through pairs of links that share the same temporal coordinate:

$$T_{\alpha\beta\gamma\delta_0}(t) = U^*_{\alpha\beta}(x,t)\,U_{\gamma\delta}(x+r\hat{v},t) \tag{3.57}$$

where all links have temporal direction. If we write down explicitly these new operators in the product of two Polyakov loops we obtain:

$$\begin{aligned}\Phi(x)^*\,\Phi(x+r\hat{v}) = \big\{U_{\alpha\epsilon_0}(x,0)\cdots U_{\epsilon_{L-1}\alpha}(x,L-a)\big\}^*\cdot \\ \cdot\big\{U_{\gamma\rho_0}(x+r\hat{v},0)\cdots U_{\rho_{L-1}\gamma}(x+r\hat{v},L-a)\big\}\end{aligned} \tag{3.58}$$

where the indexes $\epsilon_i$ and $\rho_i$ are contracted within the multiplications of link variables along the Polyakov loop, while $\alpha$ and $\gamma$ are contracted at the beginning and at the end of the lattice.

Let us collect all 2–link operators:

$$\begin{aligned}&= \big\{U^*_{\alpha\epsilon_0}(x,0)U_{\gamma\rho_0}(x+r\hat{v},0)\big\}\cdots\big\{U^*_{\epsilon_{L-a}\alpha}(x,L-a)U_{\rho_{L-a}\gamma}(x+r\hat{v},L-a)\big\} \\ &= T_{\alpha\epsilon_0\gamma\rho_0}(0)\cdots T_{\epsilon_{L-a}\alpha\rho_{L-a}\gamma}(L-a) \\ &= \{T(0)T(a)\ldots T(L-a)\}_{\alpha\alpha\gamma\gamma}\end{aligned} \tag{3.59}$$

We managed to rewrite the product of two Polyakov loops as a function of tensor with 4 indices. We define the multiplication law of such tensor as:

$$T_{\alpha\epsilon\gamma\rho}\cdot T'_{\epsilon\beta\rho\delta} = T''_{\alpha\beta\gamma\delta} \tag{3.60}$$

By breaking down $\Phi^*(x)\Phi(x+r\hat{v})$ into smaller pieces, we can construct the factors $F$ into which decompose the expectation value of $G(r)$.

### 3.3.2 G(r) Decomposition

Let us divide the lattice into $k$ temporal slices as in Fig.3.4. The number of $T$ operators inside these subsets differs depending on the slice thickness.

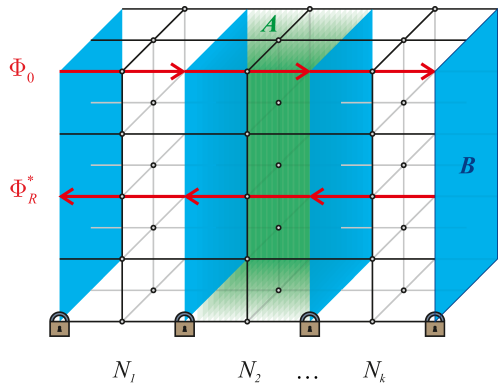


Figure 3.4: *Lattice decomposition into smaller time slices. The label A denotes links and plaquettes inside these slides, while B denotes the ones lying on the boundaries.*

Wilson action involves elementary plaquettes, so it is possible to decouple the Monte Carlo dynamics into such different slices. This means that we can make the system evolve independently within each subset, by freezing the links lying on the boundaries. Then the observable is built up combining the independent measurements performed within every sub-lattice.

Let us call $b_{ts}$ a link inside the slice and $\Box_{ts}$ the corresponding plaquette loop. We define the expectation value restricted to such links by:

$$[O] = \frac{1}{Z_{ts}} \int \prod_{b_{ts}} dU(b_{ts}) O\left(\{U(b_{ts})\}\right) \exp\left(-S_{ts}\right) \tag{3.61}$$

with

$$Z_{ts} = \int \prod_{b_{ts}} dU(b_{ts}) \exp\left(-S_{ts}\right) \tag{3.62}$$

where the action depends only by $P_{ts}$ plaquettes

$$S_{ts} = \beta \sum_{\Box_{ts}} \left(1 - \frac{1}{N} \mathrm{ReTr}\, P_{ts}\right). \tag{3.63}$$

Suppose that the thickness of each sub-lattice is composed of $h$ lattice spacing. The product of two Polyakov loops can be decomposed into $k \equiv L/h$ tensors $\mathbb{T}$ with 4 indices, each of them formed by $h$ 2–link operators:

$$\begin{aligned} \{\mathbb{T}\}_{\alpha\beta\gamma\delta} &= T_{\alpha\epsilon_0\gamma\rho_0}(0) \cdot T_{\epsilon_0\epsilon_1\rho_0\rho_1}(1) \cdots T_{\epsilon_{h-1}\beta\rho_{h-1}\delta}(h-1) \\ &= \{T(0) \ldots T(h-1)\}_{\alpha\beta\gamma\delta} \end{aligned} \tag{3.64}$$

For example if $h = 2a$, we have:

$$\begin{aligned} \Phi(x)^* \, \Phi(x + r\hat{v}) &= \{T(0)T(1)\}_{\alpha\epsilon_1\gamma\rho_1} \cdots \{T(L-2a)T(L-a)\}_{\epsilon_{L-2}\alpha\rho_{L-2}\gamma} \\ &= \{\mathbb{T}_1\}_{\alpha\epsilon_1\gamma\rho_1} \cdots \{\mathbb{T}_k\}_{\epsilon_k\alpha\rho_k\gamma} \end{aligned} \tag{3.65}$$

Each of these tensors belong to a different time slice, whose dynamics has been decoupled to the rest of the lattice. The expectation value defined in (3.61) can evaluated separately for every $\mathbb{T}$ operator. The observable $G(r)$ can be reconstructed from:

$$G(r) = \langle \Phi(x)^* \, \Phi(x + r\hat{v}) \rangle = \langle [\mathbb{T}_1] \cdots [\mathbb{T}_k] \rangle_B \tag{3.66}$$

where the expectation value $\langle \ldots \rangle_B$ is taken over different configurations of $U(b_B)$. These variables are built up from those links $b_B$ lying on the boundary between each time slice. These variables are held fixed during the evolution of the sub-lattices and represent the so-called *background field*.

The statistical error affecting the value of $G(r)$ obtained through (3.66) depends on the number of $N_B$ of sub-lattice updates:

$$\delta G(r) = \frac{s_k}{\sqrt{N_B}} \tag{3.67}$$

The product $[\mathbb{T}_1] \cdots [\mathbb{T}_k]$ leads to the exponential error reduction explained in Section 3.3.1.

The validity of (3.66) remains to be showed. Consider Fig.3.4 where the label $A$ denotes links and plaquettes inside the time-slice, while $B$ denotes the ones lying on the boundaries. The former can be further divided into $b_1, \ldots, b_k$ and into plaquette loops $\square_1, \ldots, \square_k$ depending on the sub-lattice they belong to.

Using this notation, the Wilson action decomposes as:

$$\begin{aligned} S &= S_A + S_B \\ &= \beta \sum_{\square_A} \left( 1 - \frac{1}{N} \mathrm{ReTr}\, P_A \right) + \beta \sum_{\square_B} \left( 1 - \frac{1}{N} \mathrm{ReTr}\, P_B \right) \\ &= \beta \sum_{\square_1} \left( 1 - \frac{1}{N} \mathrm{ReTr}\, P_1 \right) + \ldots + \beta \sum_{\square_k} \left( 1 - \frac{1}{N} \mathrm{ReTr}\, P_k \right) + \\ &+ \beta \sum_{\square_B} \left( 1 - \frac{1}{N} \mathrm{ReTr}\, P_B \right) = S_1 + \ldots + S_k + S_B \end{aligned} \tag{3.68}$$

The partition function $Z$ can be also decoupled using the links $b_A$ and $b_B$ as:

$$\begin{aligned} Z &= \int \prod_b dU(b)\, \mathrm{e}^{-S} = \int \prod_{b_A} dU(b_A) \prod_{b_B} dU(b_B)\, \mathrm{e}^{-S_A} \mathrm{e}^{-S_B} = \\ &= \left( \int \prod_{b_A} dU(b_A)\, \mathrm{e}^{-S_A} \right) \left( \int \prod_{b_B} dU(b_B)\, \mathrm{e}^{-S_B} \right) = Z_A \, Z_B \end{aligned} \tag{3.69}$$

We can also decompose $Z_A$ into factors related to different time slices $b_1 \ldots b_K$:

$$Z_A = Z_1 \ldots Z_K \tag{3.70}$$

The correlator of two Polyakov loops can be expressed using (3.65):

$$G(r) = \frac{1}{Z} \int \prod_b dU(b)\, \mathrm{e}^{-S} \{\mathbb{T}_1\}_{\alpha\epsilon_1\gamma\rho_1} \cdots \{\mathbb{T}_k\}_{\epsilon_k\alpha\rho_k\gamma} \tag{3.71}$$

Keeping in mind this link partitioning we now split the functional integral, and using results (3.69) and (3.70) we obtain:

$$\begin{aligned} G(r) &= \frac{1}{Z_B\, Z_1 \ldots Z_K} \int \prod_b dU(b)\, \mathrm{e}^{-S} \{\mathbb{T}_1\}_{\alpha\epsilon_1\gamma\rho_1} \cdots \{\mathbb{T}_k\}_{\epsilon_k\alpha\rho_k\gamma} = \\ &= \frac{1}{Z_B} \int \prod_{b_B} dU(b_B)\, \mathrm{e}^{-S_B} \frac{1}{Z_1} \int \prod_{b_1} dU(b_1)\, \mathrm{e}^{-S_1} \cdots \frac{1}{Z_K} \int \prod_{b_K} dU(b_K)\, \mathrm{e}^{-S_K} \cdot \\ &\qquad \cdot \{\mathbb{T}_1\}_{\alpha\epsilon_1\gamma\rho_1} \cdots \{\mathbb{T}_k\}_{\epsilon_k\alpha\rho_k\gamma} \end{aligned} \tag{3.72}$$

The integration over the $i$-th time slice is performed over the $i$-th operator $\mathbb{T}$ belonging to such sub-lattice and over the Boltzmann factor related to $b_i$. This determines the restricted expectation value (3.61):

$$\frac{1}{Z_i} \int \prod_{b_i} dU(b_i) \{\mathbb{T}_i\}_{\epsilon_{i-1}\epsilon_i\rho_{i-1}\rho_i} \mathrm{e}^{-S_i} = \left[\{\mathbb{T}_i\}_{\epsilon_{i-1}\epsilon_i\rho_{i-1}\rho_i}\right] \tag{3.73}$$

Using this relation in (3.72) we obtain (3.66):

$$\begin{aligned} G(r) &= \frac{1}{Z_B} \int \prod_{b_B} dU(b_B) [\{\mathbb{T}_1\}_{\alpha\epsilon_1\gamma\rho_1}] \cdots [\{\mathbb{T}_k\}_{\epsilon_k\alpha\rho_k\gamma}]\, \mathrm{e}^{-S_B} = \\ &= \langle [\mathbb{T}_1] \cdots [\mathbb{T}_k] \rangle_B \,. \end{aligned} \tag{3.74}$$

When performing a numerical simulation with the single level algorithm, one has to fix the value of 3 parameters: the temporal sub-lattice thickness $h$, the number $N_k$ of sub-lattice measurements of $\mathbb{T}$ and the number $M$ of background field configurations to carry out. These 3 parameters are related among themselves and finding their optimal choice is a non trivial step. Moreover, they also depend on the temporal extension $L$ of the whole lattice and on the distance $r$ between the two Polyakov loops.

The final error bar of the measure of $\langle \Phi_0^* \Phi_r \rangle$ is the combination of the uncertainties of the sub-lattice averages $\mathbb{T}$ (depending on $N_k$) and of the fluctuations of $\mathbb{T}$ due to different background fields (depending on $M$). If we suppose to have fixed $h$, the larger is $r$ the bigger must be both $N$ and $M$. Typically, $N$ is order of several thousands and $M$ of few hundreds. We note that $N$ does not depend on $L$ while $M$ does since it is related to the number of frozen time-slices.

We have now collected all necessary tools to perform a lattice gauge theory simulation. In the next Chapter we will present the results of the numerical study subject of this dissertation.

# Chapter 4

# Results

## 4.1 Introduction

In this Chapter we present the results of Monte Carlo simulations used to study the behavior of the width of the flux tube at finite temperature.

Numerical simulations have always been an important tool, since for the first time in the 1980s this model has been proposed [14, 15, 22], and its predictions have been explored.

Universality of the Lüscher term has been noticed in many works: such correction in fact does not depend on the effective action adopted. That's why simulation could be carried on choosing among many gauge groups, from $\mathbb{Z}_2$ up to $SU(N)$.

From a computational point of view, the efficiency of simulations' algorithms running discrete groups such as $\mathbb{Z}_2$ gained them lots of popularity concerning the lack of computing power.

Numerical studies [35, 36] on $\mathbb{Z}_2$ showed how in the infrared limit, the static quark potential slightly deviates from the area law. These corrections were in very good agreement with the free string action.

In 2002 Lüscher and Weisz [27] introduced the "multi-level" algorithm which enhanced the efficiency of simulations.

This allowed the autointeraction sector of the effective theory to be studied as well. For example works [23, 21, 37, 38] tested the Nambu-Goto model and realized that in a finite temperature setting results were compatible with the model's predictions.

The developing of computers enabled the more power consuming pure gauge theories with a continuous gauge group to be studied.

Effective string theory was then tested [39, 20] in the context of $SU(2)$ and $SU(3)$ in 3 and 4 spacetime dimensions. The free action gained more and more support in the infrared sector, whether next-to-leading order terms were not in good agreement especially when $R$ is lowered.

Finally we can finish by saying that effective theory has gained large

approval throughout many numerical studies

## 4.2 Model and Settings

Throughout this Chapter we consider $(2+1)-d$ Yang-Mills $SU(2)$ gauge theory on a cubic lattice of size $R \times R \times L$ with the Euclidian time extent $L$ determining the inverse temperature $\beta$. We consider the standard Wilson plaquette action:

$$S[U] = -\frac{2}{g^2} \sum_{x,\mu,\nu} \mathrm{Tr}[U_{x,\mu} U_{x+\hat{\mu},\nu} U^{\dagger}_{x+\hat{\nu},\mu} U^{\dagger}_{x,\nu}], \tag{4.1}$$

for parallel transporter variables $U_{x,\mu} \in SU(2)$ in the fundamental representation of the gauge group, located on the link $b(x,\hat{\mu})$. The parameter $g$ is the bare gauge coupling and $\hat{\mu}$ is a unit-vector pointing in the $\mu$-direction. All dimensionful quantities are expressed in units of the lattice spacing which is set to 1.

The bare gauge coupling was chosen to be $4/g^2 = 9.0$. This we will find out in Section 4.5 that corresponds to a lattice spacing $a \sim 0.072fm$. At this value of the gauge coupling the deconfinement transition takes place at the inverse temperature of about 6 in lattice units. The expansion parameter that appears in the effective theory is of the form $(\sigma R^2)^{-1}$. Starting from this observation, we can consider $R_c \equiv \sqrt{1.5/\sigma} \sim 7.5$ as a rough estimate of the scale below which the effective string picture is no longer expected to be valid.

There are some important differences between Yang-Mills $SU(2)$ gauge theories in $(2+1)-d$ or in $(3+1)-d$ . The gauge coupling $g^2$ of Yang-Mills theory in $(2+1)-d$ has dimensions of mass. Hence the theory is not scale invariant already at the classical level. In $(3+1)-d$ the gauge coupling $g^2$ is dimensionless and the theory is classically scale-invariant. However its quantum fluctuations generate a mass scale by dimensional transmutation. Nonetheless these theories share their important dynamical properties, that we briefly review. First of all both theories become free at short distances. In $(2+1)-d$ the effective dimensionless expansion parameter on a scale $l$ will be

$$g^2_{d=3}(l) \equiv l g^2 \stackrel{l\to 0}{\longrightarrow} 0 \tag{4.2}$$

In $(3+1)-d$ the coupling is dimensionless and runs as:

$$g^2_{d=4}(l) \simeq \frac{c}{\ln(l\Lambda)} \stackrel{l\to 0}{\longrightarrow} 0 \tag{4.3}$$

In both cases the interactions vanish as $l \to 0$.

The counterpart of the couplings becoming weak at short distances is that they become strong at large distances. This is immediate if we let

$l \uparrow$ in eqns(4.2,4.3). Thus in both 3 and 4 dimensions the physics at small distances is nonperturbative.

In $(2+1)-d$ the mass scale for the theory is explicitly set by the coupling. In $(3+1)-d$ the coupling is dimensionless, but through the phenomenon of dimensional transmutation, the coupling runs and this introduces a mass scale through the rate at which it runs. We then have $m_i = c_i\Lambda$ where $\Lambda$ is as in (4.3).

Finally both theories confine with a linear potential. We cannot prove this, but many lattice simulations show that this is the case.

These are the main reasons that led us to study $(2+1)-d$ gauge theories.

## 4.3 Data Analysis

The statistical analysis of the measurements is the important final step of a Monte Carlo simulation. This analysis should also provide one with the information how many updating sweeps have to be discarded before configurations in equilibrium are produced and how many sweeps are necessary between two measurements. The final product of the statistical analysis is the average value which one quotes for an observable and an estimate for the corresponding statistical error.

### 4.3.1 Statistical analysis for uncorrelated data

Let $(x_1, x_2, \ldots, x_N)$ be the values of some observable for a sequence of Monte Carlo-generated configurations after thermalization. Each of the values of the sample corresponds to a random variable $X_i$ . All these variables have the same expectation value and variance, so $\langle X_i \rangle = \langle X \rangle$ and $\sigma^2_{X_i} = \left\langle (X_i - \langle X_i \rangle)^2 \right\rangle = \sigma^2_X$. Candidates for unbiased estimators for these values are:

$$\widehat{X} = \frac{1}{N}\sum_{i=1}^{N} X_i\,, \quad \widehat{\sigma}^2_X = \frac{1}{N-1}\sum_{i=1}^{N}\left(X_i - \widehat{X}\right)^2 \tag{4.4}$$

As usual if the $X_i$ are uncorrelated one finds for $i \neq j$ $\langle X_i X_j \rangle = \langle X \rangle^2$ and the variance $\widehat{\sigma}^2_X$ gives the statistical error of $\widehat{X}$. To see this first note that the sample mean value $\widehat{X}$ is an estimator for the correct mean value: $\langle \widehat{X} \rangle = \langle X \rangle$. It is, however, itself a random variable, since its value may change from one set of $N$ configurations to another set. The variance of

that estimator is:

$$\begin{aligned}\sigma^2_{\widehat{X}} &= \left\langle \left(\widehat{X} - \langle X\rangle\right)^2 \right\rangle = \left\langle \left(\frac{1}{N}\sum_{i=1}^{N}\left(X_i - \langle X\rangle\right)\right)^2 \right\rangle \\ &= \frac{1}{N^2}\left\langle \sum_{i,j=1}^{N}\left(X_i - \langle X\rangle\right)\left(X_j - \langle X\rangle\right)\right\rangle \\ &= \frac{1}{N}\left\langle X^2\right\rangle - \langle X\rangle^2 + \frac{1}{N^2}\sum_{i\neq j}\langle X_i X_j\rangle\end{aligned} \tag{4.5}$$

For uncorrelated $X_i$ the contributions from $i \neq j$ factorize and

$$\sigma^2_{\widehat{X}} = \frac{1}{N}\sigma^2_X \tag{4.6}$$

This is the well-known result for uncorrelated measurements. Thus, for the observable based on $N$ measurements, the statistical error, i.e., the standard deviation (s.d.), is $\sigma_{\widehat{X}}$. The value $\sigma_X$ on the right-hand side of (4.6) is approximated using $\widehat{\sigma}_X$ from (4.4). For the case of $N$ uncorrelated measurements one quotes the final result as $\widehat{X} \pm \sigma$ with $\sigma = \sigma^2_X/\sqrt{N}$.

The important message of this equation is that the statistical error decreases like $N^{-1/2}$ with the number $N$ of uncorrelated configurations.

### 4.3.2 Autocorrelation

Since in our case the data sample is the result of a (computer-)time series in our Monte Carlo simulation it may happens, depending on the algorithms implemented, that the observables are correlated. This autocorrelation leads to a non-vanishing autocorrelation function, which we define as:

$$C_X\left(X_i, X_{i+t}\right) = \langle X_i X_{i+t}\rangle - \langle X_i\rangle\langle X_{i+t}\rangle\,. \tag{4.7}$$

For a Markov chain in equilibrium the autocorrelation function depends only on the (computer time) separation $t$ and we write:

$$C_X(t) = C_X\left(X_i, X_{i+t}\right) \tag{4.8}$$

Note that $C_X(0) = \sigma_X$. For large time separations, the normalized correlation function $\Gamma_x$ decreases exponentially with a typical time scale $\tau_X$:

$$\Gamma_X(t) \equiv \frac{C_X(t)}{C_X(0)} \sim \exp\left(-\frac{t}{\tau_{X,\mathrm{exp}}}\right) \tag{4.9}$$

The complete expression for $\Gamma_X(t)$ involves a sum over several such terms.

Autocorrelations lead to systematic errors which are $\mathcal{O}(\exp(-t/\tau_{\mathrm{exp}}))$ if the computer time between subsequent measurements is $t$.

For correlated random variables $X_i$ the terms with $i \neq j$ in the second line of (4.5) do not vanish and one can continue this equation to obtain for the correlated case:

$$\begin{aligned}\sigma^2_{\widehat{X}} &= \frac{1}{N^2}\sum_{i,j=1}^{N} C_X(|i-j|) = \frac{1}{N^2}\sum_{t=-(N-1)}^{N-1}\sum_{k=1}^{N-|t|} C_X(|t|) \\ &= \sum_{t=-N}^{N}\frac{N-|t|}{N^2}C_X(|t|) = \frac{C_X(0)}{N}\sum_{t=-N}^{N}\Gamma_X(|t|)\left(1-\frac{|t|}{N}\right) \\ &\approx \frac{\sigma^2_X}{N}2\left(\frac{1}{2}+\sum_{t=1}^{N}\Gamma_X(|t|)\right) \equiv \frac{\sigma^2_X}{N}2\tau_{X,\mathrm{int}}\end{aligned} \tag{4.10}$$

where we have introduced $\tau_{X,\mathrm{int}} = 1/2 + \sum_{t=1}^{N}\Gamma_X(|t|)$ as the integrated autocorrelation time. This definition is motivated by the observation of the exponential behavior in (4.9).

In the last step of (4.10) we have neglected the factor $1-|t|/N$ which is justified for large enough $N$ due to the exponential suppression of $\Gamma_X(|t|)$. Computing $\tau_{X,\mathrm{int}}$ in a realistic situation one has to cut off the sum in $\tau_{X,\mathrm{int}}$ at a value of $t$ where the values of $\Gamma_X(t)$ become unreliable. Usually one then assumes exponential behavior for the part not explicitly taken into account in the sum.

The variance $\sigma^2_{\widehat{X}}$ computed in this way is larger than the variance computed from (4.6), which assumes an uncorrelated sample. The number of effectively independent data out of N values is therefore

$$N_{\mathrm{indep}} = \frac{N}{2\tau_{X,\mathrm{int}}} \quad \text{and} \quad \sigma^2_{\widehat{X},\,\mathrm{corrected}} = 2\tau_{X,\mathrm{int}}\,\sigma^2_{\widehat{X}}. \tag{4.11}$$

For equilibration from a given start configuration one should discard at least $20\tau$. For more detailed discussions, see [40].

Summing up our results we find that for the correlated case the result one quotes is given by:

$$\widehat{X} \pm \sigma \quad \text{with} \quad \sigma = \sqrt{\frac{1}{N}2\tau_{X,\mathrm{int}}\,\widehat{\sigma}^2_X}. \tag{4.12}$$

### 4.3.3 Techniques for smaller data sets

If it is too expensive to compute the autocorrelation time, and unfortunately this is often the case in Monte Carlo simulations for quantum field theories on the lattice, there are simpler statistical methods for obtaining at least some estimate for the correlation of the data.

**Data blocking methods** One divides the set of measurements into blocks of $K$ successive measurements. Then one computes the block mean values, and considers them as new variables $X_i$ . The squared variance of the blocked variables then should decrease like $1/K$ if the original data were independent. One repeats this for increasing values of $K$. As soon as the $1/K$ behavior is observed for large enough $K$, one considers these block variables as statistically independent.

Once the minimal size of the block has been estimated, one can determine the expectation values of the observable of interest and its error. Often, however, the number of data is too small to get a reliable estimate of the variance of the computed expectation values. Another obstacle may be that error propagation is unreliable or impossible to determine. There are some efficient and easy-to-use methods dealing with both problems. They assume that the data are not correlated.

**Jackknife** Given a set of $N$ data, assume that we are interested in some observable $\theta$ which may be estimated from that set. Let us call the value of the observable obtained from the original data set $\hat{\theta}$. One now constructs $N$ subsets by removing the $n$-th entry of the original set ($n = 1, \ldots, N$) and determines the value $\theta_n$ for each set. Then

$$\sigma_{\hat{\theta}}^2 \equiv \frac{N-1}{N} \sum_{n=1}^{N} \left(\theta_n - \hat{\theta}\right)^2 \tag{4.13}$$

The square root of the variance gives an estimate for the standard deviation of $\hat{\theta}$. For the final result one quotes either $\langle\theta\rangle = \hat{\theta} \pm \sigma_{\hat{\theta}}$ or replaces $\hat{\theta}$ by the unbiased estimator. The bias may be determined from:

$$\tilde{\theta} \equiv \frac{1}{N} \sum_{n=1}^{N} \theta_n \tag{4.14}$$

leading to $\hat{\theta} - (N-1)\left(\tilde{\theta} - \hat{\theta}\right)$ as the unbiased estimator for $\langle\theta\rangle$.

In a practical implementation jackknife may be combined with blocking by organizing the data in blocks and constructing subsets by removing blocks instead of only single values. Another characteristic aspect of Monte Carlo simulations is the fact that often the observables one is interested in, are not simple averages but quantities that are obtained from a fit. An example is the energy levels obtained from an exponential fit to a Euclidean correlator. A single measurement of the correlator is fluctuating far too much for a reasonable fit. Thus one first has to average many measurements of the correlator before the fit can be performed. A powerful feature of the jackknife methods is the fact that it can be applied to the determination of the statistical error for fitted quantities.

## 4.4 String Tension at Low Temperature

As we observed in Chapter 2, the calculation of the broadening of the color flux tube, in the context of the effective string theory, requires two low energy parameters: the string tension $\sigma$ and the length $R_0$ appeared in (2.96). Remarkably, when we consider finite temperatures, there is no adjustable parameter. This feature makes apparent the predictive power of the theory himself.

We now present data simulated at low temperature and from these we will extract the values of the low energy parameters that we will use to analyze the results of the Monte Carlo simulations.

We report here on simulations performed on a $54 \times 54 \times 48$ lattice, used to extract the string tension at low temperature. As a first step we will introduce the observables we are going to measure.

### 4.4.1 Observables

As we discussed in Section 1.3, the interaction between two static charges at temperature $T = 1/L$ ($L$ being the lattice size in the periodic temporal direction) can be extracted by measuring the correlation function $G(R)$ of two Polyakov loops $\Phi_x$ at distance $R$:

$$G(R) \equiv \langle \Phi_0 \, \Phi_R^* \rangle \equiv \mathrm{e}^{-F(R,L)} \quad . \tag{4.15}$$

The free energy $F(R, L)$ of the static quark-antiquark pair is then related to the static quark potential $V(R)$ by

$$V(R) \equiv \frac{1}{L} F(R, L) = -\frac{1}{L} \log G(R) \tag{4.16}$$

According to the low-energy effective string theory at leading order illustrated in Chapter 2 the potential is expected to have at large $R$ the following form:

$$V(R) \simeq \sigma R + \mu + \frac{\gamma}{R}, \qquad \gamma = -\frac{\pi(d-2)}{24}. \tag{4.17}$$

We show in Fig. 4.1 the behavior of the potential extracted from the numerical data.

Another observable we are interested in is the derivative of the potential. There is no unique way to differentiate lattice functions, but a sensible prescription should be such that the correct continuum limit is obtained and that no artificially large lattice effects are introduced. The definition of the first derivative $F(r) = V'(r)$ proposed by Sommer [41] fulfills these conditions:

$$Q(\bar{R}) \equiv V(R+1) - V(R) = -\frac{1}{L} \log \left[ \frac{G(R+1)}{G(R)} \right] \tag{4.18}$$

| $R$ | $\bar{R}$ | $R$ | $\bar{R}$ |
|---|---|---|---|
| 3 | 2.379 | 12 | 11.478 |
| 4 | 3.407 | 13 | 12.480 |
| 5 | 4.432 | 14 | 13.481 |
| 6 | 5.448 | 15 | 14.483 |
| 7 | 6.458 | 16 | 15.484 |
| 8 | 7.464 | 17 | 16.485 |
| 9 | 8.469 | 18 | 17.486 |
| 10 | 9.473 | 19 | 18.486 |
| 11 | 10.475 | 20 | 19.487 |

Table 4.1: *Values of* $\bar{R}(R)$ *up to* $R = 20$.

where the function $\bar{R}$ is defined as:

$$\bar{R}(R)^{-1} = 2\pi \left[\Delta_2(R-a) - \Delta_2(R)\right]/a \tag{4.19}$$

where $\Delta_2(R)$ is the Green function between the origin and the point $(R, 0)$ of the lattice Laplacian in 2 dimensions and the dependence on the lattice spacing $a$ is explicited. In table 4.1 we report the values of $\bar{R}(R)$ up to $R = 20$.

Let us write down explicitly the predictions of the effective string description in the low temperature regime. We will consider only the $\mathcal{O}(1/R^2)$ correction coming from the free bosonic string case when $2R < L$. We take the derivative of (2.34) considering the first 10 elements of the series. We get:

$$Q_1(R) \simeq \sigma - \frac{\pi}{24R^2} + \frac{\pi}{R^2} \sum_{n=1}^{10} \frac{n}{1 - e^{n\pi \frac{L}{R}}} \tag{4.20}$$

The correction to the force coming by the Nambu-Goto model truncated at the second order would be of $\mathcal{O}(1/R^4)$. We shall then neglet the Nambu-Goto contribution in the fit for the string tension. So we are considering the following fitting function with 2 free parameters $\sigma$ and $\gamma$:

$$f(x) = \sigma - \frac{\gamma}{R^2} + \frac{\pi}{R^2} \sum_{n=1}^{10} \frac{n}{1 - e^{n\pi \frac{L}{R}}} \tag{4.21}$$

and later check that $\gamma$ is compatible with the Lüscher term $\pi/24$. As we pointed out before the effective string picture holds for large separation of the quark–antiquark pair. In order to obtain a good fit we should consider data for $R > R_c \gtrsim 10$. Besides this, to avoid finite size effect, we shall neglect data $R \gtrsim 20$.

With this prescriptions we show the results in Fig.4.2. We get for the string tension the result $\sigma = 0.025897(15)$. For the Lüscher term we obtain

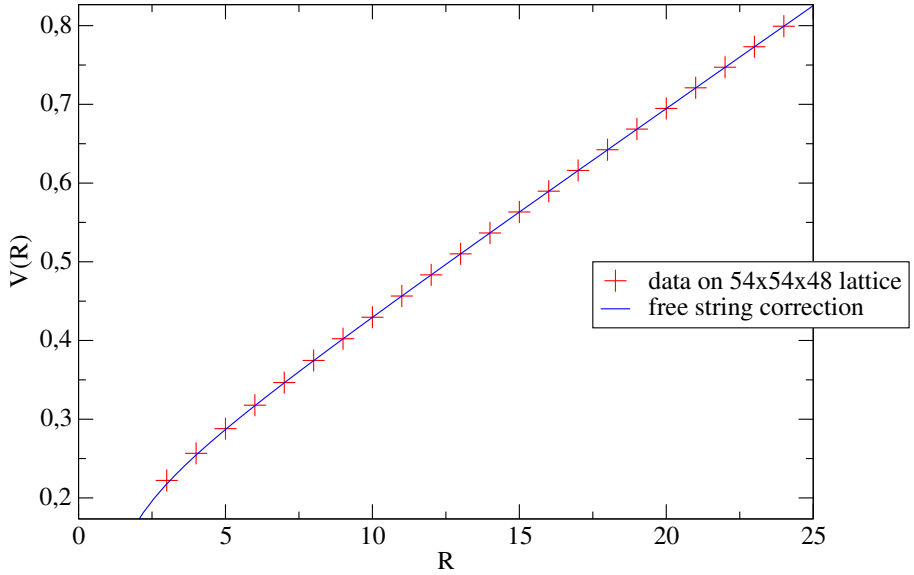


Figure 4.1: *Static quark potential obtained from the correlator of two Polyakov loops as* $V(R) = -\frac{1}{L}\log\langle\Phi_0\,\Phi_R^*\rangle$. *The solid line represent the free string correction (2.36) to the potential, where* $\sigma$ *is the string tension obtained from the fit (4.21) of the force.*

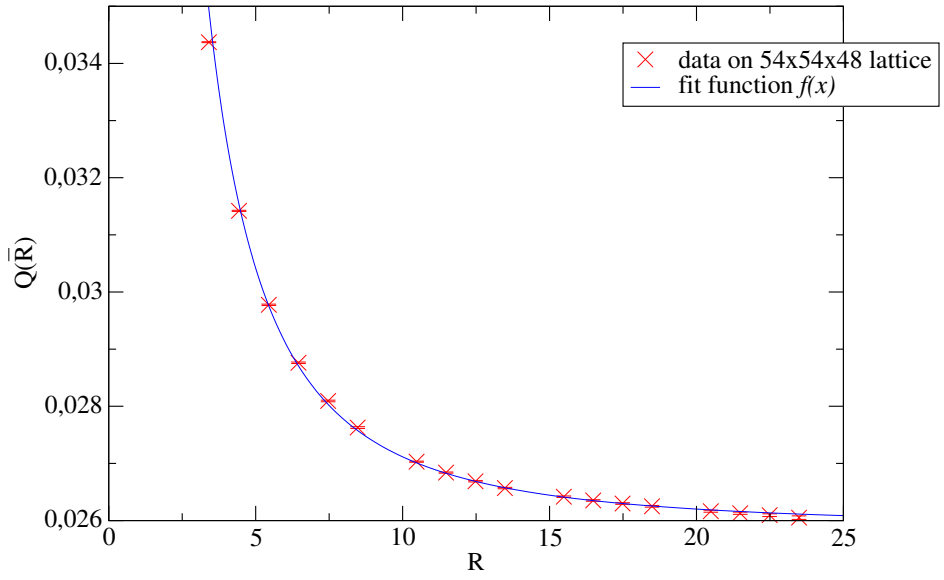


Figure 4.2: *Plot of the discretized derivative* $Q(\bar{R})$ *of the static quark potential. The solid line is the result of the fit (4.21) with parameters* $\sigma = 0.025897(15)$ *and* $\gamma = 0.124(4)$.

$\gamma = 0.124(4)$ which is in good agreement with the expected value $\pi/24 \simeq 0.130$.

## 4.5 Setting the Physical Length

With the estimate of the string tension obtained in the last Section, we shall address now the procedure needed to extract the value of the lattice spacing in our simulations. There is no unique way to do that, but we choose to assign to the square root of the string tension, that has the dimension of mass, the experimental value of 440 MeV [3]. Even if the $(2+1)-d$ $SU(2)$ Yang-Mills theory has no physical counterpart, we follow this recipe to have an idea of what is the scale.

From the simulations we obtain a dimensionless value for the string tension $\sigma$ and the lattice spacing is obtained from:

$$a = \frac{\sqrt{\sigma}}{(\sqrt{\sigma})_{exp}} \simeq \frac{\sqrt{K}}{440}\,\mathrm{MeV}^{-1} \simeq (0.448 \times \sqrt{\sigma})\,\mathrm{fm} \simeq 0,072 fm \tag{4.22}$$

where *exp* is to remind that it is an experimental value. Once we have obtained the lattice spacing we can express all the observable of the theory into physical units.

## 4.6 The Width of the Flux Tube at Zero Temperature

In this Section we discuss the width of the flux tube at zero temperature. The data are taken from [42].

Numerical simulations have been carried on a $54 \times 54 \times 48$ lattice and have been performed using the Lüscher-Weisz technique [27] described in Section 3.3.

### 4.6.1 Observables

As we discussed in Chapter 2 we can extract the width of the fluctuating string from the connected correlation function

$$C(x_3) = \frac{\langle \Phi_0 \Phi_R P_x \rangle}{\langle \Phi_0 \Phi_R \rangle} - \langle P_x \rangle, \tag{4.23}$$

of a pair of Polyakov loops $\Phi$ with a single plaquette

$$P_x = \frac{1}{2}\mathrm{Tr}[U_{x,1} U_{x+\hat{1},2} U^{\dagger}_{x+\hat{2},1} U^{\dagger}_{x,2}], \tag{4.24}$$

in the 1-2 plane (see figure 4.3). Since we are in $d = 3$ dimensions the tube fluctuates in just 1 dimension along which the color-electric field is

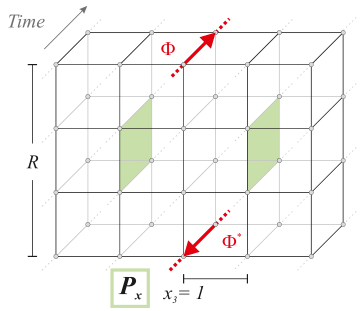


Figure 4.3: *Observable for the width of the color flux tube. The red arrows represent the two Polyakov loops in Eq. (4.23) while the green colored square represents the plaquette.*

measured as a function of the transverse displacement $x_3$. The plaquette is located at the symmetry point $x = (R/2, 0, x_3)$ at the maximal distance $R/2$ from the external quark charges. The correlation function at distance $R = 19$ is illustrated in Fig. 4.4. The pattern of data shows a Gaussian-type distribution. However small deviations are found so we shall fit the data using the ansatz:

$$\frac{\langle \Phi_0 \Phi_R P_x \rangle}{\langle \Phi_0 \Phi_R \rangle} = A \exp(-x_3^2/T) \frac{1 + B \exp(-x_3^2/T)}{1 + D \exp(-x_3^2/T)} + K, \tag{4.25}$$

where $A$, $B$, $D$, $T$, and $K$ are fit parameters. This function always provides an excellent fit of the data. The squared width of the string is then obtained as the second moment of the correlation function

$$w^2(R/2) = \frac{\int dx_3 \; x_3^2 C(x_3)}{\int dx_3 \; C(x_3)}. \tag{4.26}$$

Other fit functions have been considered in order to investigate the systematic uncertainties due to the fitting ansatz. This procedure did not produce significant effect on the string width. In Fig. 4.5 we illustrate the dependence of the squared string width $w^2(R/2)$ on the distance $R$ between the external static quarks.

### 4.6.2 Estimate of the Parameter $R_0$

When the probe approaches $R \approx 14$ the effective field theory successfully describes Monte Carlo data with the functional form of (2.95). It should be noted that the string tension has already been determined from the static quark potential. As we discussed in the beginning of the chapter, the only free parameter in the fit of the Monte Carlo data for the width at low temperature is the scale $R_0$. We obtain $R_0 = 2.26(2)$ such that $R_0\sqrt{\sigma} = 0.364(3)$.

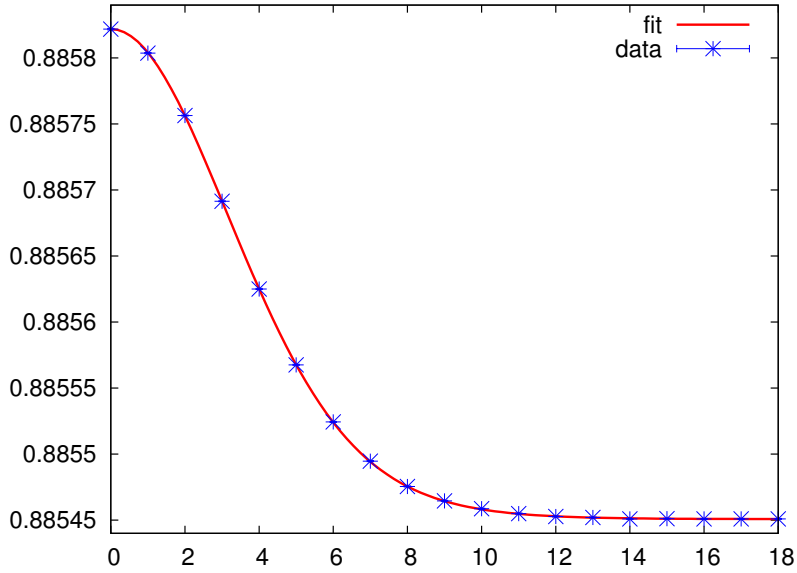


Figure 4.4: *The ratio* $\langle \Phi_0 \Phi_R P_x \rangle / \langle \Phi_0 \Phi_R \rangle$ *as a function of the transverse displacement* $x_3$ *at fixed distance* $R = 19$ *between the external static quarks. The solid line is a fit of the numerical data using Eq.(4.25).*

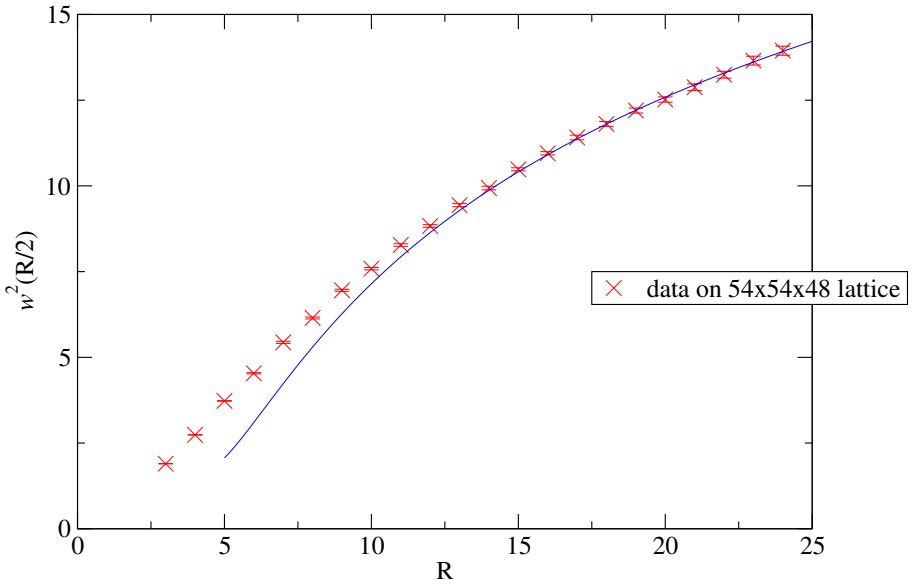


Figure 4.5: *The squared width string* $w^2(R/2)$ *at its midpoint as a function of the distance* $R$ *between the external quark charges. The solid curve is a fit to the next-to-leading order prediction of the low-energy effective field theory from Eq.(2.95).*

| $R$ range | updates |
|---|---|
| 4-8 | 3200 |
| 9-15 | 24000 |
| 16-22 | 32000 |
| 23-25 | 80000 |

Table 4.2: *Number of sub-lattice updates of the single level Lüscher-Weisz algorithm for various ranges of distances between the static sources.*

We considered the plaquette orientation parallel to the string world-sheet. Different choice of the probes — and thus different ways of defining the string width — will results on different values of the low energy parameter $R_0$. However we expect these to be very similar, and we have considered different orientations of the plaquette in the definition of Eq.(4.23). In Fig. 4.6 we show the normalized probability distribution $C(x_3)/\int dx_3\, C(x_3)$ for the 3 different orientations of the plaquette at fixed distance $R = 12$ between the external static quarks. Numerical data show that the normalized probability distribution is not significantly affected by the different probes used to extract the color flux tube width.

## 4.7 Finite Temperature Width

In the last Sections we presented simulations performed at zero temperature. In this Section we investigate the width of the flux tube at finite temperature, remaining however below the deconfinement transition $\beta = L < T_c$.

Simulations have been performed over a $90 \times 90 \times 16$ lattice, corresponding to $T/T_c \approx 0.38$. The highly efficent Lüscher-Weisz technique [27] was implemented with a single level and with slices of thickness 4. We report in table 4.2 the parameter of the simulation for various ranges of distances between the static sources.

The force (4.18) between the two static quarks has been extracted from the simulation following the procedure outlined in Section 4.4.1. We plot the result in Fig. 4.7.

From the calculations of Section 2.5, the leading order approximation is given by:

$$F_{lo}(r) = \sigma - \frac{\pi}{6\beta^2} + \frac{1}{2\beta r}. \tag{4.27}$$

This contribution is represented by the solid line in Fig. 4.7. At next-to-leading order the force can be obtained from the derivative of Eq. (2.71):

$$F(r) = F_{lo}(r) - \frac{\pi^2}{72\sigma\beta^4} - \frac{1}{8\sigma\beta^2 r^2}. \tag{4.28}$$

which is the dotted line in Fig. 4.7.

It is important to stress that $\sigma = 0.025897(15)$ is the zero-temperature string tension and there is no free parameter. The next-to-leading order expression already provides a very good description of the numerical data. Considering the accuracy of the data, it is reasonable to expect that the residual tiny discrepancy can be described by the next-to-next-to-leading order correction. For the measurement of the string width, the ansatz for the correlation function is again given by (4.25) and the squared width of the string is defined as (4.26).

In Fig. 4.8, we show the bell-shaped correlation function (4.23) as a function of the transverse displacement of the plaquette from the plane of the string world-sheet. The data refer to a pair of static sources at fixed distance $R = 17$. The solid line is a fit of the data using the ansatz (4.25). The scale that determines the logarithmic broadening of the string at zero temperature was determined in the last Section as $R_0 = 2.26(2)$.

It is important to note that $\sigma$ and $R_0$ are the only low-energy parameters entering the 2-loop expressions. Hence we can perform a very stringent check of the next-to-leading formula for the width of the color flux tube.

Fig.4.9 shows the results for the flux tube width as a function of the distance between sources. In this figure the solid line represents the fully constrained prediction of the low-energy effective string theory corresponding to the choice $R_0 = 2.26$. Excellent agreement is achieved for sufficiently large separation of the sources.

Again we compare the value of the tube width using different orientation of the plaquette and the result is showed in Fig. 4.10.

Finally we note that the calculated temperature dependence of the string tension in (2.72) does not alter the next-to-leading expression (2.100) for the width. That is because the 2-loop result contains terms of order $1/(\sigma\beta^2)$ and the corrections to the string tension $1/(\sigma\beta^2)^2$ would appear as 3-loop corrections to the width. The accuracy of the data in Fig. 4.9 does not allow to detect the tiny difference to the next-to-leading correction to the string tension, that are instead apparent in the direct measurement of the force of figure 4.7.

## 4.8 Conclusions

We have explored the low energy features of the physics of two static quarks in $(2 + 1)$-d $SU(2)$ Yang-Mills theory. Using the efficient Lüscher-Weisz multi-level simulation technique we obtained a high level of accuracy for the Monte Carlo simulations. This allowed us to study the systematic corrections of the string picture. In particular we compared the results for the finite temperature string width with analytic 2-loop calculations. Since the low-energy parameters $\sigma$ and $R_0$ were already determined at zero temperature, there were no further adjustable parameters in the comparison of

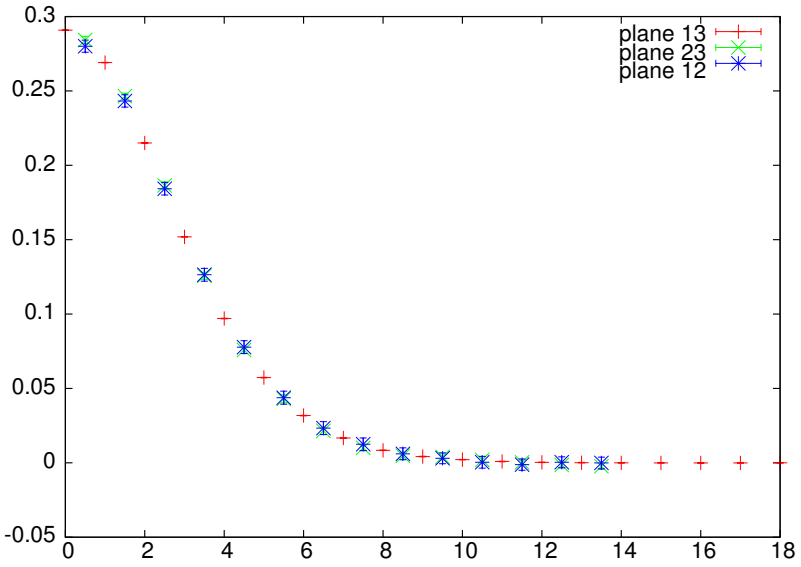


Figure 4.6: *Probability distribution* $C(x_3)/\int dx_3\ C(x_3)$ *using the 3 possible orientations of the plaquette in Eq.(4.23). The data points for the 2 orientations orthogonal to the string world-sheet are put at the midpoint between 2 lattice sites.*

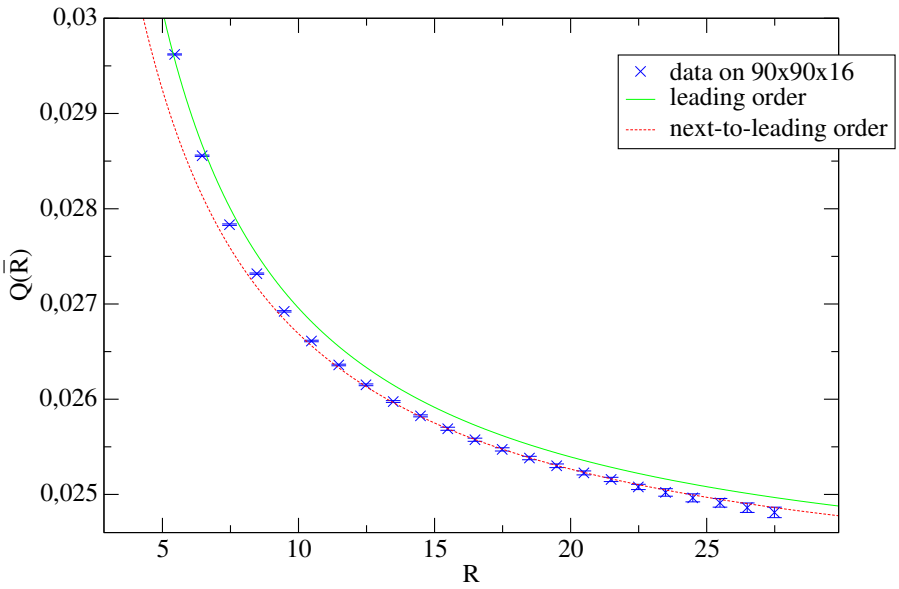


Figure 4.7: *The force* $Q(\bar{R})$ *as a function of the distance between the two static quarks. The solid line and the dotted line are the leading order approximation of Eq.(4.27) and the next-to-leading order approximation of Eq.(4.28), respectively.*

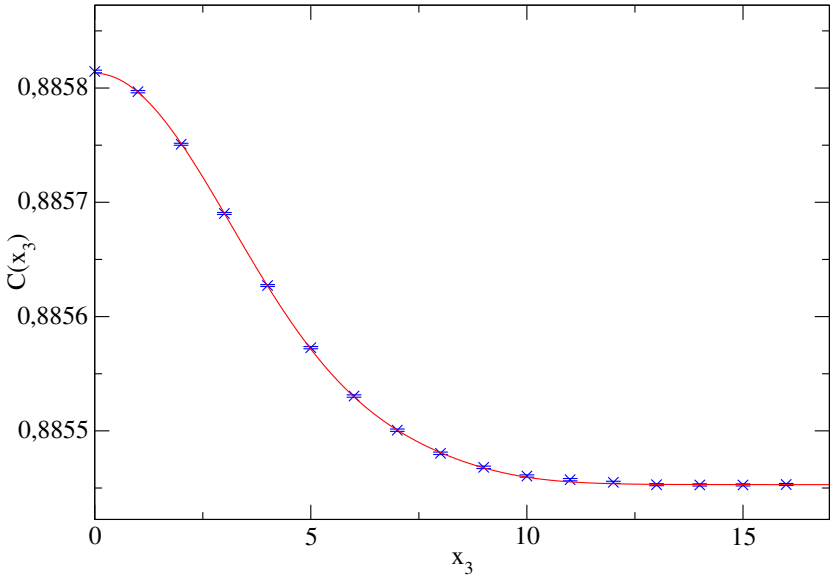


Figure 4.8: *The ratio* $\frac{\langle \Phi_0 \Phi_R P_x \rangle}{\langle \Phi_0 \Phi_R \rangle}$ *as a function of the transverse displacement* $x_3$ *of the plaquette from the plane of the string world-sheet. The distance between the two static sources is* $R = 17$*. The solid curve is a fit using Eq.(4.25).*

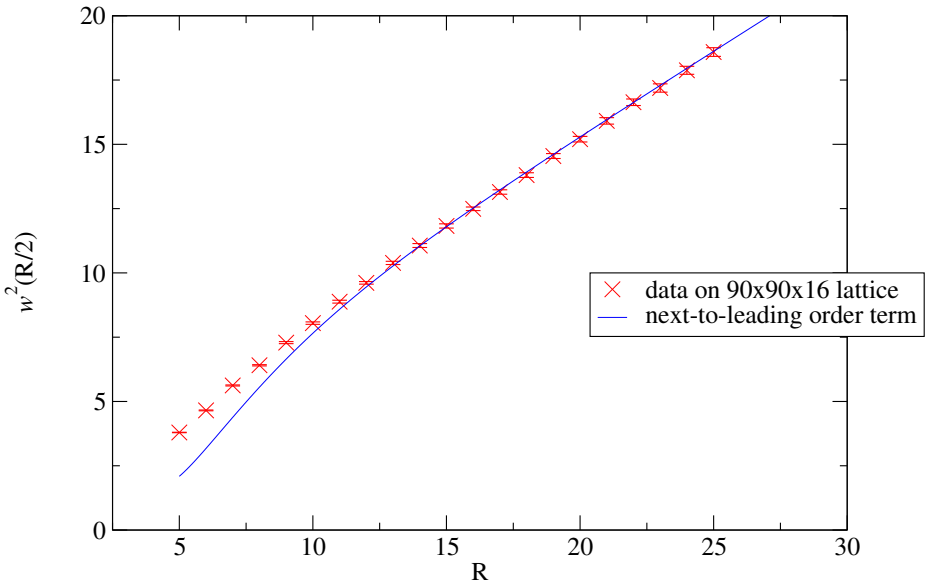


Figure 4.9: *The squared width of the confining string at its midpoint* $w^2(R/2)$ *as a function of the separation of the static sources* $R$*. The solid line represent the 2-loop prediction of the low-energy effective string theory using* $R_0 = 2.26$*.*

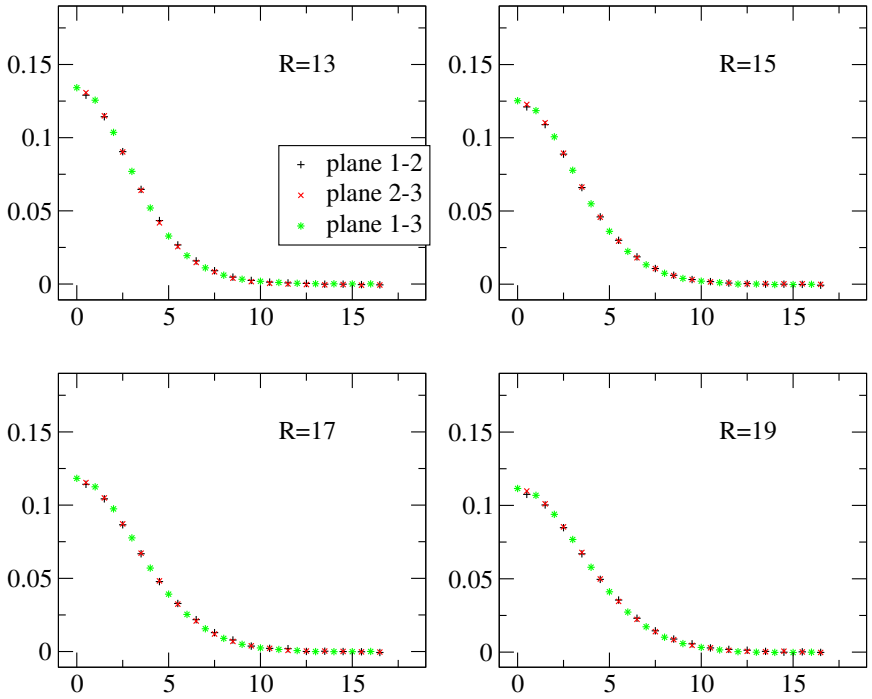


Figure 4.10: *Probability distribution* $C(x_3)/\int dx_3\ C(x_3)$ *using the 3 possible orientations of the plaquette in Eq.(4.23). The data points for the 2 orientations orthogonal to the string world-sheet are put at the midpoint between 2 lattice sites.*

the effective theory with the numerical simulations of the lattice Yang-Mills theory. We found the latter in very good agreement with the theoretical predictions, confirming the quantitative correctness of the effective string theory.

An interesting perspective would be to study the theory in a $4d$ space-time, which would require much more computational power. In addition $SU(3)$ Yang-Mills theory would give us much more insight in the low energy aspects of QCD.

# Appendix A

# The Propagator on the Cylinder

In appendix A of [43] is given an explicit expression for the propagator on the torus:

$$G(z) = -\frac{1}{2\pi\sigma}\Re e\left[\log\frac{2\pi z}{R} - \sum_{k=1}^{\infty}\frac{G_k(2\pi)^{2k}}{2k}\left(\frac{z}{R}\right)^{2k}\right] + \frac{(t-t')^2}{2\,\sigma\,L\,R} \qquad (A.1)$$

with

$$z = x - x' + i(t-t')\ ,\ G_k = 2\frac{\zeta(2k)}{R^{2k}}\,E_{2k}(iu)\ ,\quad u = \frac{L}{R}\ , \qquad (A.2)$$

and the Eisenstein series $E_{2k}(\tau)$ are defined as

$$E_{2k}(\tau) = 1 + (-1)^k\frac{4k}{B_k}\sum_{n=1}^{\infty}\frac{n^{2k-1}q^n}{1-q^n}\ , \qquad (A.3)$$

where $B_k$ are the Bernoulli numbers, defined through the expansion

$$\frac{z}{\mathrm{e}^z - 1} = 1 - \frac{z}{2} - \sum_{k=1}^{\infty}(-1)^k\frac{B_k}{(2k)!}z^{2k}\ . \qquad (A.4)$$

On a torus of size $R \times L$ this satisfies the equation:

$$-\Delta G(x,t;x't') = \frac{1}{\sigma}\delta(x-x')\,\delta(t-t') - \frac{1}{\sigma\,L\,R}\ . \qquad (A.5)$$

where the term $1/\sigma\,L\,R$ is intended to subtract the zero-mode, making the Laplace operator $\Delta$ invertible in the orthogonal subspace. Inserting A.3 in (A.1) we get

$$\begin{aligned} 2\pi\sigma G(z) &= \frac{\pi(\Im m z)^2}{L\,R} - \Re e\left[\log\frac{2\pi z}{R} - \sum_{k=1}^{\infty}\frac{B_k(2\pi)^{2k}}{(2k)!}\frac{1}{2k}\left(\frac{z}{R}\right)^{2k}\right] \\ &+ 2\,\Re e\left[\sum_{k=1}^{\infty}\frac{(-1)^k}{(2k)!}\left(\frac{2\pi z}{R}\right)^{2k}\sum_{n=1}^{\infty}\frac{n^{2k-1}q^n}{1-q^n}\right]\ . \end{aligned} \qquad (A.6)$$

We now re-sum all terms enclosed in the first square brackets using (A.4):

$$\sum_{k=1}^{\infty}(-1)^k \frac{B_k\, w^{2k}}{(2k)!}\frac{1}{2k} = \sum_{n=1}^{\infty}\frac{\mathrm{e}^{-n\,w}}{n} - \frac{w}{2} + \log w = -\log(1-\mathrm{e}^{-w}) - \frac{w}{2} + \log w, \tag{A.7}$$

with $w = -2\pi i z/R$. Interchanging the order of the two sums in the last bracket of eq. (A.6), we recognize the Taylor expansion of the cosine and arrive at the simpler expression

$$\begin{aligned} 2\pi\sigma G(z) = \frac{\pi(t-t')(t-t'-L)}{L\,R} + \Re e\Big[ &-\log(1-\mathrm{e}^{2\pi i z/R}) \\ &+2\sum_{n=1}^{\infty}\frac{n^{-1}q^n}{1-q^n}\cos\frac{2\pi n z}{R} + 2\log q^{-1/24}\eta(iu)\Big]\ , \end{aligned} \tag{A.8}$$

where the Dedekind $\eta$-function has already been defined in 2.27. Note that the sum in A.8 satisfies:

$$\sum_{n=1}^{\infty}\frac{n^{-1}q^n}{1-q^n} \equiv \sum_{k=1}^{\infty}\sum_{n=1}^{\infty}\frac{q^{k\,n}}{n} = -\sum_{k=1}^{\infty}\log\left(1-q^k\right) = -\log\varphi(\tau)\ , \tag{A.9}$$

Inserting A.9 in A.8 and expanding the first logarithm in powers of $\mathrm{e}^{2\pi i z/R}$, we obtain:

$$G(x,t) = \frac{t(t-L)}{2\sigma L R} + \frac{1}{2\pi\sigma}\sum_{n=1}^{\infty}\cos\left(\frac{2\pi n x}{R}\right)\frac{\mathrm{e}^{-2\pi n t/R} + q^n\,\mathrm{e}^{2\pi n t/R}}{n(1-q^n)} + K, \tag{A.10}$$

where

$$u = \frac{L}{R}, \qquad q = \mathrm{e}^{-2\pi u}, \qquad K = \frac{L}{12\sigma R} + \frac{1}{\pi\sigma}\log\eta(iu). \tag{A.11}$$

This expression converges in the range $q < 1$ and $0 \le t - t' \le L$.

The form of the Gaussian correlator $G(x,t;x',t') \equiv \langle h(x,t)\,h(x',t')\rangle_0$ on a cylinder of size $R \times L$ with fixed boundary conditions at $x = 0$ and $x = R$ and periodic boundary conditions in $t$ with period $L$ is obtained from the above correlators $G_t$ on the torus when its size is $2R \times L$:

$$\begin{aligned} G(x,t;x',t') &= G_t(z-z') - G_t(z+z'^*) \\ &= \frac{1}{\pi\sigma}\sum_{n=1}^{\infty}\sin\frac{\pi n x}{R}\ \sin\frac{\pi n x'}{R}\,\frac{\mathrm{e}^{-\pi n(t-t')/R} + \mathrm{e}^{-\pi n(L-t+t')/R}}{n(1-q^n)}\ . \end{aligned} \tag{A.12}$$

where $z' = x' + it'$ and $z'^* = x' - it'$. This is the expression used in Section 2.5.

# Ringraziamenti

Ringrazio prima di tutto il Dottor Michele Pepe, che con pazienza ed esperienza ha guidato il mio lavoro negli ultimi mesi.

Questo studio è stato realizzato grazie all'utilizzo della FARM del gruppo di fisica teorica dell'Università degli Studi di Milano. A questo proposito vorrei ringraziare soprattutto Emanuele Bagnaschi per avere installato MPI e per essere sempre stato pronto a risolvere ogni mio problema.

I miei ringraziamenti vanno anche al mio relatore, il Professore Sergio Caracciolo, per avermi dato fiducia sin dall'inizio.

Un ringraziamento particolare va ad Antonio Rago senza il quale non avrei mai intrapreso questa strada.

Vorrei ringraziare tutti i miei compagni di fisica teorica Alessandro, Pier, Vittore, Roberto, Enrico, Margherita, Pietro, Ulisse e Davide che hanno condiviso con me tantissimi momenti.

Ringrazio i miei amici e compagni di avventure di sempre Fabio, Luca e Danilo con i quali nell'ultimo anno ci siamo arrampicati sulle pareti più impensate.

Tra gli amici un pensiero speciale va ai due Ale, il biologo e il ferroviere, per avermi sempre ascoltato e consigliato quando ne avevo bisogno.

Molti sono i parenti, ma tra questi vorrei ringraziare i miei zii Donatella e Antonio e i miei cuginetti Giulia e Davide, a cui sarò sempre legato.

Infine, ringrazio i miei genitori e mia sorella, che mi sono stati vicini in tutti questi anni e che hanno reso possibile tutto questo.

# Bibliography


[1] Michael E Peskin and Daniel V Schroeder. *An Introduction to Quantum Field Theory; 1995 ed.* Westview, 1995.

[2] Michel Le Bellac. *Quantum and Statistical Field Theory.* Oxford University Press, USA, 1992.

[3] J. Greensite. The confinement problem in lattice gauge theory. *Prog. Part. Nucl. Phys.*, 51:1, 2003.

[4] I. Montvay and G. Munster. *Quantum fields on a lattice.* Cambridge University Press, 1997.

[5] Kenneth G. Wilson. Confinement of Quarks. *Phys. Rev.*, D10:2445–2459, 1974.

[6] A. M. Polyakov. Compact gauge fields and the infrared catastrophe. *Physics Letters B*, 59(1):82–84, 1975.

[7] M. Creutz. *Quarks, Gluons and Lattices.* Cambridge University Press, 1983.

[8] K. Osterwalder and E. Seiler. Gauge Field Theories on the Lattice. *Ann. Phys.*, 110:440, 1978.

[9] Michael Creutz, Laurence Jacobs, and Claudio Rebbi. Monte Carlo Computations in Lattice Gauge Theories. *Phys. Rept.*, 95:201, 1983.

[10] M. Lüscher, G. Munster, and P. Weisz. How Thick Are Chromoelectric Flux Tubes? *Nucl. Phys.*, B180:1, 1981.

[11] G. Munster. *Nucl. Phys.*, B180:23, 1981.

[12] M. Creutz. Monte Carlo Study of Quantized SU(2) Gauge Theory. *Phys. Rev.*, D21:2308, 1980.

[13] Anna Hasenfratz, Etelka Hasenfratz, and Peter Hasenfratz. Generalized Roughening Transition And Its Effect On The String Tension. *Nucl. Phys.*, B180:353, 1981.

[14] M. Lüscher, K. Symanzik, and P. Weisz. Anomalies of the Free Loop Wave Equation in the WKB Approximation. *Nucl. Phys.*, B173:365, 1980.

[15] M. Lüscher. Symmetry Breaking Aspects of the Roughening Transition in Gauge Theories. *Nucl. Phys.*, B180:317, 1981.

[16] Cheng. *Gauge theory of elementary particle physics: Problems and solutions*. 2000. Oxford, UK: Clarendon (2000) 306 p.

[17] K. Dietz and T. Filk. On The Renormalization Of String Functionals. *Phys. Rev.*, D27:2944, 1983.

[18] M. Lüscher and P. Weisz. String excitation energies in su(n) gauge theories beyond the free-string approximation. *JHEP*, (0407):014, 2004.

[19] Robert D. Pisarski and Orlando Alvarez. Strings at finite temperature and deconfinement. *Phys. Rev.*, D26:3735, 1982.

[20] M. Caselle, M. Pepe, and A. Rago. Static quark potential and effective string corrections in the (2+1)-d SU(2) Yang-Mills theory. *JHEP*, 10:005, 2004.

[21] M. Caselle, M. Hasenbusch, and M. Panero. Short distance behaviour of the effective string. *JHEP*, 05:032, 2004.

[22] Yoichiro Nambu. QCD and the String Model. *Phys. Lett.*, B80:372, 1979.

[23] M. Caselle, M. Hasenbusch, and M. Panero. String effects in the 3d gauge Ising model. *JHEP*, 01:057, 2003.

[24] M. Lüscher. Construction of a Selfadjoint, Strictly Positive Transfer Matrix for Euclidean Lattice Gauge Theories. *Commun. Math. Phys.*, 54:283, 1977.

[25] Ofer Aharony and Eyal Karzbrun. On the effective action of confining strings. *Journal of High Energy Physics*, 2009(06):012, 2009.

[26] F Gliozzi, M Pepe, and U J Wiese. The width of the color flux tube at 2-loop order. Technical Report arXiv:1006.2252, Jun 2010. Comments: 15 pages, no figures.

[27] Martin Lüscher and Peter Weisz. Locality and exponential error reduction in numerical lattice gauge theory. *JHEP*, 09:010, 2001.

[28] Heinz J. Rothe. *Lattice gauge theories : an introduction / Heinz J. Rothe*. World Scientific, Singapore :, 2nd ed. edition, 1997.

[29] Nicholas Metropolis, Arianna W. Rosenbluth, Marshall N. Rosenbluth, Augusta H. Teller, and Edward Teller. Equation of state calculations by fast computing machines. *The Journal of Chemical Physics*, 21(6):1087–1092, 1953.

[30] A. D. Kennedy and B. J. Pendleton. Improved heatbath method for monte carlo calculations in lattice gauge theories. *Physics Letters B*, 156(5-6):393–399, 1985.

[31] Martin Lüscher. A portable high-quality random number generator for lattice field theory simulations. *Computer Physics Communications*, 79(1):100–110, 1994.

[32] Donald Ervin Knuth. *The art of computer programming / Donald E. Knuth.* Addison-Wiley, Reading, Mass., :, 1968.

[33] Mark Galassi, Jim Davies, James Theiler, Brian Gough, Gerard Jungman, Michael Booth, and Fabrice Rossi. *Gnu Scientific Library: Reference Manual*. Network Theory Ltd., 2003.

[34] George Marsaglia, B. Narasimhan, and Arif Zaman. A random number generator for PC's. *Comput. Phys. Commun.*, 60:345–349, 1990.

[35] M. Caselle, R. Fiore, F. Gliozzi, M. Hasenbusch, and P. Provero. String effects in the Wilson loop: A high precision numerical test. *Nucl. Phys.*, B486:245–260, 1997.

[36] M. Caselle et al. Rough interfaces beyond the Gaussian approximation. *Nucl. Phys. Proc. Suppl.*, 42:755, 1995.

[37] M. Caselle, M. Panero, P. Provero, and M. Hasenbusch. String effects in Polyakov loop correlators. *Nucl. Phys. Proc. Suppl.*, 119:499–501, 2003.

[38] Michele Caselle, Martin Hasenbusch, and Marco Panero. Effective string picture for confinement at finite temperature: Theoretical predictions and high precision numerical results. *Nucl. Phys. Proc. Suppl.*, 129:593–595, 2004.

[39] Martin Lüscher and P Weisz. Quark confinement and the bosonic string. *J. High Energy Phys.*, 07(hep-lat/0207003. CERN-TH-2002-138. MPI-TH-2002-024):049. 21 p, Jul 2002.

[40] Alan D. Sokal. Monte carlo methods in statistical mechanics: Foundations and new algorithms. Lecture Notes Cours de Troisieme Cycle de la Physique en Suisse Romande, Lausanne, Switzerland, (unpublished, 1989).

[41] R. Sommer. A New way to set the energy scale in lattice gauge theories and its applications to the static force and alpha-s in SU(2) Yang-Mills theory. *Nucl. Phys.*, B411:839–854, 1994.

[42] F. Gliozzi, M. Pepe, and U. J. Wiese. The Width of the Confining String in Yang-Mills Theory. *Phys. Rev. Lett.*, 104:232001, 2010.

[43] M. Caselle, F. Gliozzi, Ulrika Magnea, and S. Vinti. Width of Long Colour Flux Tubes in Lattice Gauge Systems. *Nucl. Phys.*, B460:397–412, 1996.